NASA/CR—97-206591

IN-17

Rain Fade Compensation for Ka-Band Communications Satellites

W. Carl Mitchell
Space Systems/LORAL, Palo Alto, California

Lan Nguyen, Asoka Dissanayake, Brian Markey, and Anh Le
COMSAT Laboratories, Clarksburg, Maryland

December 1997

The NASA STI Program Office ... in Profile

Since its founding, NASA has been dedicated to the advancement of aeronautics and space science. The NASA Scientific and Technical Information (STI) Program Office plays a key part in helping NASA maintain this important role.

The NASA STI Program Office is operated by Langley Research Center, the lead center for NASA's scientific and technical information. The NASA STI Program Office provides access to the NASA STI Database, the largest collection of aeronautical and space science STI in the world. The Program Office is also NASA's institutional mechanism for disseminating the results of its research and development activities. These results are published by NASA in the NASA STI Report Series, which includes the following report types:

- TECHNICAL PUBLICATION. Reports of completed research or a major significant phase of research that present the results of NASA programs and include extensive data or theoretical analysis. Includes compilations of significant scientific and technical data and information deemed to be of continuing reference value. NASA counter-part of peer reviewed formal professional papers, but having less stringent limitations on manuscript length and extent of graphic presentations.

- TECHNICAL MEMORANDUM. Scientific and technical findings that are preliminary or of specialized interest, e.g., quick release reports, working papers, and bibliographies that contain minimal annotation. Does not contain extensive analysis.

- CONTRACTOR REPORT. Scientific and technical findings by NASA-sponsored contractors and grantees.

- CONFERENCE PUBLICATION. Collected papers from scientific and technical conferences, symposia, seminars, or other meetings sponsored or co-sponsored by NASA.

- SPECIAL PUBLICATION. Scientific, technical, or historical information from NASA programs, projects, and missions, often concerned with subjects having substantial public interest.

- TECHNICAL TRANSLATION. English-language translations of foreign scientific and technical material pertinent to NASA's mission.

Specialized services that help round out the STI Program Office's diverse offerings include creating custom thesauri, building customized databases, organizing and publishing research results ... even providing videos.

For more information about the NASA STI Program Office, you can:

- Access the NASA STI Program Home Page at http://www.sti.nasa.gov/STI-homepage.html

- E-mail your question via the Internet to help@sti.nasa.gov

- Fax your question to the NASA Access Help Desk at (301) 621-0134

- Phone the NASA Access Help Desk at (301) 621-0390

- Write to:
  NASA Access Help Desk
  NASA Center for AeroSpace Information
  800 Elkridge Landing Road
  Linthicum Heights, MD 21090-2934

NASA/CR—97-206591

Rain Fade Compensation for Ka-Band Communications Satellites

W. Carl Mitchell
Space Systems/LORAL, Palo Alto, California

Lan Nguyen, Asoka Dissanayake, Brian Markey, and Anh Le
COMSAT Laboratories, Clarksburg, Maryland

Prepared under Contract NAS3–27559

National Aeronautics and
Space Administration

Lewis Research Center

December 1997

Available from

NASA Center for Aerospace Information
800 Elkridge Landing Road
Linthicum Heights, MD 21090-2934
Price Code: A08

National Technical Information Service
5287 Port Royal Road
Springfield, VA 22100
Price Code: A08

CONTENTS

Section **Page**

CONTENTS (Continued)

CONTENTS (Continued)

CONTENTS (Continued)

ILLUSTRATIONS

ILLUSTRATIONS (Continued)

ILLUSTRATIONS (Continued)

TABLES

EXECUTIVE SUMMARY

This report provides a review and evaluation of practical rain fade compensation alternatives for Ka-band satellite systems. This report includes a description of and cost estimates for performing three rain fade measurement and compensation experiments.

The evaluated rain fade characteristics include rain attenuation or fade depth, rain and ice depolarization, tropospheric scintillation, fade duration, inter-fade interval, fade rate, frequency scaling of fade, correlation of fades within a 1-GHz bandwidth, simultaneity of rain events over extended areas, and antenna wetting. The evaluated fade measurement techniques include satellite beacon power, modem AGC, pseudo bit error ratio, bit error ratio from channel coded data, bit error ratio from known data pattern, and signal-to-noise ratio. The evaluated fade compensation techniques include built-in link margin, overdriven satellite transponder, uplink power control, diversity techniques (i.e., frequency diversity, site diversity through routing, and back-up terrestrial network), information rate and FEC code rate changes, downlink power sharing (i.e., active phased array, active lens array, matrix or multi-port amplifier, and multi-mode amplifier), and an ABR feedback flow control technique for varying the information rate from the source. Three experiments have also been proposed to assess the implementation issues related to these techniques. The first experiment deals with rain fade measurement techniques while the second one covers the rain fade compensation techniques. A feedback flow control technique for the ABR service (i.e., for ATM-based traffic) is addressed in the third experiment.

Based on the evaluation criteria of measurement accuracy and time, and implementation complexity, the three measurement techniques selected for further evaluation in the first two experiments are beacon power, bit error ratio from channel coded data, and signal-to-noise ratio. The two compensation techniques selected for further evaluation in the second experiment are uplink power control, and information rate and FEC code rate changes. Implementation of the ABR feedback flow control technique is carried out in the third experiment.

From this study, the following conclusions can be made:

(1) Due to severe fading in Ka-bands in a number of rain zones, sufficient system margins should be allocated for all carriers in a network. In a Ka-band satellite system, for the link from earth station A to earth station B, the system margin generally consists of a fixed clear-sky margin and an additional margin, which is dynamically allocated through the rain fade compensation technique being implemented. The fixed clear-sky margin is typically in the range of 4-5 dB. It is not

uncommon to provide more than 15 dB in the dynamic range of a typical uplink power control system in moderate and heavy rain zones.

(2) In order to provide a high system margin, it is desirable to combine the uplink power control technique with the technique that implements the source information rate and FEC code rate changes. The use of the second technique alone will contribute up to about 4.5 dB toward the dynamic part of the system margin.

(3) The three proposed experiments are intended to assess the feasibility of the selected fade measurement and compensation techniques, and ABR feedback flow control technique. The first experiment, planned for a ten-month period, will compare the beacon power, bit error ratio from channel coded data, and signal-to-noise ratio techniques in terms of implementation issues such as measurement accuracy and reliability, stability of measured data, and ease of operation. The second experiment, also planned for a ten-month period, will address the implementation issues related to the uplink power control technique and the technique which implements the source information rate and FEC code rate changes, and the combination of both techniques. The third experiment, planned for a twelve-month period, will address the implementation issues related to the ABR feedback flow control technique.

SECTION 1 — INTRODUCTION

In the last two years, a number of companies have begun plans to implement commercial Ka-band satellite systems. For example, in 1995 alone, 14 U.S. companies submitted filings to the Federal Communications Commission (FCC) to request its authorization to construct and launch Ka-band (30/20 GHz) satellites in order to begin operation in the 1998-2001 time frame [1]. A majority of these emerging systems proposed to use advanced on-board processing (OBP) technologies [2], [3] & [4] to offer, on a global scale, services such as voice, data, video, multimedia, Internet, etc. The on-orbit feasibility of some of these technologies have been demonstrated by the Advanced Communications Technology Satellite (ACTS) program [5]. Through these services, applications typically include distance learning, corporate data distribution and training, tele-medicine, direct-to-home (DTH) video, distribution of software, music, scientific data, financial, and weather information, etc. The successful deployment of these systems would firmly establish satellite communications as an important and economical means in the realization of the national and global information infrastructures (NII/GII).

It is well known that as the carrier frequency increases from the C-band (6/4 GHz) and Ku-band (14/12 GHz) to Ka-band (30/20 GHz), the carrier performance becomes more severely affected (due to rain attenuation, increase in receive system noise temperature, depolarization, etc.) during periods of rain in the uplink or downlink transmission path between the earth station and satellite. In a viable Ka-band satellite system, it is imperative that suitable adaptive fade compensation means be implemented at earth stations to alleviate the severe impairment effects due to rain. This report provides a review and evaluation of practical rain fade compensation alternatives for Ka-band satellite systems, and includes a number of proposed rain fade measurement and compensation experiments, and cost estimates for performing these experiments.

Section 2 presents a general overview of conventional bent-pipe and more advanced OBP spacecraft architectures. The rain fade characterization including rain attenuation, depolarization, tropospheric scintillation, fade dynamics, simultaneity of fade events, and antenna wetting effects is described in Section 3. Section 4 provides a detailed evaluation of fade measurement techniques such as beacon power, modem automatic gain control (AGC), pseudo bit error ratio, bit error ratio from channel coded data, bit error ratio from known data pattern, and signal-to-noise ratio. An assessment of the cost of implementing these techniques on the earth station or terminal is also included. Section 5 provides a detailed evaluation of the rain fade compensation techniques such as built-in link margin, overdriven satellite transponder, uplink power control, frequency and site diversity, back-up terrestrial network, information rate and forward error correction (FEC) code rate changes, and downlink power sharing. A comparison of these techniques is also provided.

The fade compensation technique for the asynchronous transfer mode (ATM) available bit rate (ABR) service is presented in Section 6. From the above relevant results, a set of requirements is derived to serve as the baseline system design requirements. These requirements are presented in Section 7. The rain fade measurement experiments, rain fade compensation experiment and the ATM experiment are described in Section 8. Section 9 gives the summary and conclusions. The references are given in Section 10. The Appendix contains an error analysis for each fade measurement technique applied to a bent-pipe satellite operating with back-off, a bent-pipe satellite operating in saturation and an on-board processing satellite.

SECTION 2 — SPACECRAFT ARCHITECTURES

In general, there are two types of spacecraft architectures employed in commercial communications satellites, namely, bent-pipe and on-board processing. Most current C- and Ku-band communications satellite systems are of the bent-pipe type while most proposed Ka-band systems are of the OBP type.

2.1 BENT-PIPE ARCHITECTURE

In a conventional bent-pipe satellite, carriers or signals transmitted from earth stations in the uplink are received by the satellite. As shown in Figure 2-1, on-board the satellite, the carriers undergo a number of major steps: amplification by low-noise amplifiers (LNAs), down conversion from uplink frequencies to downlink frequencies, separation into individual channels or transponders, final amplification by traveling-wave tube amplifiers (TWTAs) or solid state power amplifiers (SSPAs), and transmission in the downlink to earth stations. An inherent characteristic of transparent or bent-pipe satellite systems is that, for a link from earth station A to earth station B, the total carrier-to-noise ratio received at B depends on several major components (e.g., [6], [7], & [8]) such as uplink thermal noise and uplink interference; intermodulation [9] and modulation transfer [10]; and downlink thermal noise and downlink interference. Uplink and/or downlink interference entries are due to intra-system interference (co-channel interference due to frequency reuse), intersystem interference (adjacent satellite interference), and interference from terrestrial radio relay systems sharing the same bands. In particular, the carrier performance of a link can be limited or controlled by any one component or by a combination of various components.

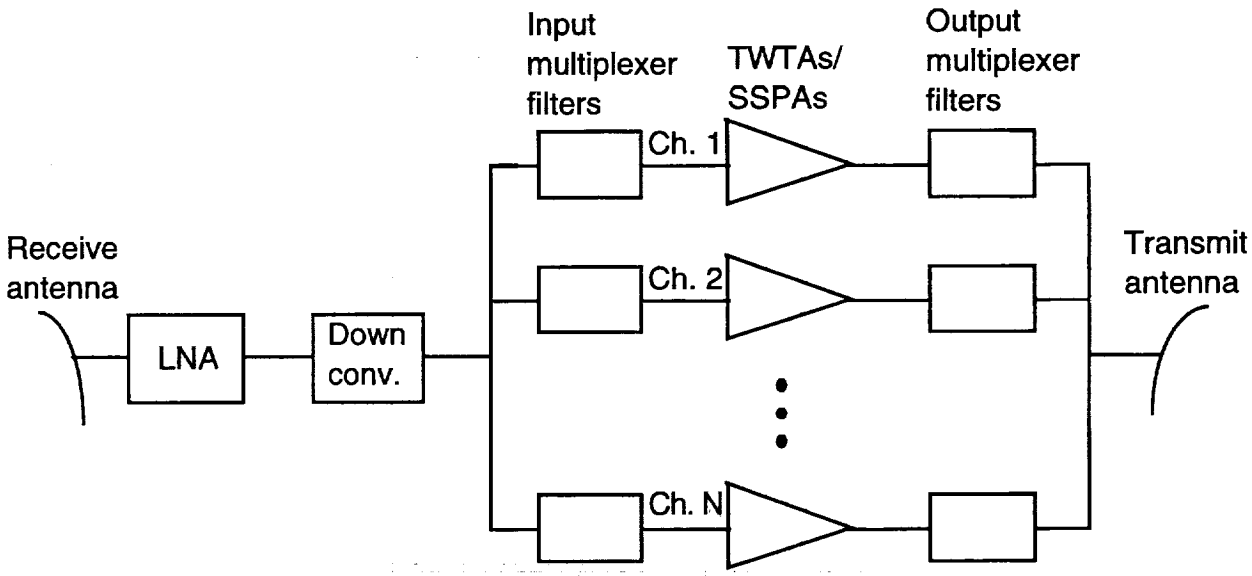

Figure 2-1. Simplified Block Diagram of A Bent-Pipe Satellite

2.2 ON-BOARD PROCESSING ARCHITECTURES

OBP satellites are more complex than bent-pipe satellites. Benefits arising from the added complexities are numerous [2]-[4], and vary as the degree of complexity is implemented in a specific OBP design. Depending on network requirements, an OBP satellite (Figure 2-2) can be designed to include a combination of capabilities such as demultiplexing/multiplexing, demodulation/modulation, decoding/encoding, beam switching, baseband switching (time slots or packets), etc. OBP communications payloads can be grouped into three types as follows.

(1) In the first type, the main function of the payload is to route or channelize (demultiplex/multiplex) traffic from upbeams (i.e., uplink beams) into downbeams (i.e., downlink beams) according to certain operational network requirements. For example, in the INTELSAT VI satellite-switched time-division multiple access (SS-TDMA) system [11], [12], TDMA bursts arriving on various upbeams can be routed by the microwave switch matrix (MSM) on board the satellite to various downbeams according to specific switch state time plans. It should be noted that, in this situation, the TDMA carrier link performance also depends on a number of components as described in Section 2.1 since, once a switch state is established, the transponders behave like bent-pipe transponders during that switch state duration.

(2) The second type refers to regenerative payloads in which uplink carriers are first demodulated and decoded into baseband signals. These signals can then be further processed, and encoded and modulated before transmission onto downlinks. Since baseband signals are available on board the satellite, it is possible to implement dynamic connectivity among all beams and channels (users) using a baseband switch and a processor. The principal benefit realized with this architecture is the complete isolation between uplink degradations and downlink degradations, thereby improving substantially the carrier bit error ratio (BER) performance [2],

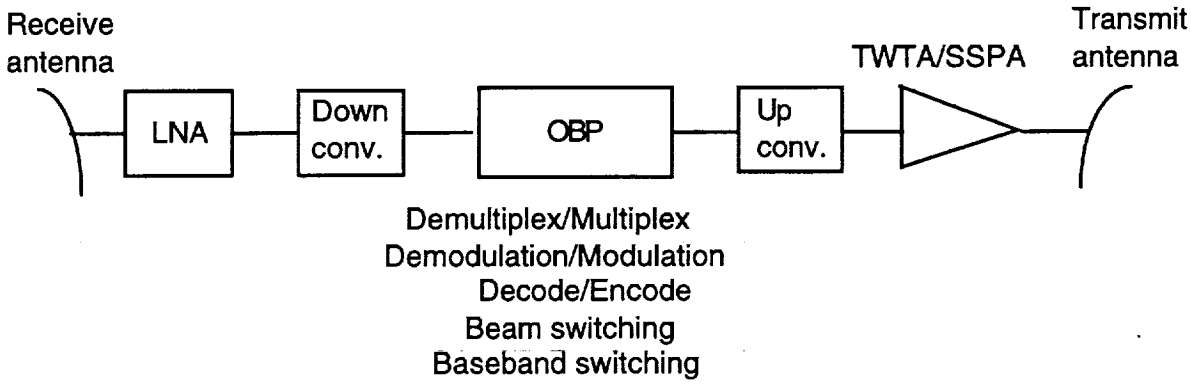

Figure 2-2. Simplified Block Diagram of An OBP Satellite

[13]. Proposed Ka-band systems which utilize regeneration and baseband circuit switching [3] include, for examples, the CyberStar [14] and Galaxy/Spaceway [15] systems.

(3) In the third type, regeneration and a more advanced form of baseband switching, called fast packet switching, with capabilities similar to those of an Asynchronous Transfer Mode (ATM) swich are utilized [3]. Here, the same benefit with respect to the improvement of the carrier BER performance is also realized. A proposed Ka-band system utilizing this architecture is the Astrolink system [16].

In this study, the two architectures evaluated are bent-pipe and regenerative with baseband circuit switching. In particular, for the latter, in the uplinks, TDMA carriers will access the satellite in the frequency-division multiple access (FDMA) mode; and, large time-division multiplex (TDM) carriers will be transmitted in the downlinks. It should be noted that only a high-level evaluation will be performed for these two architectures with respect to rain fade compensation techniques since very little technical information was provided in [14] and [15].

SECTION 3 — RAIN FADE CHARACTERIZATION

Propagation factors that affect Ka-band satellite links operating at moderate to high elevation angles include:

- gaseous absorption
- cloud attenuation
- melting layer attenuation
- rain attenuation
- rain and ice depolarization
- tropospheric scintillation

Gaseous absorption, cloud attenuation, melting layer attenuation, and rain attenuation are absorptive effects producing both signal attenuation and a proportionate increase in the thermal noise received at the antenna port. Systems employing orthogonal polarization to implement frequency reuse suffer from interference produced by rain and ice depolarization. Tropospheric scintillation is non-absorptive and produce signal attenuation as well as enhancements. Due consideration must be given to the different impairment factors when designing fade mitigation schemes. In this respect, fade rates, fade durations, and frequency scaling behavior of fading mechanisms are of special importance. A brief review of the various impairment factors are presented below.

3.1 GASEOUS ABSORPTION

Compared to other absorptive effects gaseous absorption arising from oxygen and water vapor present in the atmosphere is relatively small. Absorption due to oxygen is nearly constant and that due to water vapor varies slowly with time in response to variations in temperature and humidity [17]. Gaseous absorption at 5°C and 25°C as a function of relative humidity is shown in Figures 3-1 and 3-2 for typical Ka-band up- and down-link frequencies; elevation angle is 40°. As evidenced, the gaseous absorption increases with the relative humidity as well as the temperature. Closeness of the down-link frequency to the water vapor absorption line at 22.2 GHz makes the absorption at the down-link frequency exceed that at the up-link frequency. This occurs when the water vapor absorption is significantly larger than the oxygen absorption. It is seen that for moderate elevation angles the gaseous absorption amounts to less than 1.5 dB under most conditions. The fade ratio between the two frequencies are also shown in the figures. The fade ratio is a function of both humidity and temperature and varies approximately between 1.5 for complete dry conditions and 0.8 under high humidity conditions. For practical purposes the ratio can be considered equal to unity.

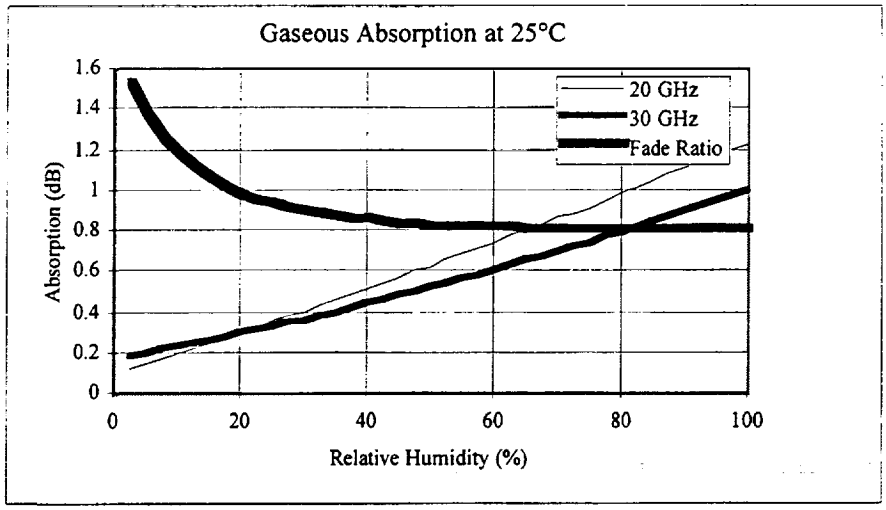

Figure 3-1. Gaseous absorption at 20 and 30 GHz; temperature: 5°C, elevation angle 40°

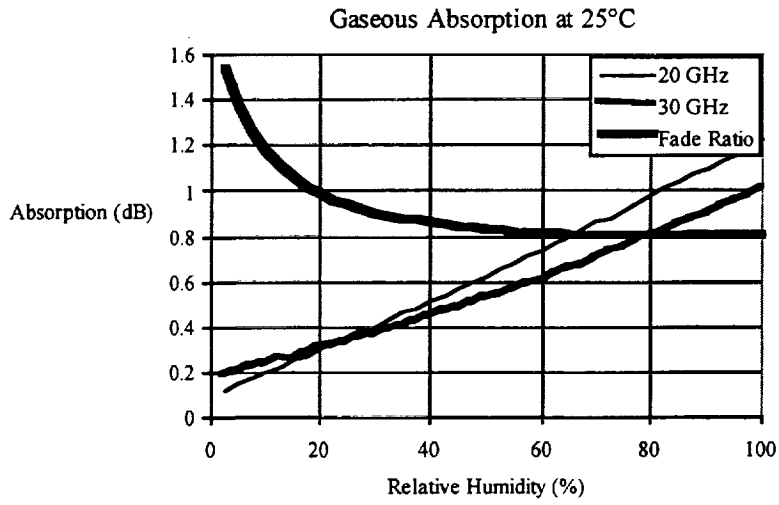

Figure 3-2. Gaseous absorption at 20 and 30 GHz; temperature: 25°C, elevation angle 40°

3.2 CLOUD ATTENUATION

At Ka-band frequencies clouds containing liquid water can produce both signal attenuation and amplitude scintillations [18]; ice clouds, in general, do not produce these effects. The small size of cloud particles relative to the wavelength makes cloud attenuation essentially a function of cloud temperature and the integrated liquid water content along the propagation path. Figure 3-3 show the relationship between cloud attenuation, frequency, and cloud temperature. The specific attenuation coefficient shown is defined as the specific attenuation (dB/km) for a liquid water content of 1 gm/m^3. Table 3-1 shows average properties of several cloud types and the levels of expected attenuation for an elevation angle of 40°. Attenuation levels are calculated assuming a uniform distribution of the liquid water within the cloud. It is seen that significant amounts of cloud attenuation can be expected at the up-link frequency of 30 GHz. The fade ratio between two frequencies is approximated by [19]:

$$\frac{A_1}{A_2} = \left(\frac{f_1}{f_2}\right)^2 \tag{3-1}$$

where A_1 are A_2 are attenuation (dB) at frequencies f_1 and f_2, respectively.

Although reliable information on fading rates associated with clouds is generally lacking, fade rates are thought to be relatively small (in the range 0.1 to 1 dB/min).

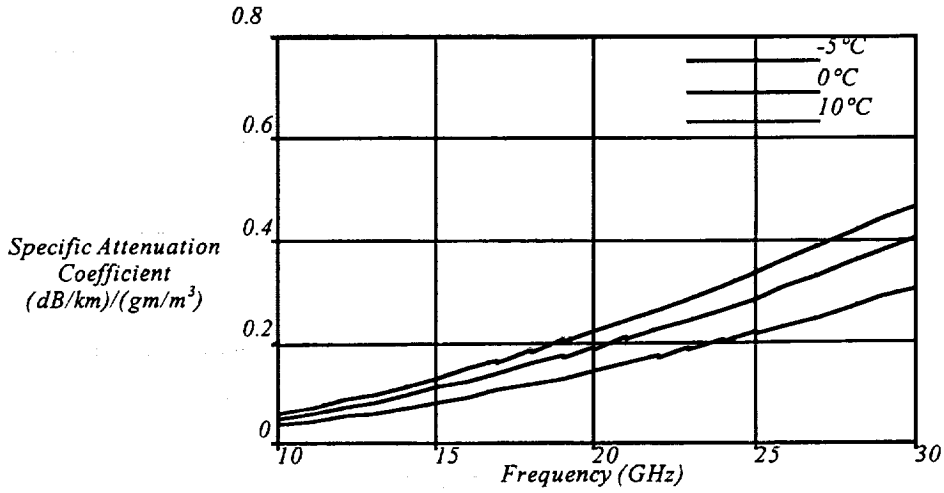

Figure 3-3. Specific Attenuation of Clouds as a Function of Frequency and Temperature

Table 3-1. Average Properties of Different Cloud Types

Cloud Type	Density (g/m3)	Vertical Extent (km)	20 GHz Attenuation (dB)	30 GHz Attenuation (dB)
Cumulus	1.0	1.0 - 3.5	0.8	1.8
Stratus	0.15	0.5 – 2.0	0.4	0.9
Stratocumulus	0.55	0.5 – 1.0	0.6	1.3
Altostratus	0.4	2.5 – 3.0	0.4	0.9

3.3 RAIN ATTENUATION

Rain attenuation is the dominant propagation impairment at Ka-band frequencies. Rain attenuation is a function of frequency, elevation angle, polarization angle, rain intensity, rain drop size distribution and rain drop temperature. Fade durations and rates are closely correlated with the rain type; e.g. stratiform rain are conducive to longer fade durations and slower fade rates. Frequency scaling of rain attenuation is largely determined by the raindrop size distribution and the rain temperature. As a first order approximation, the same frequency scaling relationship given in equation 3-1 may be used for rain as well. A more rigorous scaling law can be found in [17].

Figure 3-4 shows the distribution of signal attenuation observed at 20.2 and 27.5 GHz at Clarksburg, MD. The data were collected using the beacon signals on the ACTS satellite [20]; elevation angle is 39°. Total path attenuation that include gaseous absorption and other clear-air effects are included in the distributions. Also shown in the figure is the rain rate distribution. It is seen that the annual raining time for the measurement site is around 5%. Annual time percentage for which rain attenuation is present along the observation path is somewhat higher due to the fact that rain attenuation is produced by the presence of rain along the satellite path and the rain rate distribution pertains only to a point measurement near the earth station antenna. Due to the presence of other factors such as cloud attenuation, raining time along the path can not be easily discerned. As shown in the figure, fade depths at 27.5 GHz under moderate elevation angles exceed 20 dB for 0.1% of an average year. Fading becomes worse for low-elevations and/or severe rainfall climates. Figure 3-5 shows the fade distributions at 20 GHz for different rain climates as defined by the ITU-R; elevation angle is 40°. The distributions have been derived using the ITU-R rain attenuation prediction model. Both fade durations and fade rates associated with rain attenuation are found to be distributed in a log-normal fashion; these are discussed in detail in subsection 3.8 on fade dynamics.

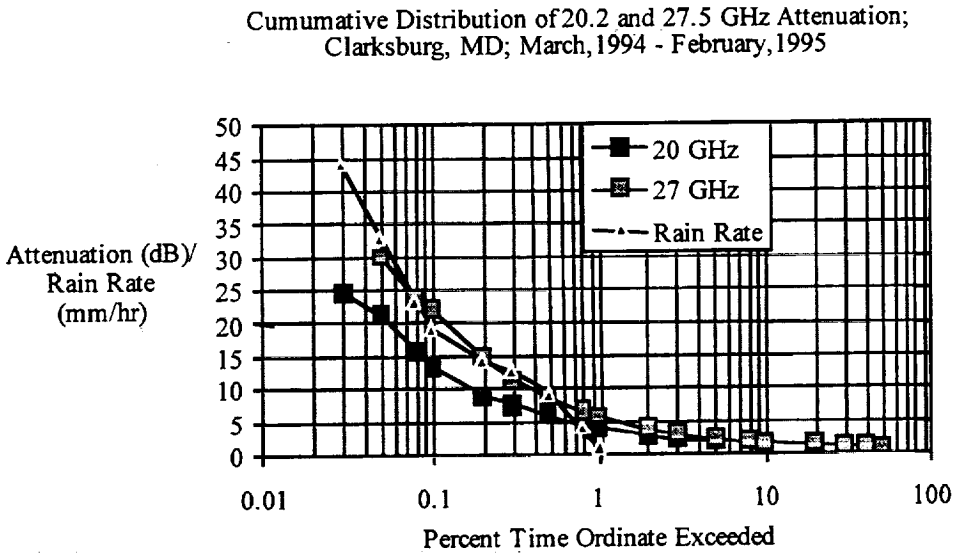

Figure 3-4. Attenuation and Rain Rate Cumulative Distributions for Clarksburg, Maryland. Elevation angle 39°

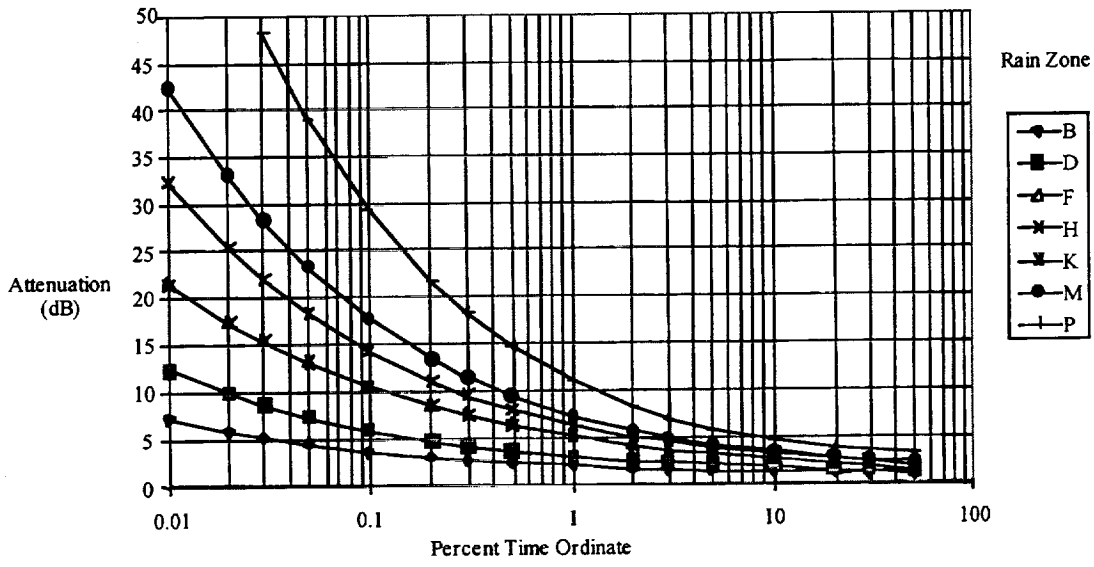

Figure 3-5. Rain Attenuation Distribution at 20 GHz for Different Rain Climates; Elevation Angle 40°

3.4 MELTING LAYER ATTENUATION

The melting layer is the region around the 0°C isotherm where snow and ice particles from aloft melt to form rain. The presence of a well defined melting layer or radar bright band is mainly associated with precipitation from stratiform clouds and for low rain rates. The width of the layer is of the order of 500 m. Specific attenuation in the melting layer, however, is expected to be higher than that in the rain below. Therefore, under light rain conditions, melting layer attenuation may become a significant factor in the total path attenuation; typically, fade levels up to about 3 dB can be expected at 30 GHz [21]. Fade rates are similar to those produced by rain under low fade conditions.

3.5 TROPOSPHERIC SCINTILLATIONS

Tropospheric scintillations are amplitude fluctuations produced by refractive inhomogenieties present in the lower part of the troposphere. Scintillation can occur with or without fading on the path; the former is known as dry scintillations and the latter as wet scintillations since it is accompanied by rain on the path. The magnitude of scintillation increases with the increase of frequency, decrease of elevation angle, and decrease of the antenna diameter. Figure 3-6 shows statistical distribution of amplitude scintillation fading at 20 GHz for several elevation angles [17]; a 1.2 m diameter antenna, 80% relative humidity, and 20° C surface temperature are assumed. Figure 3-7 shows the corresponding distributions at 30 GHz. Signal enhancements due to scintillations follow similar statistics albeit somewhat smaller in magnitude. The frequency scaling of scintillation approximately follows the relationship [17]:

$$\frac{A_1}{A_2} = \left(\frac{f_1}{f_2}\right)^{\frac{7}{12}} \tag{3-2}$$

where A_1 and A_2 are attenuation or enhancement (dB) at frequencies f_1 and f_2, respectively. Frequency spectrum of scintillations are limited to a maximum frequency of around 2 Hz. Associated fade rates are a function of the peak-to-peak scintillation magnitude and the frequency content. Under severe scintillation conditions fade rates of several dB/s can be expected.

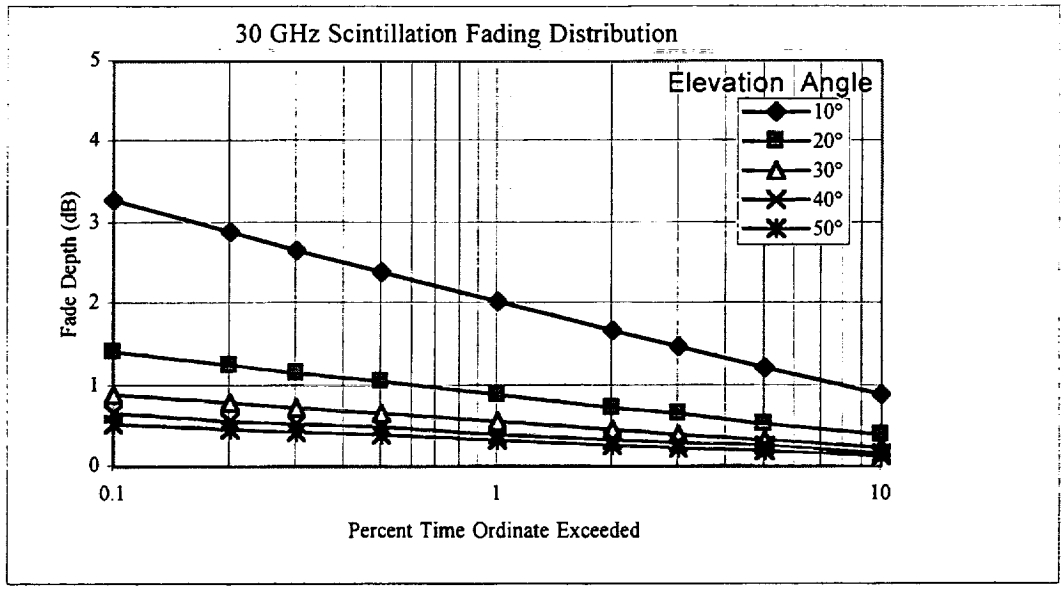

Figure 3-6. Cumulative Distribution of Scintillation Fading at 20 GHz

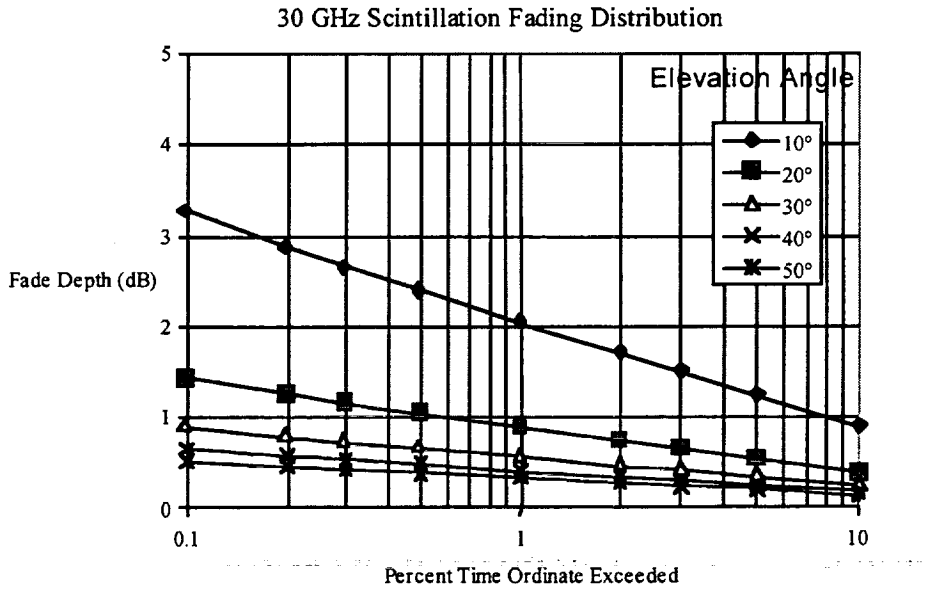

Figure 3-7. Cumulative Distribution of Scintillation Fading at 30 GHz

3.6 RAIN AND ICE DEPOLARIZATION

Satellite systems employing frequency re-use by means of orthogonal polarization may suffer from interference through coupling between wanted and unwanted polarization states. Such coupling arises from antenna imperfections and atmospheric depolarization caused by precipitation particles. Non-spherical particles such as spheroidal rain drops and needle or plate like ice particles can produce coupling between orthogonal polarization states. Depolarization is a function of the polarization state, elevation angle, and the frequency. In the case of linear polarization, depolarization increases with the polarization tilt angle with respect to the local horizontal, and reaches a maximum when the tilt angle is 45°. Depolarization for a circularly polarized signal is same as that for a linearly polarized signal having a 45° tilt angle. At Ka-band frequencies rain depolarization becomes significant only at fade levels in excess of about 10 dB. On the other hand ice depolarization may be experienced without significant fading along the link.

Rain and ice depolarization may be predicted using empirical techniques such as the one recommended by the ITU [17]. Figure 3-8 shows the distribution of the cross-polar discrimination (XPD) at 20 and 30 GHz due to atmospheric precipitation particles; the XPD is defined as:

$$XPD = 10\log\left(\frac{\textit{signal power in the wanted polarization}}{\textit{signal power in the unwanted polarization}}\right) \qquad (3\text{-}3)$$

The figure pertains to an elevation angle of 40°, circular polarization, and a rain climate typical of a US mid-Atlantic location. A comparison of rain attenuation levels shown in Figure 3-4 with depolarization levels in Figure 3-8, it may be surmised that for availability time greater than about 99% depolarization is of secondary importance compared to fading. However, when fade compensation is applied through power control the interference caused by depolarization increases proportionately to the amount of power control applied, and due care must be taken to avoid excessive interference.

3.7 COMBINED EFFECT OF PROPAGATION FACTORS

The preceding subsections outlined the individual propagation impairments affecting Ka-band satellite links. In general, most of these impairments can occur simultaneously. This is illustrated in Figure 3-9 where the time series of a fade event recorded at Clarksburg, MD, using the ACTS beacon signals are shown. In Figure 3-10 power spectrum of the time series at the two frequencies are shown, and Figure 3-11 shows the ratio of the spectral components at the two frequencies (ratio of logarithmic value of spectral components). It is seen that different propagation factors can be easily identified through the spectral ratio. The lowest frequency components of the spectral ratio are identified with the gaseous

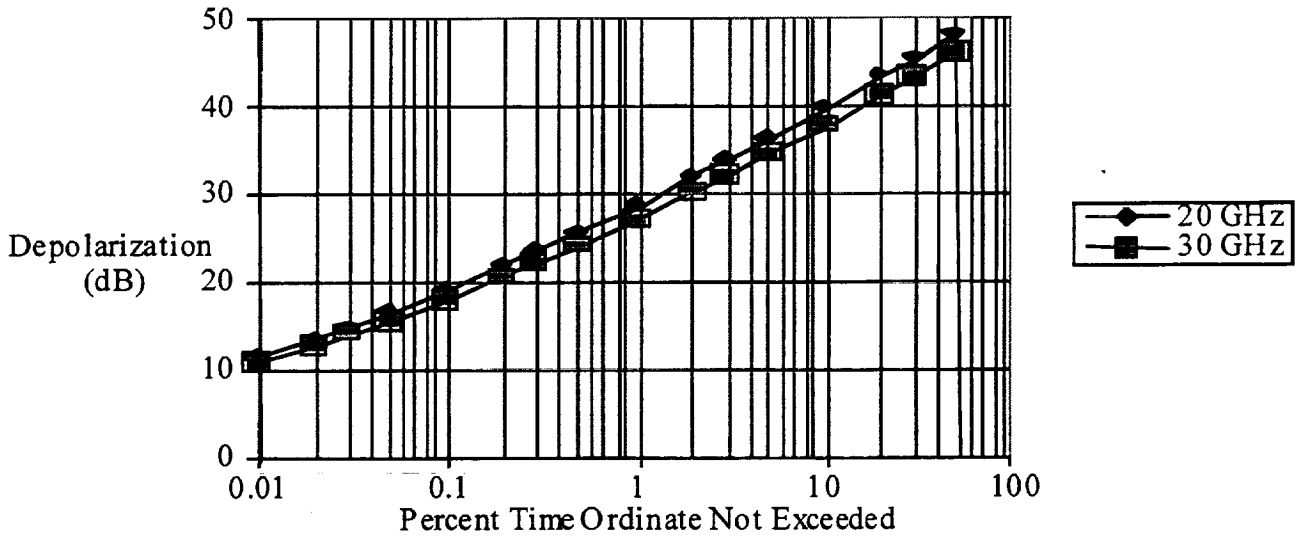

Figure 3-8. Distribution of XPD at 20 and 30 GHz

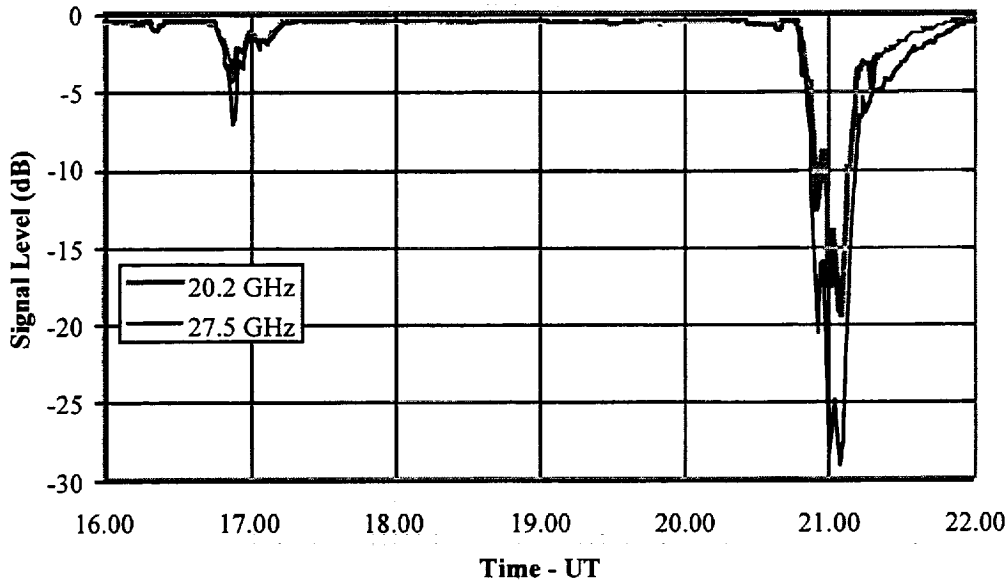

Figure 3-9. Rain event observed at Clarksburg. Signal attenuation on 20.2 and 27.5 GHz ACTS beacon signals are shown; elevation angle 39°

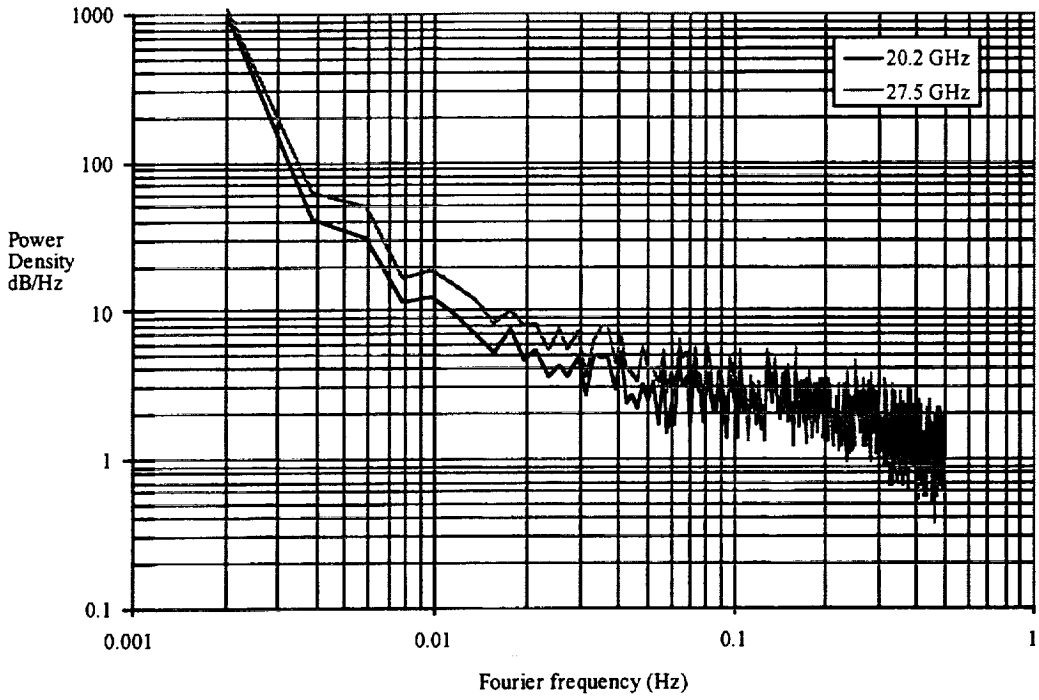

Figure 3-10. Power Spectra of the Fading Event Depicted in Figure 3-9

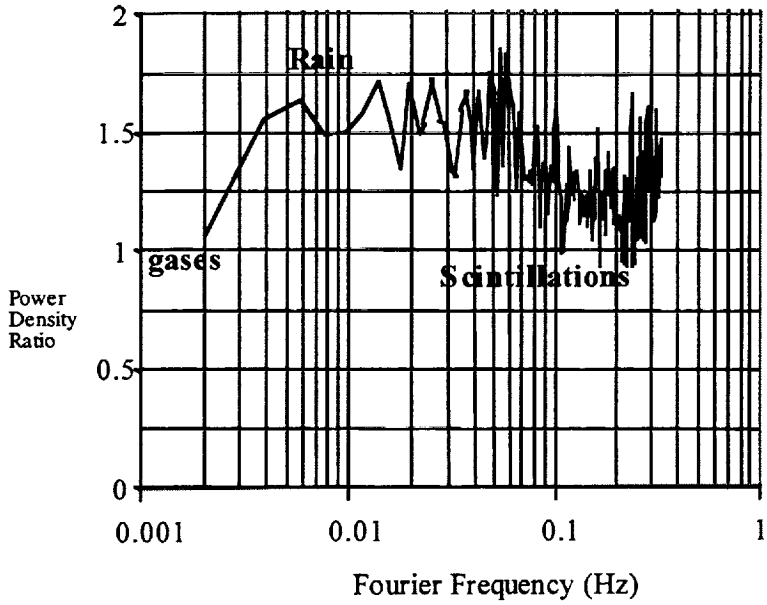

Figure 3-11. Ratio of Spectral Components at 27.5 and 20.2 GHz

absorption; mid frequencies are associated with clouds and rain attenuation, and higher frequencies are produced by scintillation activity. As such, frequency domain separation of propagation factors can be gainfully employed when implementing fade mitigation techniques.

3.8 FADE DYNAMICS

Dynamics of fade events are of importance in the design and implementation of fade mitigation techniques employing power control, diversity, coding, and resource sharing. In addition, they need to be considered when specifying performance objectives of digital networks employing satellite links. Fade duration, or the time interval during which the signal attenuation exceeds a given threshold, intervals between fade episodes, intervals between fade events, and the rate of change of attenuation are the most important dynamic features relevant to system modeling.

Within a precipitation event, the fade level varies considerably, crossing a given fade threshold several times over a relatively short time interval; precipitation events themselves are separated by a longer time span as illustrated in Figure 3-12. A precipitation event starts when the fade level exceeds a given threshold and ends when the fade level falls below the threshold and is followed by a long gap during which the fade level is closer to the clear-air value.

Within the event, there may be several short duration peaks separated by several short gaps. The peaks are called fade episodes and the gaps are known as inter-episode gaps or inter-fade intervals. The relatively longer time interval between fade events is the inter-event interval. Tropospheric scintillations often accompany precipitation events, and the

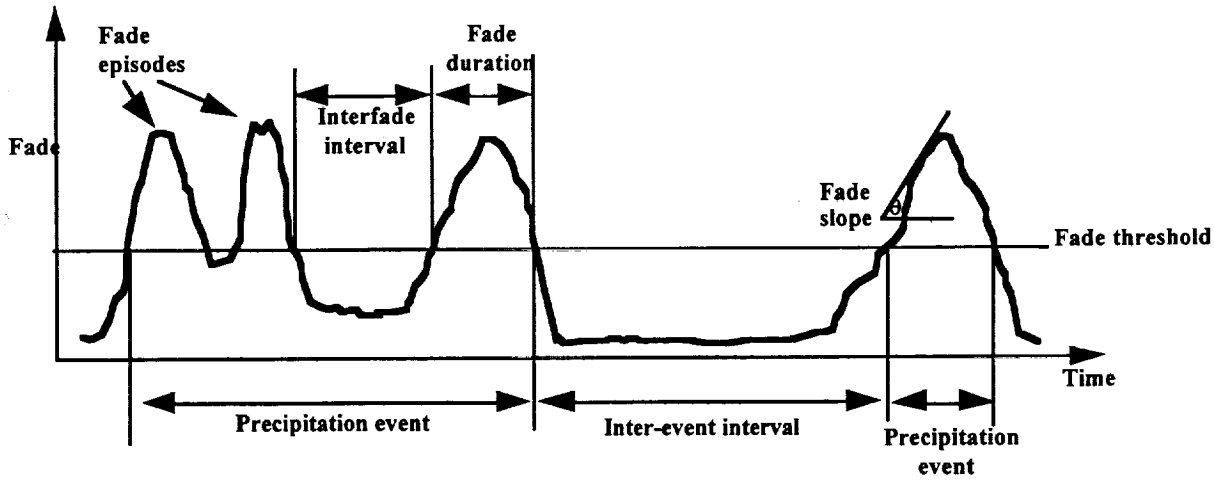

Figure 3-12. Features Commonly Used in Characterizing Precipitation Events

above features need to be characterized both in the presence and absence of scintillations. Scintillations are relatively fast variations in the signal amplitude and these can be separated from slower variations produced by precipitation particles using a low-pass filter. Filter time constants of the order of 20 to 60 seconds appear to be adequate for the purpose [20].

3.8.1 Fade Duration

In general, fade duration is a function of frequency, elevation angle, and the rain type. At a given fade threshold the fade duration will increase with an increase of frequency and a decrease of the elevation angle. Experimental evidence show that these dependencies approximately follow the rain attenuation dependence on frequency and elevation angle [23]. Thus, the frequency dependence of fade duration at a fixed elevation angle is approximately given by:

$$\frac{\text{total number of fades with A } > \text{ x dB at f1}}{\text{total number of fades with A } > \text{ x dB at f2}} \approx \left(\frac{f1}{f2}\right)^2 \tag{3-4}$$

where A is the fade depth (dB) and x is the threshold (dB) at which the fades are counted and f is frequency. A more rigorous frequency scaling law may be found in [17]. The elevation angle dependence at a fixed frequency may be approximated by:

$$\frac{\text{total number of fades } > \text{ A dB at } \theta_1}{\text{total number of fades } > \text{ A dB at } \theta_2} \approx \frac{\sin\theta_2}{\sin\theta_1} \tag{3-5}$$

where θ is the elevation angle.

The elevation angle dependence shown above is expected to hold only for moderate to high elevations where fading is produced by individual rain cells. At low elevation angles more than one rain cell often contributes to the fading process, thus leading to a more complex elevation angle dependence.

The role of the rain type in influencing fade duration stems directly from the average dwell time of rain structures. Wide spread rains tend to have longer dwell times compared to thunderstorm rains.

The average duration of fades exceeding a given threshold appears to be independent of the threshold level. This is due to the fact that the number of fades increase with the decrease of the fade threshold without any discernible relationship between the two parameters. The larger time percentage for which a lower fade threshold is exceeded is distributed among a larger number of fades, and the lower time percentage at a higher fade

threshold is distributed among a smaller number of fades. An example of average fade duration is given in Figure 3-13. An average fade duration of approximately 2 min. for most fade thresholds is evidenced in Figure 3-13 [20]. This seems to be typical for most paths and climates with the exception of those regions that are subject to extremely severe and widespread events such as typhoons. The spread of fade duration around the average value increases with the decrease of the fade threshold. As an example, it is common to observe fades lasting more than an hour at a threshold of 3 dB; on the other hand, a fade of 20 dB is less likely to last more than two or three times the average value. This is illustrated in the fade duration statistics shown in Figure 3-14 and 3-15 for 20.2 GHz and 27.5 GHz, respectively.

The measured data indicate the duration of fades exceeding a given threshold to have a log-normal distribution for longer duration fades composed mainly of rain induced fades. Shorter duration fades, produced largely by tropospheric scintillations, can be represented by a power-law distribution [24].

3.8.2 Inter-Fade and Inter-Event Intervals

Information on interfered intervals is important in applications such as diversity switching in which excessive switch occurrences can have a detrimental effect on system performance. Inter-event intervals, which pertain to the return period of precipitation events, are of importance in network management and reallocation of resources on a larger scale.

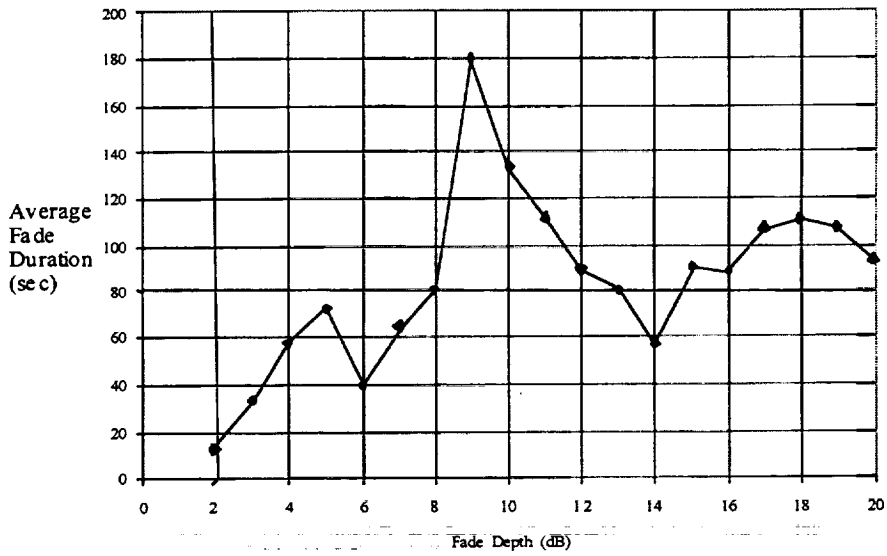

Figure 3-13. Average Fade Duration at 20.2 GHz

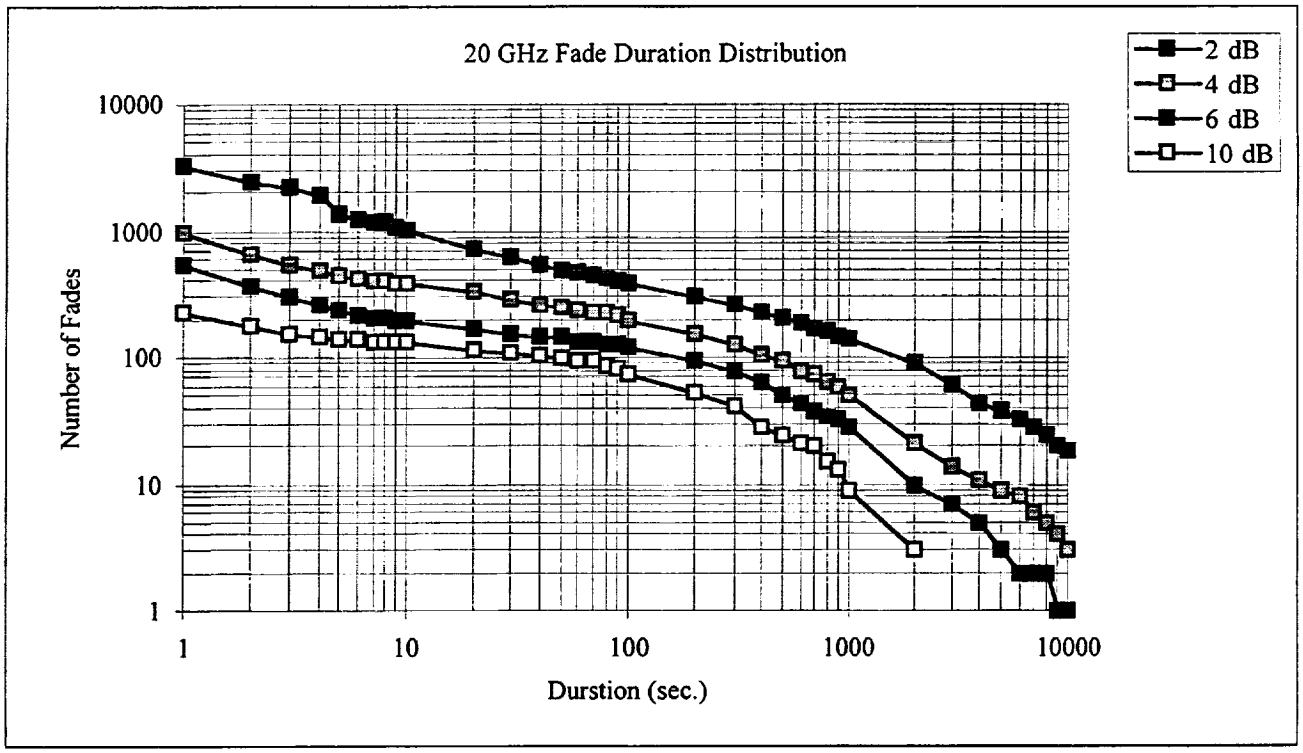

Figure 3-14. Fade Duration Distribution at 20.2 GHz

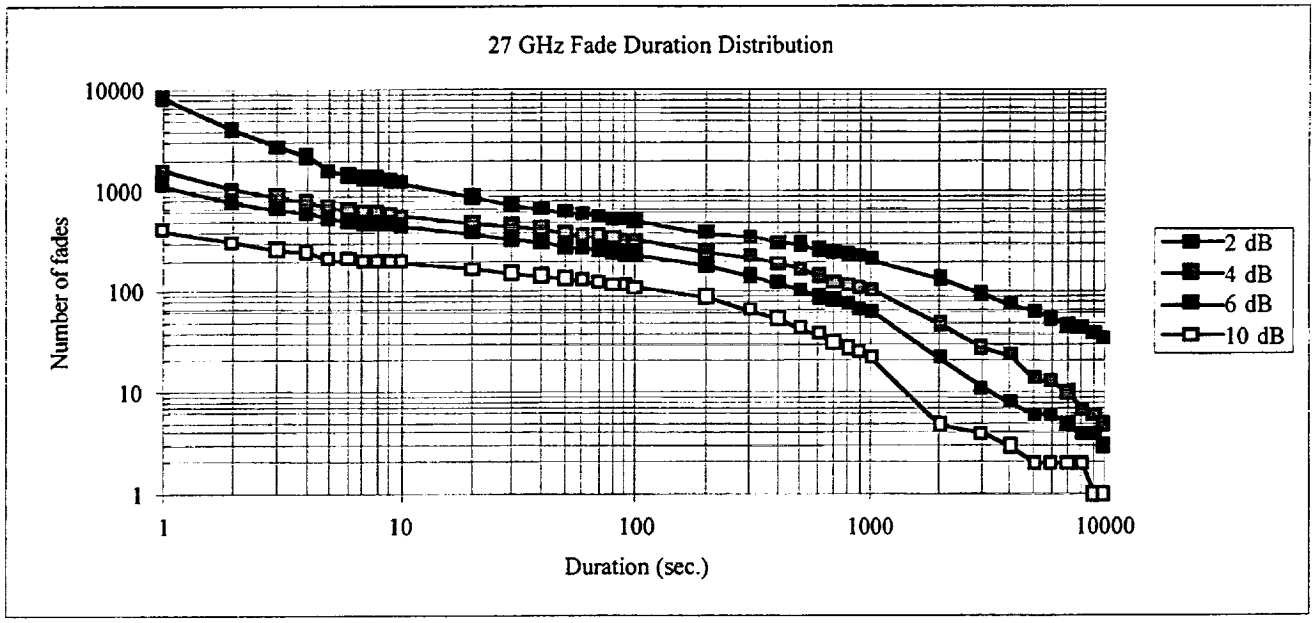

Figure 3-15. Fade Duration Distribution at 27.5 GHz

In general, rain induced inter-fade intervals and inter-event intervals are log-normally distributed [24]. Short duration inter-fade intervals resulting from tropospheric scintillations, however, are expected to follow a power-law form as found with the short-term fade duration. Figures 3-16 and 3-17 show inter-fade interval distributions derived from data collected using the ACTS beacon signals at 20.2 and 27.5 GHz; elevation angle is 40°. It can be seen that the slope of the distribution changes with the fade depth. Higher fade thresholds are characterized by longer intervals compared to those at lower fade thresholds.

Frequency and elevation angle scaling of inter-fade intervals may be attempted using the relationships given under fade duration.

3.8.3 Rate of Change of Attenuation

In a manner similar to rain fade duration statistics, the distribution of the rate of change of attenuation appears to be log-normal with a median of about 0.1 dB/s. Little difference has been observed between the positive-going (fading) and negative-going (recovering) slopes of the rate of change of attenuation for integration times of 10 s or more. In most experiments reported to date, the average fade slope does not appear to depend significantly on the fade level, with a maximum fade rate of about 1 dB/s being reported for integration time constants of the order of 10 s. Much higher fading rates are observed with integration times below 10 s and these are associated with scintillation activity.

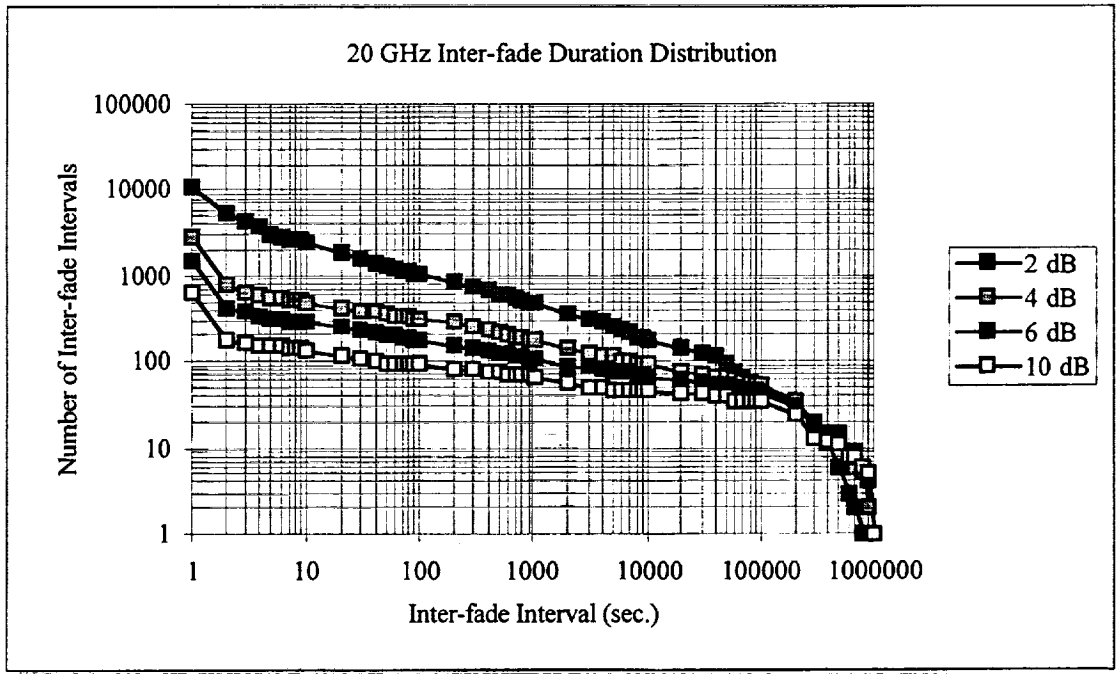

Figure 3-16. Inter Fade Interval Distribution at 20.2 GHz

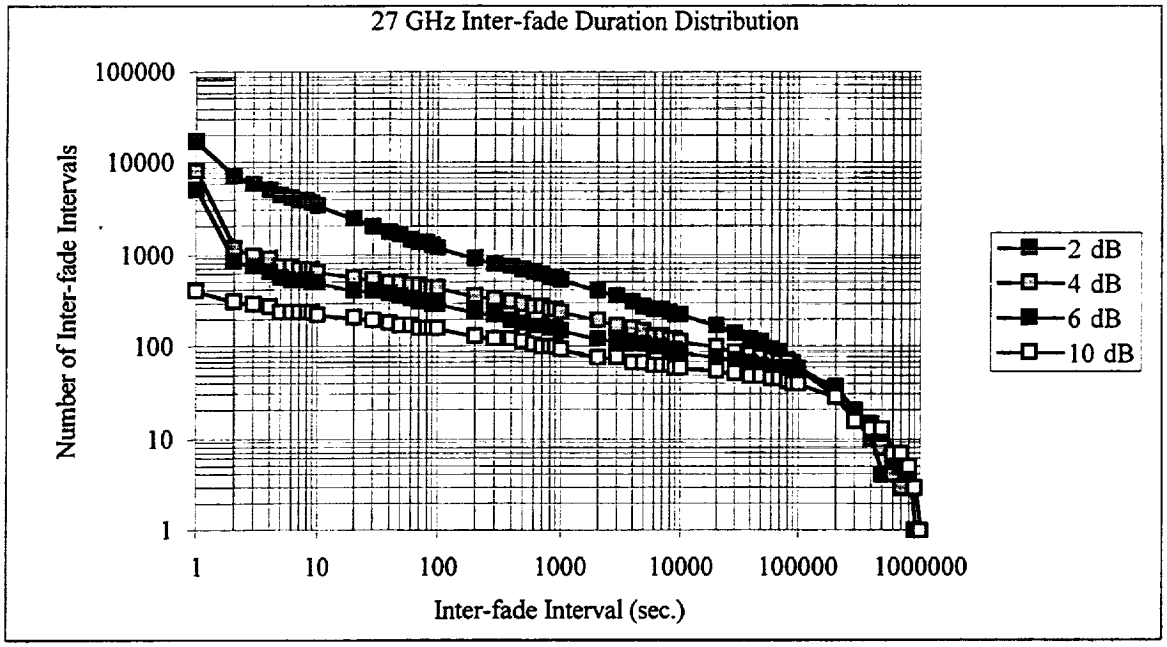

Figure 3-17. Inter Fade Interval Distribution at 27.5 GHz

Figures 3-18 and 3-19 show the cumulative distribution of fade slopes at 20.2 and 27.5 GHz for different fade thresholds. It is evident that the fade slope distributions are not sensitive to the fade threshold. Figure 3-20 shows a histogram of fade slopes at 20.2 GHz illustrating the symmetrical behavior of positive and negative going slopes.

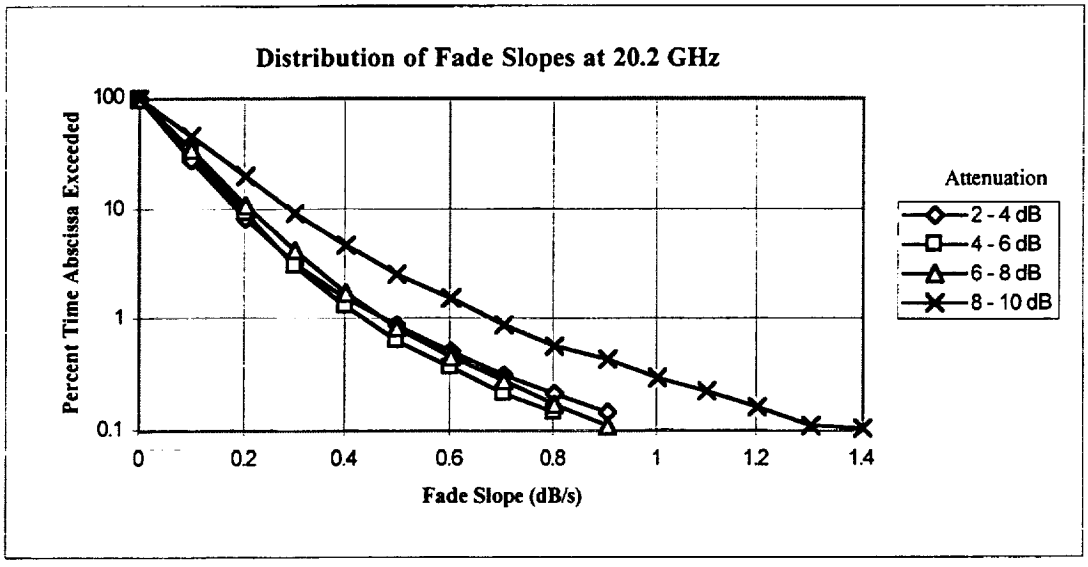

Figure 3-18. Cumulative Distribution of Fade Slopes at 20.2 GHz

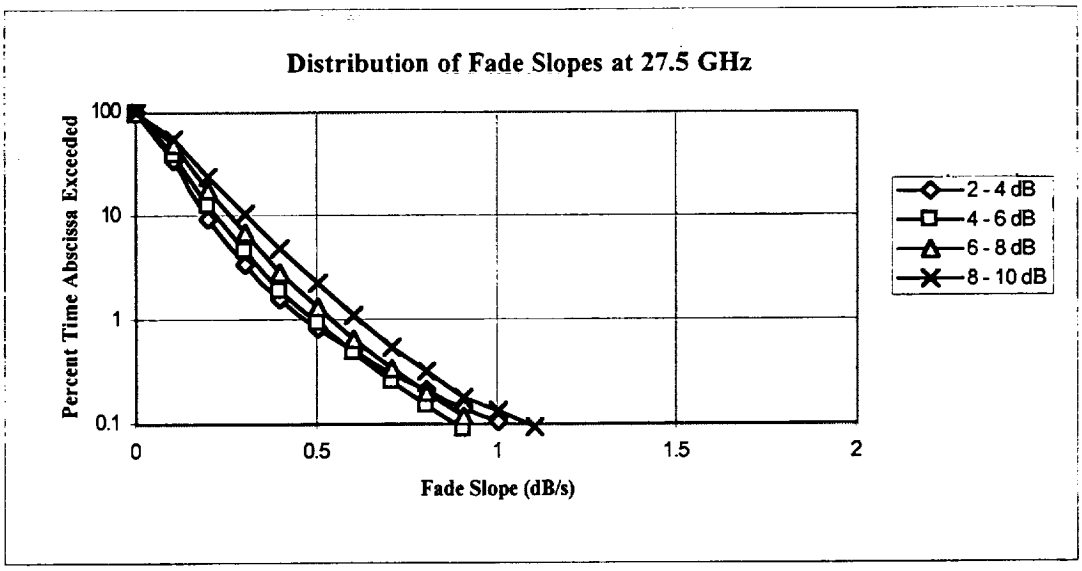

Figure 3-19. Cumulative Distribution of Fade Slopes at 27.5 Ghz

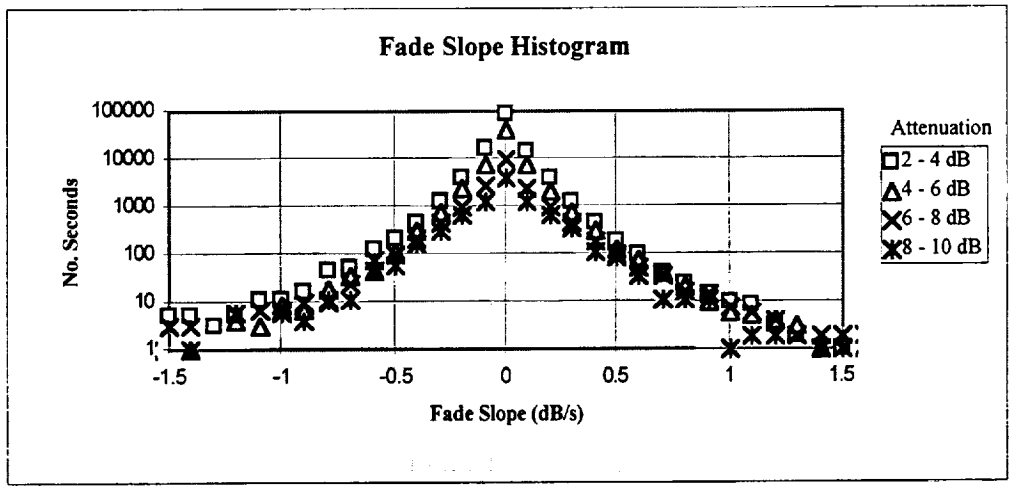

Figure 3-20. Fade Slope Histograms at 20.2 GHz

3.9 RAIN FALL CORRELATION OVER LARGE AREAS

Rain fade compensation implemented on the basis of shared resources must be designed with an understanding of the simultaneity of rain fading across the satellite coverage area. Although detailed information on simultaneous rain fading on multiple satellite links across a large area is not easily modeled, rainfall patterns over extended areas can be studied to gain sufficient knowledge to size additional resources required for fade compensation.

Meteorological data on hourly precipitation from several thousand stations scattered throughout the continental USA were analyzed to derive rain fall correlation over extended areas. Figures 3-21, 3-22, and 3-23 show the joint probability of rain for three cities: Cleveland, OH, Los Angeles, CA, and Washington, DC.

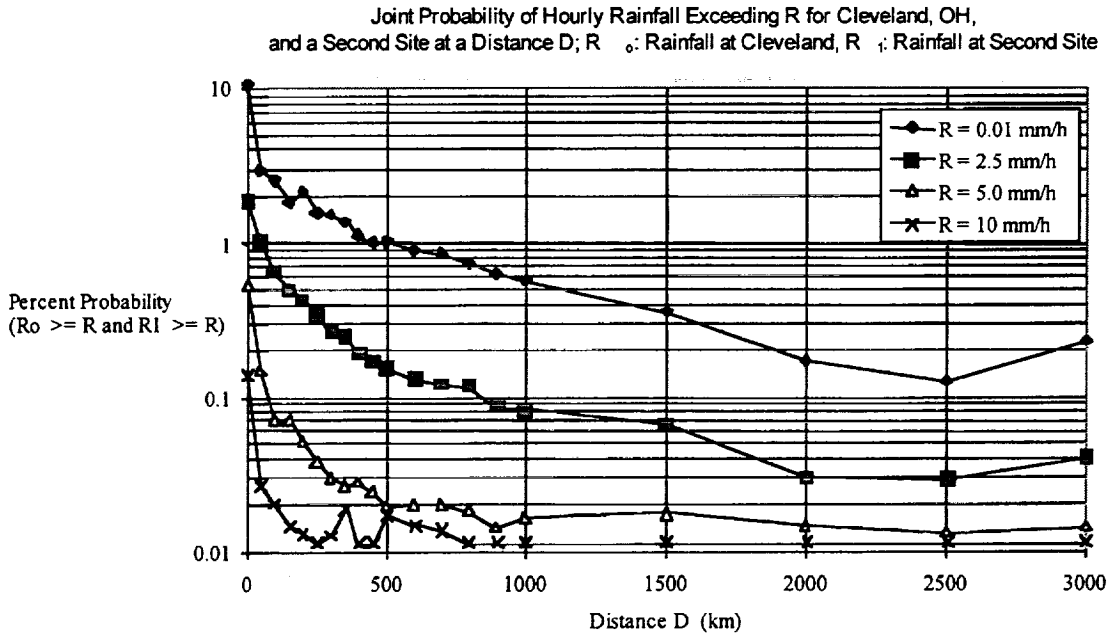

Figure 3-21. Joint Probability of Rainfall Exceeding Specified Threshold as a Function of Site Separation for Cleveland, OH

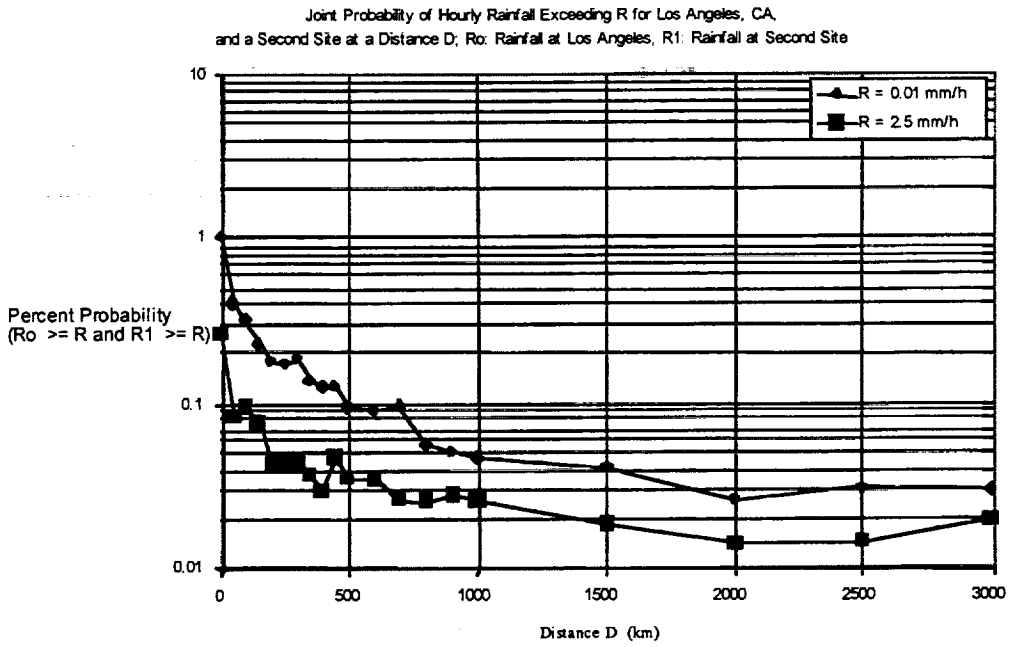

Figure 3-22. Joint Probability of Rainfall Exceeding Specified Threshold as a Function of Site Separation for Los Angeles, CA

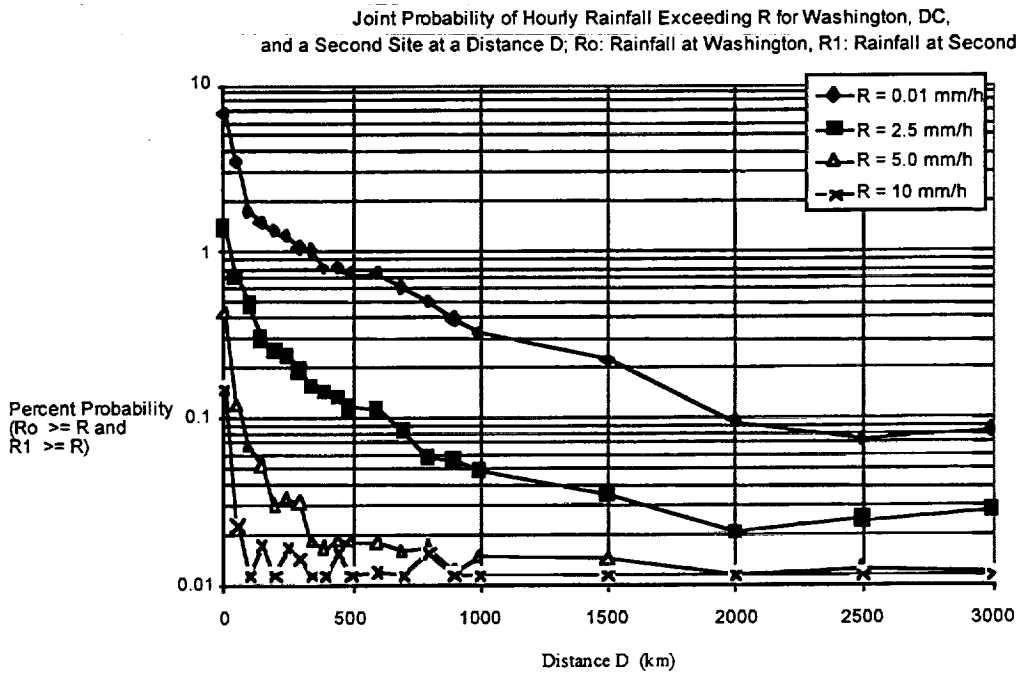

Figure 3-23. Joint Probability of Rainfall Exceeding Specified Threshold as a Function of Site Separation for Washington, DC

3.10 ANTENNA WETTING

In addition to rain fading, wetting of the antenna reflector surface and the antenna feed window can produce additional signal attenuation [25]. Signal attenuation can be especially severe at Ka-band frequencies. Antenna wetting effect can be modeled using geometrical optics techniques [26]. Figure 3-24 shows the signal attenuation at 20 GHz due to antenna reflector wetting as a function of the rain rate for an elevation angle of 40° and 80°. A reflector diameter of 1.8 m and a smooth reflector surface are assumed in the calculation. Signal attenuation at 20 GHz due to feed wetting is shown in Figure 3-25. Figures 3-26 and 3-27 show results for 30 GHz. It is seen that attenuation due to feed wetting is significantly higher than that due to reflector wetting. However, application of a hydrophobic coating on the feed window can significantly reduce the signal loss. On the other hand significant levels of attenuation may be encountered for reflector wetting when the reflector surface is not smooth as demonstrated by the ACTS propagation measurements. Fade mitigation techniques must account for the antenna wetting effects. The antenna wetting contribution can be considered an error term when measuring the fade on the satellite link.

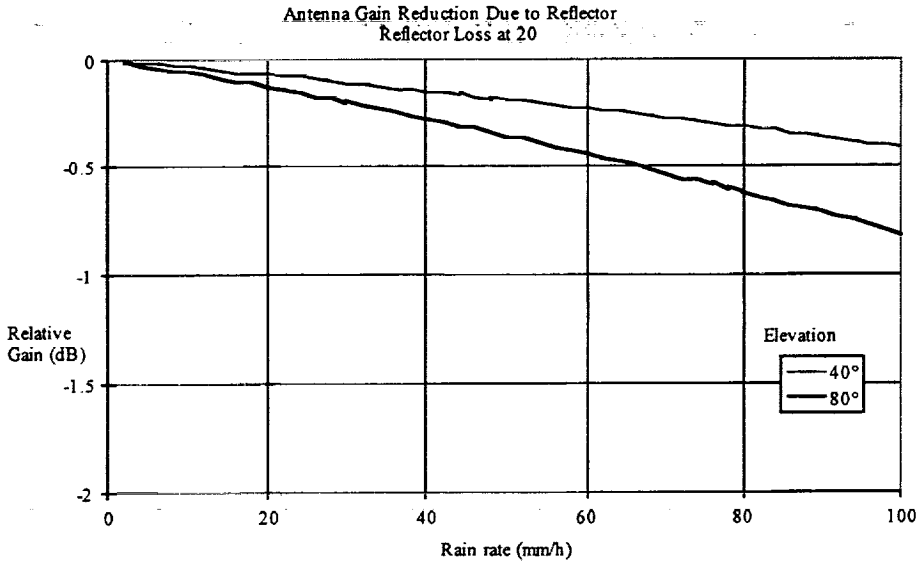

Figure 3-24. Antenna Reflector Wetting Loss at 20 GHz

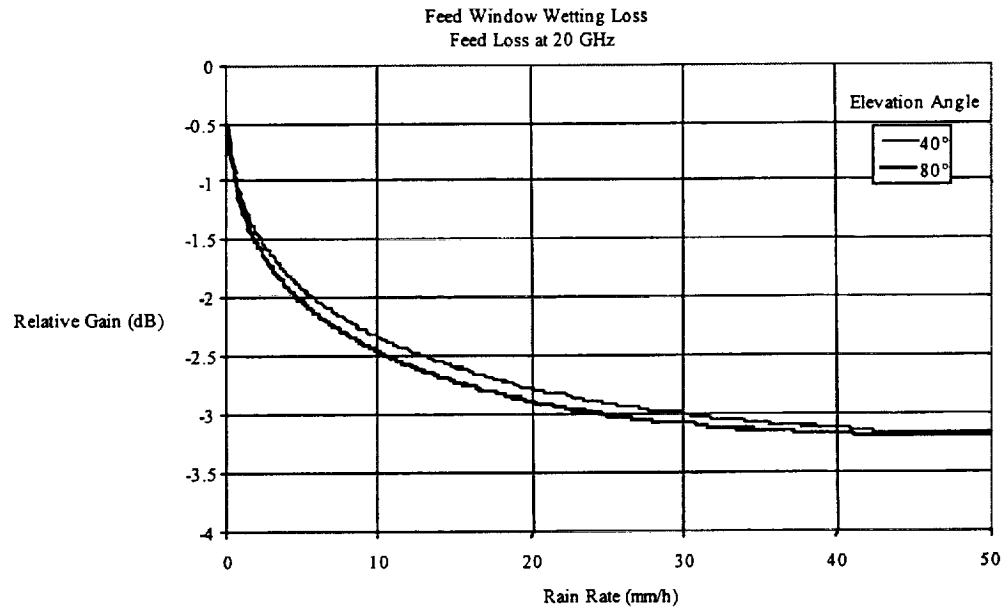

Figure 3-25. Antenna Feed Wetting Loss at 20 GHz

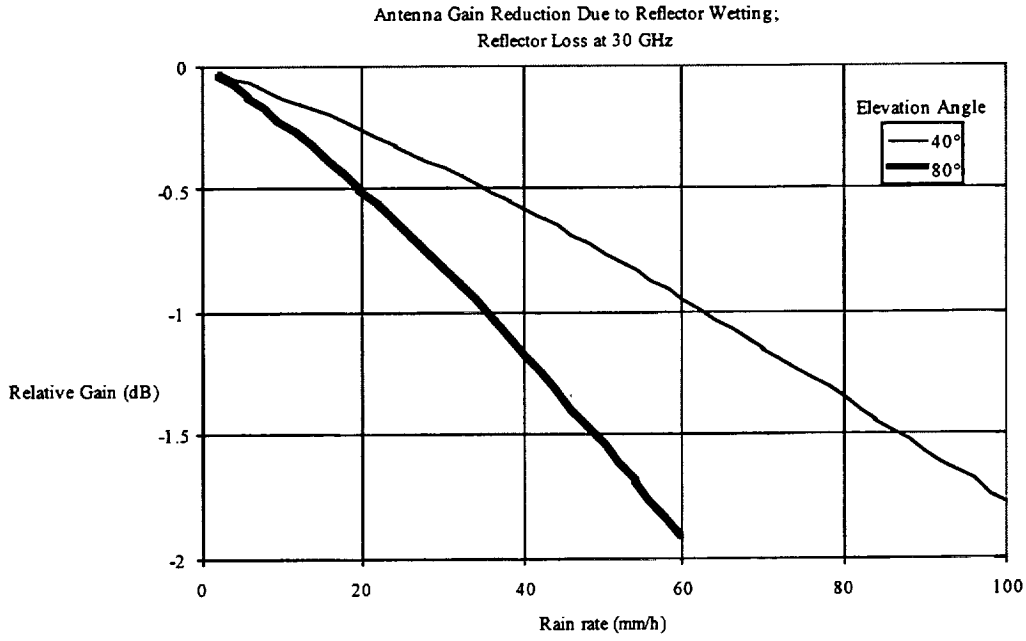

Figure 3-26. Antenna Reflector Wetting Loss at 30 GHz

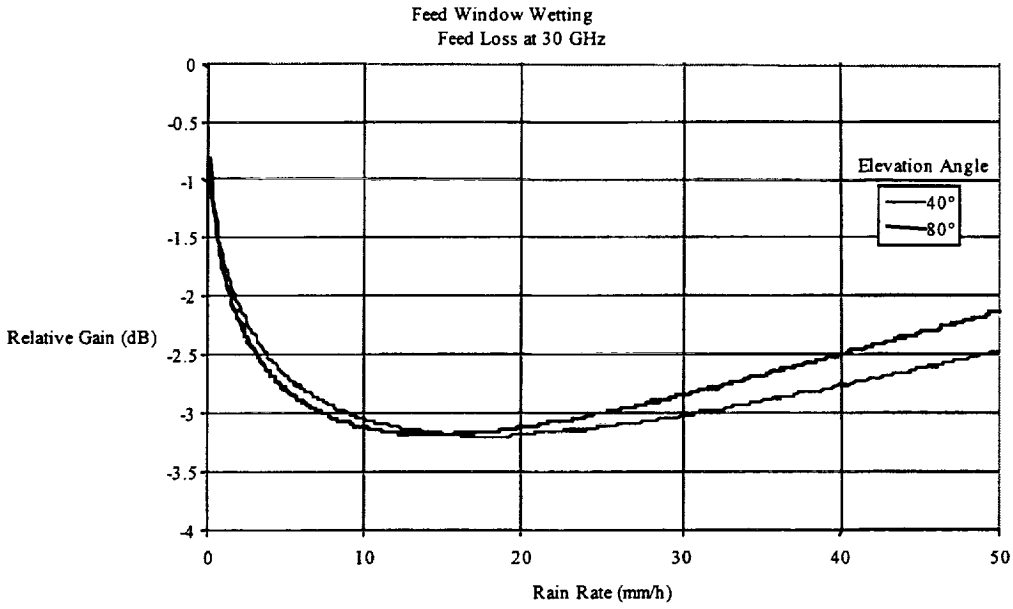

Figure 3-27. Antenna Feed Wetting Loss at 30 GHz

SECTION 4 — RAIN FADE MEASUREMENT TECHNIQUES

Rain fading is a degradation in the power of a signal received at an earth terminal caused by rain in the propagation path. Fading is typically expressed as a degradation in the received carrier in decibels. Fading and the accompanying noise temperature increase caused by rain in the propagation path combine to produce an effective fade, or downlink degradation. Downlink degradation is an indication of the signal power increase required to overcome the effects of excess propagation losses and maintain a given link quality.

Since this study is concerned with a comparative evaluation of rain fade measurement and compensation techniques for two distinct satellite architectures, bent pipe and regenerative with baseband switching, fade measurement techniques will be evaluated with respect to their ability to measure fades at earth terminals caused by rain in the downlink path. Comparison of fade measurement techniques applied to the measurement of fading caused by rain on the downlink allows comparisons to be applied to either architecture. Bent pipe satellite architectures enable the measurement of fades at earth terminals caused by rain in the uplink path while the regenerative transponder masks uplink impairments from the remote earth terminals. Also, regenerative satellites can measure uplink fading on-board the satellite while such techniques are usually not employed on bent-pipe satellites.

Six fade measurement techniques have been evaluated during phase two of this study. Criteria for comparative evaluation of these six fade measurement techniques include fade measurement accuracy, speed of response and implementation cost impact on small terminals. In all cases, accuracy refers to the accuracy of predicting downlink degradation at earth terminals where the fade measurement equipment resides. Uplink degradation can be predicted from downlink degradation measurements performed on a common path. The prediction process involves frequency scaling and the accuracy of uplink compensation, based on scaled downlink fading estimates, is degraded by the accuracy of this scaling process. Frequency scaling accuracy affects all fade measurement techniques equally and is not included in the estimated measurement accuracy. The following sections cover the six fade measurement techniques. The beacon receiver and modem SNR fade measurement procedure are covered in detail while other techniques, which are similar in nature, are covered quickly. Detailed descriptions of the assumptions made in the fade measurement accuracy analysis for each technique can be found in the appendix.

4.1 ESTIMATING FADE FROM BEACON RECEIVER

Most satellites generate beacon signals which are used as carriers for telemetry data and for propagation experiments. Beacon signals are typically transmitted in the downlink band on global coverage horns. Beacon signals can be monitored by the VSAT terminal to estimate the level of fading on its path. The absolute power of the received beacon signal is

compared with a clear-sky reference to determine rain attenuation on the path. A beacon signal is assumed to be available to all terminals and beacon reception is possible without antenna feed or LNB modifications. Beacon signals cannot be assumed to be within the IF band of all terminals though. Terminal equipment must provide beacon receiver circuitry capable of detecting the beacon within the downlink frequency band at the LNB output. This circuitry is not otherwise required and therefore increases the production cost of the VSAT equipment. The beacon receiver circuitry is envisioned to include a synthesizer and down converter to select the beacon signal from the LNB output, a beacon tracking loop and circuitry to measure the strength of the acquired beacon signal. Figure 4-1 shows the basic elements required for beacon signal power monitoring.

The complexity and cost of the beacon receiver is dependent upon the frequency accuracy of the downconverted beacon signal, the frequency accuracy of the reference provided to the beacon receiver and the carrier to noise power density of the beacon signal at the receiver input. The frequency accuracy of the reference and down converted beacon determine the width of the frequency band over which the beacon tracking PLL must search to acquire the beacon signal. If this search bandwidth is less than the capture range of the beacon tracking PLL then a static beacon receiver synthesizer setting will provide adequate performance and beacon receiver cost will be low. If the search bandwidth exceeds the capture range of the PLL then a more sophisticated search algorithm is required. The level of complexity of this algorithm can range from a simple switched filter approach, where the PLL bandwidth is opened up for signal acquisition then narrowed for tracking, to more complex processes which involve making repeated signal power measurements while tuning the synthesizer across the search band and computing the beacon frequency from symmetry calculations. An example of beacon tracking performance for the ACTS downlink beacon received by a 1.2 meter VSAT antenna is provided in section 8.1.1.

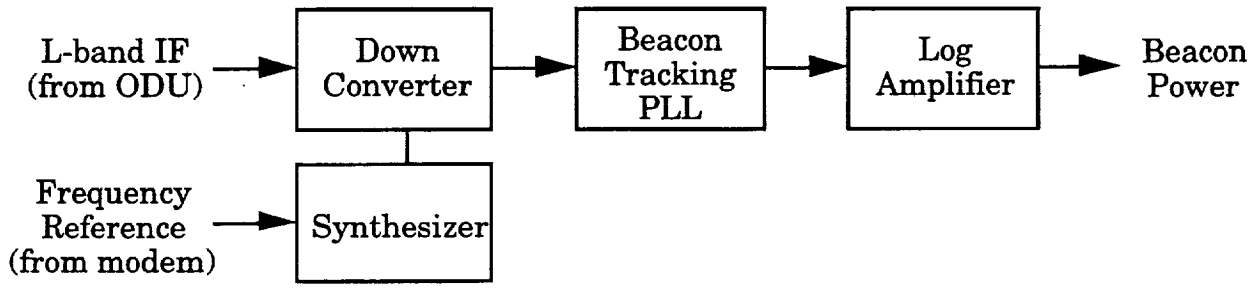

Figure 4-1. Beacon Receiver Block Diagram

Beacon signal power measurements are made on a continuous basis by the beacon receiver. When clear-sky conditions are perceived to exist, beacon power measurements are used to update a database containing average clear-sky beacon power levels. This database contains a moving average clear-sky reference beacon level for the current time-of -day thus enabling the fade estimation algorithm to correct for diurnal variations in received beacon power. When propagation conditions along the path are determined to be degraded by rain attenuation, the clear-sky reference level for the current time of day is divided by the received beacon power level to generate the rain attenuation estimate. A downlink degradation estimate is determined from the rain attenuation measurement by a look-up table which assumes a constant system noise and rain media temperatures.

4.1.1 Accuracy – Beacon Receiver

The accuracy of fade estimates generated from beacon signal power measurements is dependent upon the correlation between rain attenuation and received beacon power, beacon power measurement accuracy and the effectiveness of the algorithm used to estimate degradation from beacon power readings. Since received beacon power is the product of all gain and loss terms in the spacecraft to ground path, variation in any term will directly affect beacon power level. Table 4-1 shows the sources of fade measurement error and the residual error which contributes to fade measurement accuracy after time of day and baseline corrections.

Beacon power readings are an indication of the rain attenuation or fading on the downlink path. For direct comparison with other fade measurement techniques, the fade measurement result is used to generate a degradation estimate or effective fade. The degradation, D, is calculated from the rain attenuation, A, the system noise temperature under clear-sky conditions, T_S, and the rain temperature, T_m.

$$D \cong A + 10 \log\left(\frac{T_s + T_m\left(1 - 10^{-A/10}\right)}{T_s}\right) \tag{4-1}$$

Approximations in the above equation include insignificant feed losses, no gaseous attenuation and constant LNB noise and rain temperature. Errors in the degradation estimate are

$$\partial D = \left(1 + \frac{2.3 T_m 10^{-\frac{A}{10}}}{T_S + T_m\left(1 - 10^{-\frac{A}{10}}\right)}\right)\partial A + \left(\frac{2.3\left(1 - 10^{-\frac{A}{10}}\right)}{T_S + T_m\left(1 - 10^{-\frac{A}{10}}\right)}\right)\partial T_m + \left(\frac{2.3 T_m\left(1 - 10^{-\frac{A}{10}}\right)}{T_S\left(T_S + T_m\left(1 - 10^{-\frac{A}{10}}\right)\right)}\right)\partial T_S \tag{4-2}$$

Table 4-1. Beacon Power Measurement Fade Estimate Accuracy

Term in Link Budget	Maximum Variation, [dB]	Compensation Mechanism	Residual Error, [dB]
Beacon Power	2.00	Beacon source aging is effectively removed by long term averaging of clear sky baseline.	0.01
Satellite pointing loss	±0.0005	Level fluctuations, ΔP, are dependent on satellite orientation errors, $\Delta\theta$, according to $\Delta P = -12(\Delta\theta/\theta_{FWHM})^2$. Beacon is transmitted on conus horn with $\theta_{FWHM} \approx 4°$ and variation 0.025° is most significant mispointing using autotrack.[27]. Hourly quantization of clear sky baseline will remove all but 0.00003dB.	0.00
Path loss	±0.1	Long term averaging of clear sky baseline will reduce any range variation dependency to an insignificant level.	0.00
Scintillation	±1.2[28]	Low pass filtering of power readings will reduce scintillation to $P_o/P_i = (1+\omega^2/\omega_o^2)^{-1}$, $\omega \approx 3\ rad/sec$ for scintillation, $\omega_o \approx 0.5\ rad/sec$ filter corner.	0.04
De-polarization	-0.14 (XPD, degraded to 15 dB)	Depolarization associated with rain events is dominated by absorption. Rain causing a degradation in XPD to 15 dB, and resultant 0.14 dB co-polar attenuation, would be associated with at least a 20 dB fade from absorption at 20 GHz. Depolarization associated with ice crystals will not be accompanied with absorption and will appear to the fade measurement system as a rain event.	0.07
Gaseous absorption	±0.5 [28]	Gaseous absorption is dependent upon relative humidity and air temperature. Both of these parameters will correlate with diurnal compensation of baseline and long term(seasonal) effects will be filtered out by clear-sky baseline averaging. Most significant errors will be caused by drastic weather changes (Δ RH=20%, ΔT = 20°) in a reasonably short time frame. Frequency scaling of error will cause overcompensation during periods of changing gaseous absorption and baseline compensation under compensates for long term changes.	0.3
Cloud Attenuation	-1.2	Dynamics of cloud attenuation are indistinguishable from light rain and frequency scaling is very similar.[28] Since it is desirable to compensate for cloud attenuation, fade measurement system should respond and therefor response is not an error.	0.0
Rain Attenuation	-20	Response to rain attenuation is not an error. When attenuation exceeds dynamic range of beacon receiver, receiver will loose lock and high rain fade should be assumed.	0.0
Earth station antenna pointing error	±0.04	Diurnal variations in the satellite position relative to the earth terminal will be filtered out by diurnal compensation of clear-sky baseline. (see spacecraft orientation above) $\theta_{FWHM} \approx 0.86°,\ \Delta\theta \approx 0.05°$	0.003
Earth station antenna efficiency	-2.0	Feed window wetting is small when compared to rain attenuation at identical rain rates and will be overcompensated when frequency scaled. Two decibel wetting loss at 20 GHz would be scaled to 3.6 dB at 30 GHz while wetting loss for transmit signal should only be 2.7 dB. 0.9 dB is worst case error. Precipitation in the form of snow causes little atmospheric attenuation but a layer of melting snow or ice on the antenna surface can cause gradual deep fades. Heating systems or antenna covers are required in snowy environments.	0.9

Table 4-1. Beacon Power Measurement Fade Estimate Accuracy (Continued)

Term in Link Budget	Maximum Variation, [dB]	Compensation Mechanism	Residual Error, [dB]
LNB gain	5	LNB gain variations with temperature are approximately -0.1 dB/K. Clear-sky baseline will compensate for seasonal changes and diurnal compensation will remove a significant portion of the daily variations. Residual error will be related to worst case day-to-day temperature change at constant time of day. (assume 10°C)	1.0
Beacon receiver accuracy	1.0	Expensive beacon receivers typically have 0.25 dB long term accuracy. Inexpensive circuitry to measure beacon power level should provide 0.75 dB long term accuracy without periodic calibration.	0.75
RSS Error in attenuation		All of the above figures are worst case errors which can be assumed to be equivalent to 2 σ or 95% confidence values.	1.57
Average error		The mean square error, or 1 σ, value is one half of the above result.	0.79
Accuracy of degradation estimate		Look-up table uses fixed clear-sky system noise and rain media temperature and calculates degradation from rain attenuation estimate. (see text)	±1.25 dB

Assumed rain temperature, T_m, is 280±10 K, clear-sky system noise temperature, T_s, is 230±10 K and rain attenuation, A, is 5±0.79 dB. The Beacon Power fade measurement technique accuracy calculations are summarized for the three satellite architectures in the appendix, on pages A-1 through A-3. The overall uncertainty in the downlink degradation estimate is predicted to be ±1.25 dB for all three satellite architectures.

4.1.2 Response Time – Beacon Receiver

Logarithmic amplifiers are available which provide the desired accuracy with response times under 1 millisecond. When the degradation exceeds the beacon receiver margin, the beacon receiver will lose lock. Such an occurrence should be interpreted as a extended fade and the duration of this fade will be prolonged by the beacon receiver acquisition time.

4.1.3 Implementation – Beacon Receiver

The beacon receiver fade measurement technique is unique in that implementation is independent of the satellite architecture. The elements included in the blocks shown in Figure 4-1 are required to measure beacon power and must exist in addition to, and derive power from, the indoor unit motherboard. Many of the components including the synthesizer and receiver PLL integrated circuits are available at low cost. Table 4-2 shows a preliminary estimate of the parts cost for a simple analog beacon receiver with L-band input.

Table 4-2. Low Cost Beacon Receiver Parts Cost

Description	Manufacturer	Part Number	Unit Cost (Q=1000)
L-band synthesizer PLL	Motorola	MC145201	$3.40
L-band mixer	TriQuint	TQ9172N	$4.14
L-band VCO	Motorola	MC12149	$3.03
IF synthesizer PLL	Motorola	MC145170	$2.05
Miscellaneous discrete	Various	Various	$5.00
		Total	≅ $17

The beacon receiver must be tested in production and therefore will have a slight cost impact on the modem arising from increased testing time and the reduction of production yields. This cost impact, based on a failure rate of 10^{-2} and a unit cost of $2K is $20 per unit. Development costs are estimated to be $120K for the beacon receiver. This cost, spread over one thousand units will dominate the modem cost impact unless production quantities are much higher. This fade estimation technique is expected to have a cost impact of approximately $157 on units produced in quantities of one thousand.

4.2 ESTIMATING FADE FROM MODEM AGC VOLTAGE

Most earth terminal demodulators have variable gain amplifiers which are controlled to provide constant carrier plus noise (C+N) power at the input to the modem analog to digital converter. Downlink fading can be estimated from the control voltage of these automatic gain control (AGC) circuits. This fade measurement technique is similar to the beacon receiver in that it measures the absolute level of a signal and degradation is calculated from the measured fade. Fade measurement circuitry samples the modem AGC voltage at regular intervals and maintains a record of these samples. A fade estimation algorithm tracks the recent history of AGC voltage measurements and compares them to the clear-sky baseline for the current time-of-day. The algorithm determines whether significant fading is being experienced on the downlink path and may factor the current reading into the clear-sky baseline to follow seasonal variations. The fade estimation algorithm also estimates the fading from the current AGC voltage reading. This fade estimate is used to predict the downlink degradation from an assumed system noise and rain temperature via the same process as described in section 4.1.1 for the beacon receiver fade measurement technique.

4.2.1 Accuracy – Modem AGC Voltage

The accuracy of degradation estimates based upon modem AGC voltages are dependent on the satellite architecture and satellite performance as well as the AGC voltage measurement and fade estimation process. The received C+N power level accuracy calculations are summarized in Appendix A, on pages A-4 through A-6, for each satellite architecture. A backed-off bent pipe satellite will exhibit uplink power variations which, when combined

with satellite gain variations and downlink variations similar to the beacon power measurement, will affect the downlink carrier power. The combined effect of these uncertainties is a 1.14 dB uncertainty in the received carrier power. A saturated transponder and the on-board processing satellite will limit these variations and provide improved uncertainty of 0.66 dB and 0.65 dB respectively for the received carrier power. For satellite links operating with concatenated coding and with clear-sky link margins of 4 dB, the relationship between C+N power and fading can be approximated by Equation (4-3) which is shown in Figure 4-2 below.

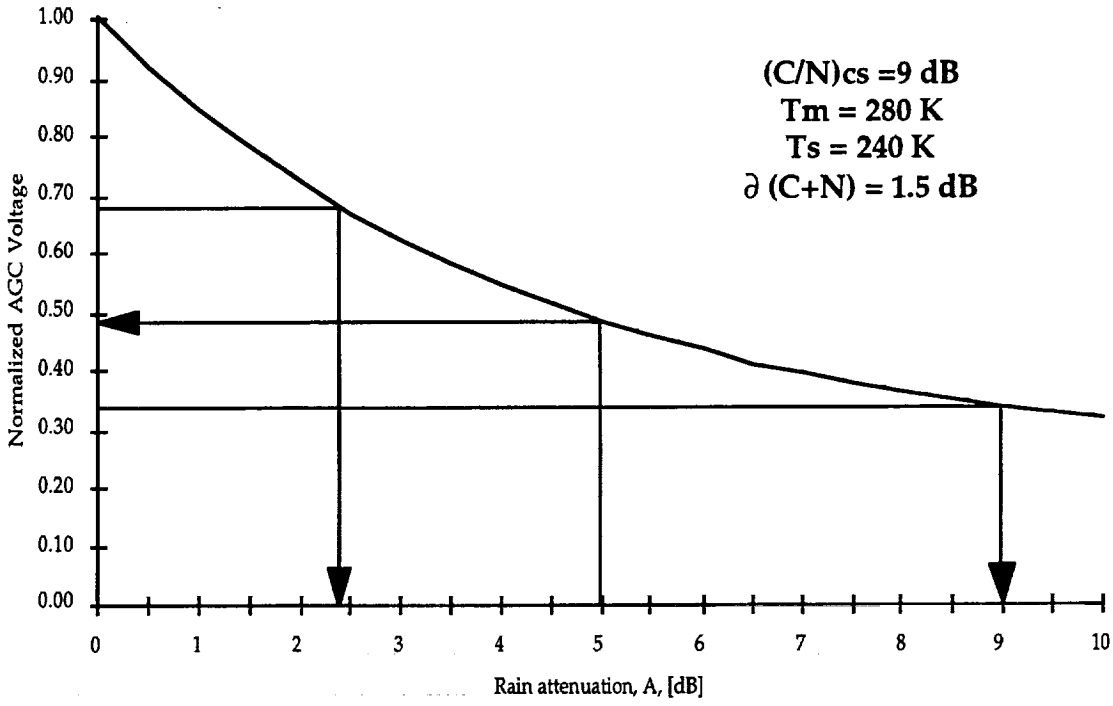

Figure 4-2. Effect of Carrier plus Noise Power Uncertainty on Estimated Fade

$$(C+N)_f = (C+N)_{cs} - A + 10\log\left(\frac{T_s + T_m\left(1-10^{-\frac{A}{10}}\right)}{T_s}\right) \qquad (4\text{-}3)$$

$(C+N)_{cs}$ = *clear sky carrier plus noise power*

$(C+N)_f$ = *faded carrier plus noise power*

$A, T_m, \& T_s$ *as previously defined.*

Received carrier plus noise power uncertainty of 1.14 dB creates a relatively large ±1.75 dB uncertainty in the estimated attenuation. This attenuation estimate is used to estimate downlink degradation and results in a degradation uncertainty of 3.94 dB. This uncertainty is much higher than those provided by the other 5 fade measurement techniques and eliminates this fade measurement technique from further investigation.

4.2.2 Response Time – Modem AGC Voltage

The modem AGC fade measurement technique can provide fade estimates whenever the modem demodulator is tuned to a received carrier. Fade estimates can be read from the demodulator circuitry at an arbitrarily high rate limited by the processing requirements of the fade estimation algorithm. The bandwidth of the AGC control loop is typically 0.01 to 0.001 times the modem symbol rate as it is undesirable for the AGC circuitry to respond to instantaneous fluctuations in the received carrier and noise power. For a QPSK modem passing an information rate of 384 kb/s, with concatenated coding and reasonable framing overhead, the symbol rate will be around 300 ksymbols/s. A typical AGC loop bandwidth would be around 1.5 kHz and the AGC voltage will follow any propagation phenomena with delays less than 10 ms.

4.2.3 Implementation – Modem AGC Voltage

Implementation of the modem AGC fade measurement technique has very low impact on modem complexity and a possible slight impact on modem parts cost. Demodulators have AGC loops in place and only an additional processor function is required to read and record the modem AGC voltage. If the AGC loop is implemented digitally then no additional parts are required. If the modem AGC loop is analog then an A/D converter may be required to measure the analog control voltage if one is not already available in the modem. A suitable, low speed converter and associated circuitry would cost approximately $10 in quantities of one thousand. Any additional features must be tested in production and therefore will have a slight cost impact on the modem arising from increased testing time and the reduction of production yields. This cost impact, based on a failure rate of 10^{-3} and a unit cost of $2K is $2 per unit. Development costs are estimated to be $80K for the fade measurement circuitry. This cost, spread over one thousand units will dominate the modem cost impact unless production quantities are much higher. The total modem cost impact for the modem AGC fade measurement circuitry is estimated to be $92.

4.3 ESTIMATING FADE FROM PSEUDO-BIT ERROR RATE

Downlink degradation can be estimated directly from measurements of channel performance parameters which depend upon E_S/N_O compared with similar measurements performed under clear-sky conditions. The Pseudo BER fade measurement technique is the first of four techniques of this type[29]. A secondary demodulator path is created and this path is intentionally degraded by establishing restricted decision thresholds. In a link

employing QPSK modulation a pseudo-error region would count as error those symbols whose phase fell into the shaded region of Figure 4-3 while the primary channel would continue to use the orthogonal axes as decision thresholds to yield the lowest BER.

The relationship between channel BER and pseudo-BER varies little over a wide range of channel conditions. Pseudo-error zone width may be selected to trade accuracy for measurement speed so that a pseudo-error measurement may be completed much more quickly than an actual BER measurement of identical accuracy.

4.3.1 Accuracy – Pseudo Bit Error Rate

The Pseudo-BER fade measurement technique, like all techniques which measure fades from E_b/N_o , is insensitive to VSAT terminal LNB gain variations. LNB gain variations affect noise power and signal power equally and therefore do not change E_b/N_o. There are still uncertainties in the received E_b/N_o that are not related to rain attenuation. These uncertainties are summarized in Appendix A, on pages A-7 through A-9, for the three satellite architectures. Assuming the measurement interval is selected to provide a degree of confidence of 0.25 on the Pseudo-BER measurement, then the degree of confidence in the actual BER is increased by the magnitude of the slope of the $\log(P_e)$ versus $\log(P_p)$ curve shown in Figure 4-5. This slope is -1.63 resulting in a degree of confidence of 0.41 for the BER measurement. This 41% range of BER values about average value of 0.01 translates to an uncertainty in the E_b/N_o value of ±0.5 dB (see Figure 4-4). The overall uncertainty in the downlink degradation estimate is predicted to be 1.06 dB for the backed-off bent pipe satellite and ±0.50 dB for the other two satellite architectures.

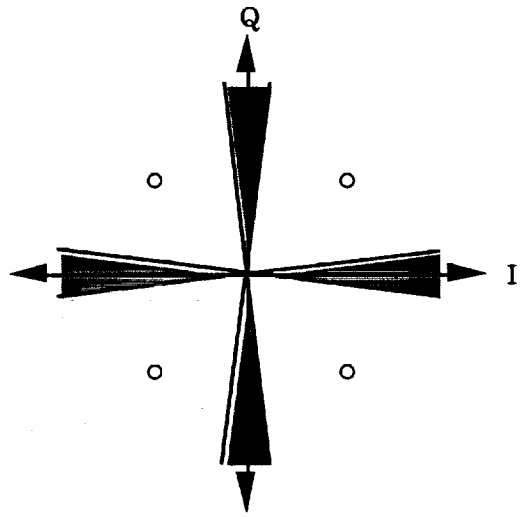

Figure 4-3. Shifted-Phase Decision Thresholds for Pseudo BER Fade Measurement

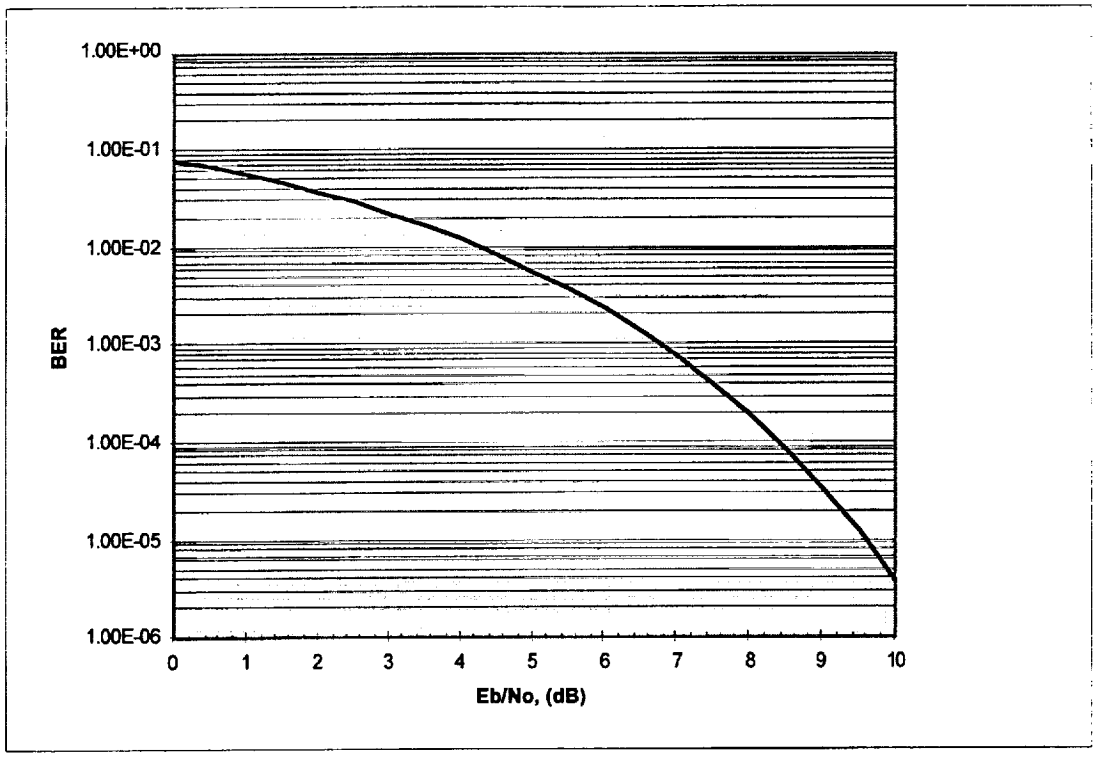

Figure 4-4. Theoretical BER Performance of QPSK Signal on Ideal Linear Channel

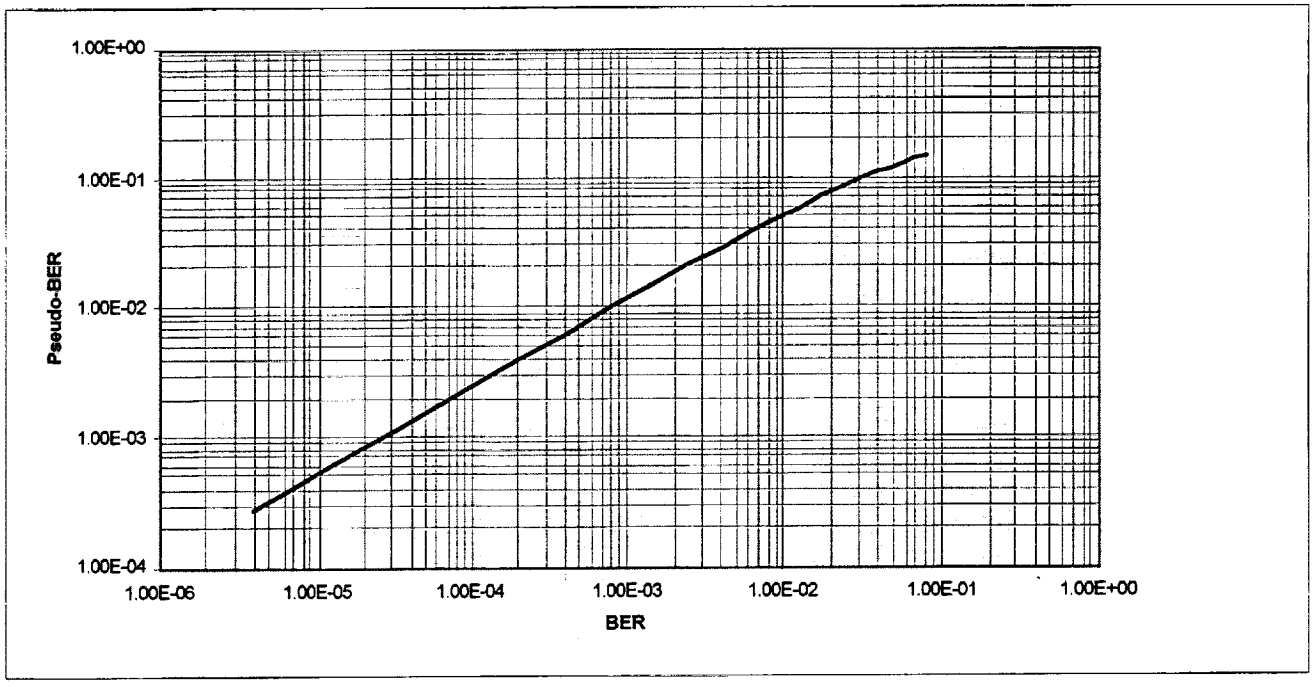

Figure 4-5. Pseudo BER Versus Actual BER on Ideal Linear Channel

4.3.2 Response Time – Pseudo Bit Error Rate

The required degree of confidence in the measurement of Pseudo-BER, P_C , can be obtained by measuring over an observation interval of $n=6.2x10^3$ symbols. For the channel rates encountered carrying a 384 kb/s information rate the QPSK symbol rate is approximately 300 ksymbol/s which results in an observation interval of 21 ms.

$$n = \frac{K_c^2}{P_c^2 P_p} \tag{4-4}$$

K_c = Number of standard errors of the mean
= 1.96 for 95% confidence level
P_c = Required confidence in Pseudo - BER measurement
= 0.25
P_p = Pseudo - BER
= 0.01 .

4.3.3 Implementation – Pseudo Bit Error Rate

The Pseudo-BER fade measurement technique is another technique which only provides useful measurements while the demodulator is locked to the desired carrier. Pseudo-BER measurements performed to estimate downlink degradation require additional circuitry to generate a pseudo-error count over the desired measurement interval. This fade measurement process can be implemented with four comparators operating at the channel symbol rate, four latches to sample the comparator outputs at the appropriate instant, a four input exclusive-or gate and a counter. Total parts cost is estimated to be less than $5. This circuitry should generate less than 10^{-3} production test failures per unit which, for a unit production cost of $2K, results in a cost impact of $2 per unit. Development cost for the fade measurement circuitry are estimated to be less than $50K resulting in a cost impact of $50 per unit for total production of 1,000 units. The sum of these cost factors is $57 per unit.

4.4 ESTIMATING FADE FROM BER ON CHANNEL CODED DATA

On systems which utilize forward error correction, measurements of channel bit error rate (BER) within the modem can be used to estimate path loss due to rain attenuation. As fading occurs the carrier to noise power ratio degrades and the decoder correction rate increases. Channel bit error rate is measured by re-encoding the decoded channel data and comparing the re-encoded data with a delayed version of the original channel data. Any discrepancies are corrections performed by the decoder. These corrections are counted and divided by the bit count to determine the channel BER.

4.4.1 Accuracy – BER from Channel Coded Data

The accuracy of fade estimates generated from channel BER measurements is dependent upon the correlation between fading and channel BER and channel BER measurement accuracy. Effects which decouple downlink C/N and rain attenuation can include uplink compensation errors, satellite gain variations, antenna gain and antenna pointing errors. Efforts to filter out these sources of error will never be completely effective and residual errors will contribute to fade measurement uncertainty. Appendix A, on pages A-10 through A-12 shows the principle sources of signal to noise ratio variations and estimates of the mean square error in the E_b/N_o ratio. This error, combined with the error in measuring channel BER , combine to reduce the accuracy of fade estimates. The overall uncertainty in the downlink degradation estimate is predicted to be ±1.04 dB for the backed-off bent pipe satellite and ±0.46 dB and ±0.45 dB for the saturated bent pipe and on-board processing satellites respectively.

4.4.2 Response Time – BER from Channel Coded Data

Assuming channel BER is measured on a 384 kb/s carrier the above accuracy can be obtained in less than 17 milliseconds. For lower baseband data rates more time would be required to accumulate statistics. On high rate data streams, such as a 90Mb/s TDM stream the response time is significantly lower.

4.4.3 Implementation – BER from Channel Coded Data

This technique can be utilized independent of satellite access schemes because it operates on the recovered data. If FEC is not utilized a similar technique can be implemented by measuring the BER of a known sequence such as the unique word in a TDMA system or framing bits in a TDM system. In this case response times will be much longer due to the limited number of bits for error measurement. All forms of this fade estimation technique can also be implemented on the satellite.

Circuitry required to implement this fade estimation technique include the re-encode circuitry, a comparator, a channel error counter, a channel bit counter and a processor to estimate the fade from the channel BER measurement. For data rates below 25 Mb/s integrated circuits are available for convolutional encoding and Viterbi decoding. These devices, which presumably already reside within the modem, have built-in re-encode circuitry, a comparator, a channel error counter and a channel bit counter. There is therefore no additional parts cost associated with this fade measurement technique. This circuitry should generate less than 10^{-3} production test failures per unit which, for a unit production cost of $2K, results in a cost impact of $2 per unit. Development cost for the fade measurement circuitry is estimated to be less than $50K resulting in a cost impact of $50 per unit for total production of 1,000 units. The sum of these cost factors is $52 per unit.

For higher rate systems, all of the circuitry to measure channel BER and compute fades impacts terminal cost. The re-encode circuitry, compare circuitry, bit counters and error counters are relatively simple when compared with the task of decoding the encoded data. The additional circuitry to accumulate BER statistics would have minor incremental cost impact. A microprocessor is still required to complete the fade estimation circuitry and implement the compensation algorithm. The terminal cost impact of this fade estimation technique for bit rates above 25 Mb/s data is approximately $50.

4.5 ESTIMATING FADE FROM BER ON KNOWN DATA PATTERN

Virtually every satellite communication channel carries some overhead bits to indicate multiplexing frame boundaries, provide carrier phase reference, provide carrier frequency reference or burst time references to receiving terminals. These overhead bits typically constitute 3% to 5% of the channel capacity. BER measurements can easily be performed on these bits because the receiving terminal has a-priori knowledge of their content. Fade estimates can then be based on the results of these measurements.

4.5.1 Accuracy – BER from Known Data Pattern

BER measurements performed on known data patterns are measurements of channel quality and do not rely on the absolute accuracy of any power level measurement. This technique for estimating fading is therefore immune to LNB gain variations and the uncertainty in the received signal quality is similar to the BER from channel coded data, SNR and pseudo-BER measurements. Assume that the known data pattern is not encoded and the channel is operating at a BER of 0.01 corresponding to a BER of 3×10^{-4} after the Viterbi decoder and quasi-error free ($10^{-10} - 10^{-11}$) after the Reed-Solomon decoder. A 40% tolerance on measuring the BER indicates that the 95% confidence interval for measured BER is $0.01 \pm 40\%$ or $0.006 < \text{BER} < 0.014$. Reading from the un-coded QPSK curve of Figure 4-4 yields an uncertainty in E_b/N_O of ±0.5 dB. This uncertainty is combined with additional uncertainties associated with the uplink and downlink uncertainties in E_b/N_O in Appendix A, on pages A-13 through A-15. The error in the degradation estimate is ±1.06 dB for the saturated bent-pipe, ±0.50 dB for the backed off bent-pipe and ±0.49 dB for the on-board processing satellite.

4.5.2 Response Time – BER from Known Data Pattern

Since the BER measurement is performed on only a small fraction of the channel bits, more measurement time is required to provide acceptable accuracy. To achieve the 40% tolerance on measured BER for a 384 kbit/s stream requires a 1,200 bit measurement interval or 0.10 seconds for a 3% known pattern content.

4.5.3 Implementation – BER from Known Data Pattern

This fade measurement technique can only provide meaningful degradation estimates when the demodulator is locked to the desired data stream. The demodulator will not have the advantage of knowing the current degradation during the link acquisition procedure. This fade measurement technique does not add any additional parts to the modem. Any known data pattern in the aggregate stream is monitored on a continuous basis by the modem to either provide or verify proper operation of the communication link. The cost associated with this technique is only that associated with the expense of developing a process to accumulate the BER statistics and can be assumed equal to the BER from Channel Coded Data fade measurement technique.

4.6 ESTIMATING FADE FROM SIGNAL TO NOISE RATIO

Measurements of signal power to noise power ratio (SNR) within the modem can also be used to estimate path loss due to rain attenuation. As fading occurs the carrier to noise power ratio degrades according to the following formula.

$$C/N \text{ degredation in decibles } = 10\log\left(\frac{T_m\left(1-10^{-0.1A}\right)+T_s}{T_s}\right)+A \qquad (4\text{-}5)$$

T_s = System noise temperature under clear sky conditions

A = Rain attenuation in decibels

T_m = Rain temperature

The first term accounts for the increase in system noise power caused by rain absorption and the second term accounts for the signal attenuation. The above relationship is plotted for several system clear sky noise temperatures in Figure 4-6. The effective fade, or degradation, is approximately 1.5 times higher than the rain induced attenuation.

When this technique is implemented on the satellite, the scaling between rain attenuation and SNR degradation is one because the noise temperature "seen" by the satellite is always high, essentially equal to the earth surface temperature.

Within the modem the baseband signal to noise ratio can be calculated from data samples. If we assume QPSK data with no inter symbol interference the signal to noise ratio is

$$SNR = \frac{\left(\sum |I|+|Q|\right)^2}{2\sum\left(I^2+Q^2\right)-\left(\sum |I|+|Q|\right)^2} \qquad (4\text{-}6)$$

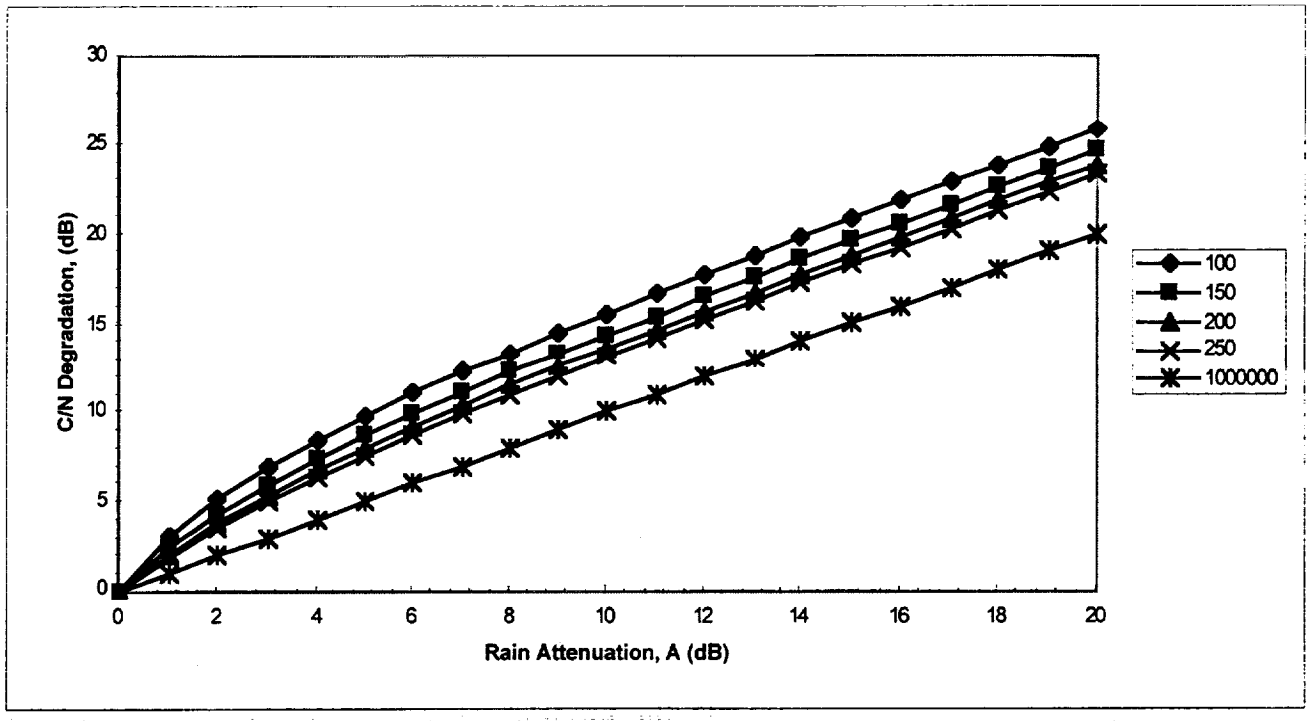

Figure 4-6. C/N Fading Caused by Rain Attenuation

Where I and Q are the I-channel and Q-channel data samples. Fade estimates are calculated from the signal to noise measurement and assumptions on the receiver noise temperature from the above graph.

4.6.1 Accuracy – Signal to Noise Ratio

The accuracy of fade estimates generated from signal to noise power measurements is dependent upon the correlation between fading and signal to noise ratio and signal to noise measurement accuracy. Effects which can decouple downlink E_b/N_o and rain attenuation include uplink compensation errors, satellite gain variations, antenna gain and antenna pointing errors. Efforts to filter out these sources of error will never be completely effective and residual errors will contribute to fade measurement uncertainty. These uncertainties are summarized in the appendix, on pages A-16 through A-18, for the three satellite architectures. The overall uncertainty in the downlink degradation estimate is predicted to be 1.03 dB for the backed-off bent pipe satellite, ±0.43 dB for the saturated bent pipe and ±0.42 dB for the on-board processing satellite architecture.

4.6.2 Response Time – Signal to Noise Ratio

Assuming Signal to Noise is measured on a 384 kb/s carrier the above accuracy can be obtained in less than 10 milliseconds. For lower baseband data rates more time would be required to accumulate statistics. On high rate data streams, such as a 90 Mb/s TDM

stream the response time trades with implementation cost. In this case response times below 10 milliseconds can be obtained at low costs.

4.6.3 Implementation – Signal to Noise Ratio

This technique can be utilized independent of satellite access schemes because it operates on the baseband signal. This fade estimation technique can also be implemented on the satellite.

Figure 4-7 shows a hardware implementation which can function in TDMA and high rate TDM environments. This implementation takes advantage of the fact that SNR readings are required only a few times per second. The First-In-First-Out (FIFO) memories are the only element which must function at the channel symbol rate. A sufficient number of successive data samples are read into the FIFO to obtain the required SNR accuracy. A microprocessor then processes the data by accumulating the required summations, calculates the SNR and implements the fade compensation algorithm. A programmable logic device is included to control the FIFO loading and perform other ancillary functions which may be required to interface with the modem. The terminal cost impact of this

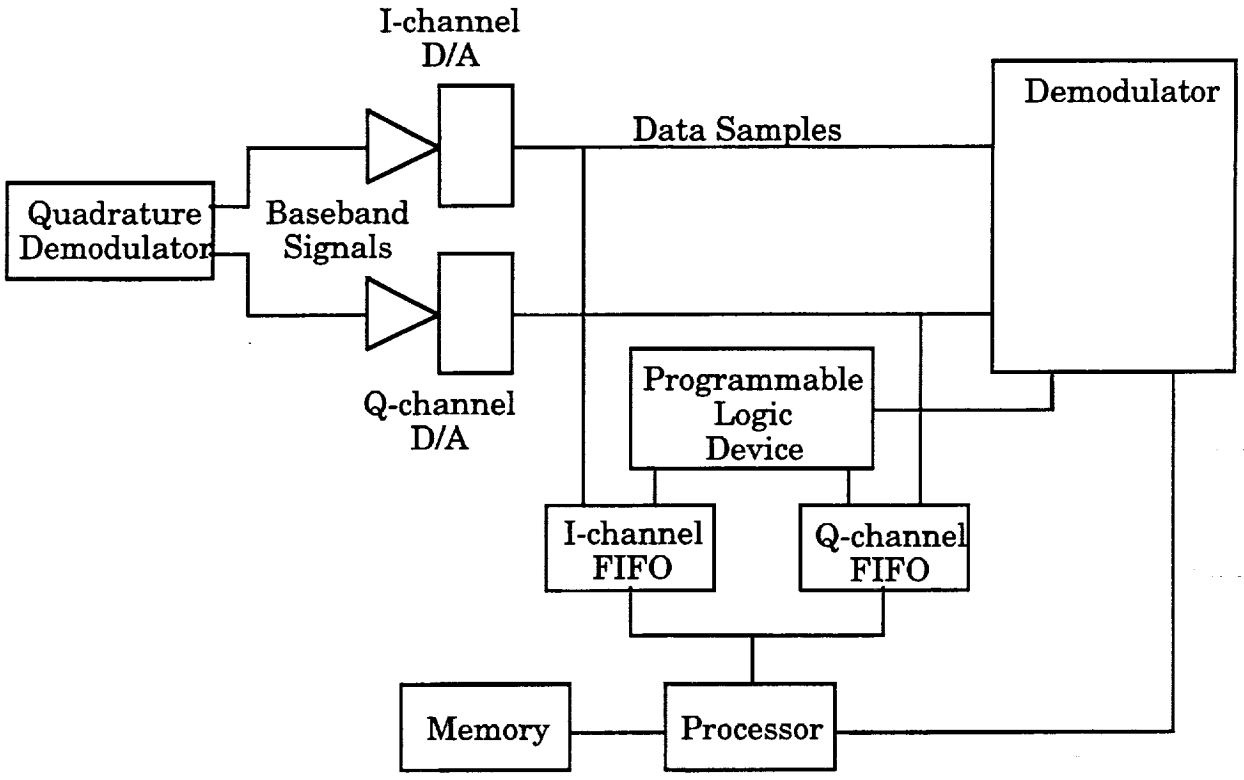

Figure 4-7. Signal to Noise Ratio Measurement Hardware

circuitry is estimated to be approximately $12 for a low speed FIFO memory integrated circuit. The processing and data handling burden is assumed to be incorporated into the modem with no parts requirement. The cost associated with reduced production yields due to a 10^{-3} test failure rate for the fade measurement circuitry is $2 for unit costs of $2K. Fade measurement circuitry development cost is estimated to be $80K which adds $80 to the per unit cost for production quantities of 1000 units. The combined cost impact of this fade measurement technique is estimated to be $94.

4.7 SUMMARY OF FADE MEASUREMENT TECHNIQUES

The six fade measurement techniques are summarized in Table 4-3. Three techniques were selected for further investigation as indicated. The beacon power measurement technique was selected because its performance is independent of satellite architecture and the cost factor will improve with higher production volumes. The Modem AGC technique was excluded based upon poor predicted accuracy. The Pseudo-BER, BER from Channel Coded Data and BER from Known Data Pattern technique are very similar in performance. BER from channel coded data was selected to represent this group because channel coding will most certainly be employed and many modems are available with this feature. The SNR technique was also included based upon low cost impact and good accuracy.

Table 4-3. Summary of Fade Measurement Techniques

Technique	Cost to Implement	Speed of Response	Accuracy of Degradation Estimate			Selected for Experiment
			Bent Pipe/ Backoff	Bent Pipe/ Saturated*	On-board Processing	
Satellite Beacon	$157	0.001 sec	1.25	1.25	1.25	✓
Modem AGC Level	$92	0.01 sec	3.94	2.17	2.17	
Pseudo BER	$57	0.02 sec	1.06	0.50	0.50	
Channel BER from a Known Data Pattern	$52	0.10 sec	1.06	0.50	0.49	
BER Monitoring from Channel Coded Data	$52	0.02 sec	1.04	0.46	0.45	✓
Modem Signal to Noise Ratio	$94	0.01 sec	1.03	0.43	0.42	✓

* Assumes that overdrive is maintained through all uplink fades. Otherwise bent-pipe with back-off accuracy is more appropriate.

SECTION 5 — RAIN FADE COMPENSATION

For satellite systems operating in frequency bands in which rain events can severely degrade the carrier performance for significant durations of time in a year (e.g., Ku- and Ka-bands), it is necessary to allocate sufficient margins for all carriers or to implement some form of rain fade compensation techniques at earth stations or on board the satellite in order to maintain the link availabilities at acceptable levels. A number of rain fade compensation techniques include built-in link margin, overdriven satellite transponder, uplink power control, diversity techniques (i.e., frequency diversity, site diversity through routing, and back-up terrestrial network), information rate and FEC code rate changes, and downlink power sharing (i.e., active phased array, active lens array, matrix or multiport amplifier, and multimode amplifier). These will be evaluated and compared in this section.

5.1 BUILT-IN LINK MARGIN

In a bent-pipe satellite, for a carrier transmitted from earth station A to earth station B, the total carrier-to-noise ratio at B is given by [6], [7]

$$\frac{1}{\left(\frac{C}{N}\right)_{total}} = \frac{1}{\left(\frac{C}{N}\right)_{up}} + \frac{1}{\left(\frac{C}{I}\right)_{up}} + \frac{1}{\left(\frac{C}{IM}\right)} + \frac{1}{\left(\frac{C}{N}\right)_{down}} + \frac{1}{\left(\frac{C}{I}\right)_{down}} \tag{5-1}$$

where

$(C/N)_{total}$ = total carrier-to-noise ratio (dB)
$(C/N)_{up}$ = uplink carrier-to-noise ratio (dB)
$(C/I)_{up}$ = uplink carrier-to-interference ratio (dB)
C/IM = carrier-to-intermodulation ratio (dB)
$(C/N)_{down}$ = downlink carrier-to-noise ratio (dB)
$(C/I)_{down}$ = downlink carrier-to-interference ratio (dB).

Equation (5-1) can also be expressed as

$$10^{-\frac{(C/N)_{total}}{10}} = 10^{-\frac{(C/N)_{up}}{10}} + 10^{-\frac{(C/I)_{up}}{10}} + 10^{-\frac{(C/IM)}{10}} + 10^{-\frac{(C/N)_{down}}{10}} + 10^{-\frac{(C/I)_{down}}{10}} \tag{5-2}$$

or

$$\left(\frac{C}{N}\right)_{total} = -10\log\left[10^{-\frac{(C/N)_{up}}{10}} + 10^{-\frac{(C/I)_{up}}{10}} + 10^{-\frac{(C/IM)}{10}} + 10^{-\frac{(C/N)_{down}}{10}} + 10^{-\frac{(C/I)_{down}}{10}}\right]. \tag{5-3}$$

As seen from Equation (5-3), if one of the five ratios becomes much smaller than the others, the total carrier-to-noise ratio is almost equal to this ratio. In this case, it is often termed that the link is limited by this component. In operational satellite systems, depending on a number of factors such as service requirements in terms of carrier bit rate, modulation and coding, required BER performance, and link availability; earth station antenna diameter and high-power amplifier (HPA) size; climate conditions at earth stations; satellite parameters (e.g., saturation flux density, EIRP, and G/T); and interference environment, the total carrier-to-noise ratio can be limited by more than one component.

In general, a link or system margin is allocated to a link in order to provide a specified link availability. A high system margin is required for a high link availability. In a bent-pipe transponder, the transponder capacity is a function of the system margin: the higher the margin the lower the capacity. As seen from Equation (5-3), this nonlinear function depends on the factors mentioned earlier. In a system in which carriers are allocated margins to provide a threshold BER performance at a specified link availability, the carrier BER performance is, under clear-sky conditions, much better than the threshold BER performance. Since these margins are permanently assigned, the capacity is fixed. Therefore, it is not possible to achieve an increase in the capacity which could have been realized had the fixed margins not been allocated or had smaller fixed margins been allocated and additional margins provided by earth stations and/or spacecraft on an adaptive basis during periods of severe rain fades.

It should be noted that, in a multicarrier-per-transponder operation, the total transponder input backoff is normally set in the quasi-linear region in order to minimize the IM impairment. Consequently, the individual carrier input backoff is set in the linear region. The uplink margin is normally equal to the system margin since an uplink fade would affect almost equally the $(C/N)_{up}$, $(C/I)_{up}$, C/IM, $(C/N)_{down}$, and $(C/I)_{down}$. For a downlink fade, the downlink margin is normally much larger than the system margin since only the last two components are affected. As an example, for the IDR (intermediate data rate) service offered in the Ku-band in the INTELSAT system, the nominal uplink margin and downlink margin are equal to 7 dB and 11 dB, respectively [30]. In a single-carrier-per-transponder operation, the total transponder input backoff is normally set in the saturation region since there is no IM impairment. (Here, nonlinear distortions due to TWTA or SSPA nonlinearities become dominant [31].) The uplink margin is normally larger than the system margin since an uplink fade would not affect equally the $(C/N)_{up}$, $(C/I)_{up}$, $(C/N)_{down}$, and $(C/I)_{down}$. For a downlink fade, the downlink margin is normally much larger than the system margin since only the last two components are affected.

In an OBP satellite, for a carrier transmitted from earth station A to earth station B, the information BER performance at B, BER_i, is given by [13]

$$BER_i = BER_{iu} + BER_{id} \tag{5-4}$$

where

BER_{iu} = uplink information BER

BER_{id} = downlink information BER.

BER_{iu} is a function of $(C/N)_{up}$ and $(C/I)_{up}$, BER_{id} a function of $(C/N)_{down}$ and $(C/I)_{down}$. It is worth noting here that uplink noise and interference components, and downlink noise and interference components do not accumulate or add up like those shown in Equation (5-3). In a special situation in which $C_{up}/(N_{up}+I_{up})$, the ratio of uplink carrier power to uplink thermal noise and interference, is equal to $C_{down}/(N_{down}+I_{down})$, the ratio of downlink carrier power to downlink thermal noise and interference, close to 3-dB advantage in system margin can be realized as compared to a similar situation using a bent-pipe satellite. In a link, the uplink or downlink margin is always larger than the system margin. From Equation (5-4), the allocation of a fixed uplink margin can be performed independently from the allocation of a fixed downlink margin, depending on climate conditions at the transmit and receive earth stations. For a large downlink TDM carrier, the allocation of a large fixed downlink margin may reduce the carrier information rate.

Therefore, while the built-in link margin technique is simple, and can reduce the complexity and cost associated with a network, the requirement of large fixed margins in the Ka-band (much larger than margins required in the Ku-band) will adversely affect the system capacity in bent-pipe and OBP satellites.

5.2 OVERDRIVEN SATELLITE TRANSPONDER

In a bent-pipe satellite, in order to minimize the effects due to high uplink rain fades, it is possible, in a single-carrier-per-transponder operation, to transmit a high-power carrier from an earth station such that the transponder TWTA operating point is set well into the overdrive region (i.e., 4 dB or more beyond saturation) as shown in Figure 5-1. For example, in the Ku-band, a 7-dB fade in the uplink will reduce the TWTA operating point from +4 dB to -3 dB. The corresponding reduction in downlink carrier EIRP is small (e.g., about 0.5 dB for a TWTA [18]). Therefore, by operating the TWTA in the overdrive region, high uplink fades can be tolerated while keeping the downlink carrier EIRP at about the same level. Consequently, the degradation due to an uplink fade on the carrier BER

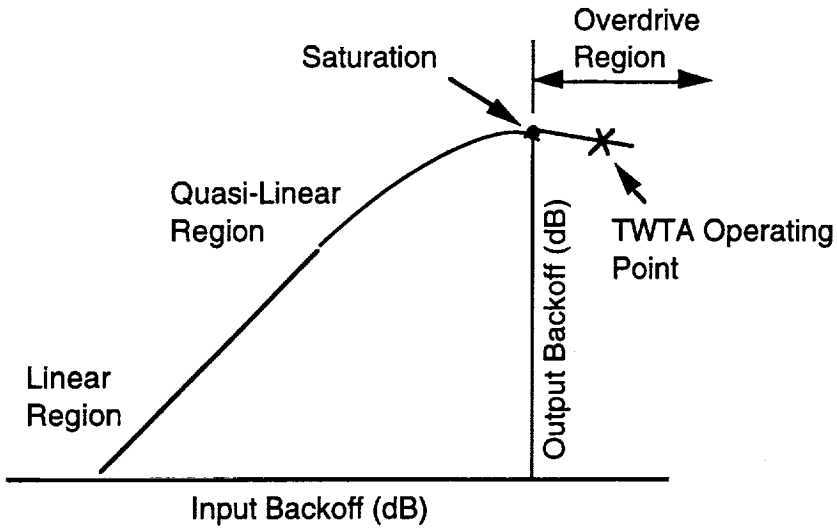

Figure 5-1. Transponder TWTA Operation in Overdrive Region

performance is almost negligible. (It has been implicitly assumed here that the link is not limited in the uplink. This is normally the case in single-carrier-per-transponder operations.)

This technique is only suitable for systems in which a single high-power carrier is transmitted through a single transponder TWTA whose operating point is set beyond saturation. Here, the nonlinear effects [32], [31] due to the TWTA on the carrier performance (i.e., BER performance, power spectrum re-growth, etc.) must be fully evaluated and accounted for in the system design and associated link budgets. This technique is not useful in commercial multicarrier operations with FDMA or code-division multiple access (CDMA) carriers due to severe IM impairments.

5.3 UPLINK POWER CONTROL

Uplink power control is a technique in which the carrier uplink EIRP is adjusted on an adaptive basis based on the continuous measurement, in the downlink, of the power of another carrier or of the same carrier. The amount of uplink power adjustment is estimated from this measured downlink fade. Depending on the satellite beam configurations (i.e., connectivities and coverages) and availability of beacons, and the earth station locations in the beam coverages, this technique can be implemented in three different ways: open-loop, closed-loop, and feedback-loop.

In an open-loop system (e.g., in a non-loopback beam), an earth station cannot receive its own transmit carrier, and needs to rely on a measurement of the downlink beacon fade. In a closed-loop system (e.g., in a global beam or loopback beam), an earth station can receive its own transmit carrier as well as carriers from other earth stations with which it is communicating . It is preferable to estimate the uplink power adjustment based on the

fade measurement of one of these carriers instead of the same carrier since the measurement of the latter is not accurate due to variations in carrier input backoff and associated variations in carrier output backoff under uplink and downlink fadings (i.e., rain at an earth station affecting simultaneously the carrier being transmitted and received). In a feedback-loop system (e.g., in an east-to-west beam and a west-to-east beam), a central control station monitors the powers of all carriers it receives in one beam, and commands, through the other beam, earth stations which undergo uplink fadings to adjust their uplink EIRP's. It is implicitly assumed here that rain does not occur simultaneously in the two beams. Among the three systems, the last one requires more space segment and ground segment resources than the first two. In addition, an earth station which undergoes uplink fadings has to wait at least two round-trip propagation delays before it can receive instructions from the central control station to increase its uplink carrier EIRP.

In a bent-pipe satellite, any one of the three selected rain fade measurement techniques (i.e., beacon power, bit error ratio from channel coded data, and signal-to-noise ratio) can be used to estimate the uplink power adjustments. In an OBP satellite, one of the last two techniques can be used on board the satellite to measure the uplink powers of all carriers. Appropriate commands can then be sent, in the downlink, to the affected earth stations to adjust their uplink carrier powers accordingly.

An experiment was conducted by COMSAT Laboratories at Clarksburg, Maryland using ACTS during the May - November 1994 to evaluate the feasibility of the open-loop uplink power control technique [28]. It was found that, under most conditions, a power control accuracy of ±2.5 dB could be maintained and uplink fades of up to 15 dB could be compensated. A summary of key ACTS experiments was described in [33].

5.4 DIVERSITY TECHNIQUES

Over the years various diversity techniques have been proposed for mitigating rain fading at frequencies above about 10 GHz. These include frequency diversity, site diversity, terrestrial backup, and orbital diversity. Some of these techniques are briefly discussed below.

5.4.1 Frequency Diversity

Rain attenuation, expressed in dB, increases with the frequency approximately in proportion to the square of the frequency. Rain attenuation at 20 GHz is almost three times that at 11 GHz. Figure 5-2 shows the rain attenuation distributions at 4, 6, 11, 14, 20, and 30 GHz for a mid-Atlantic location; elevation angle is 40°. Although frequency diversity can be used to mitigate rain fading at Ka-band frequencies, the requirement of complex feed systems or separate antennas may out weigh any advantage offered by this technique.

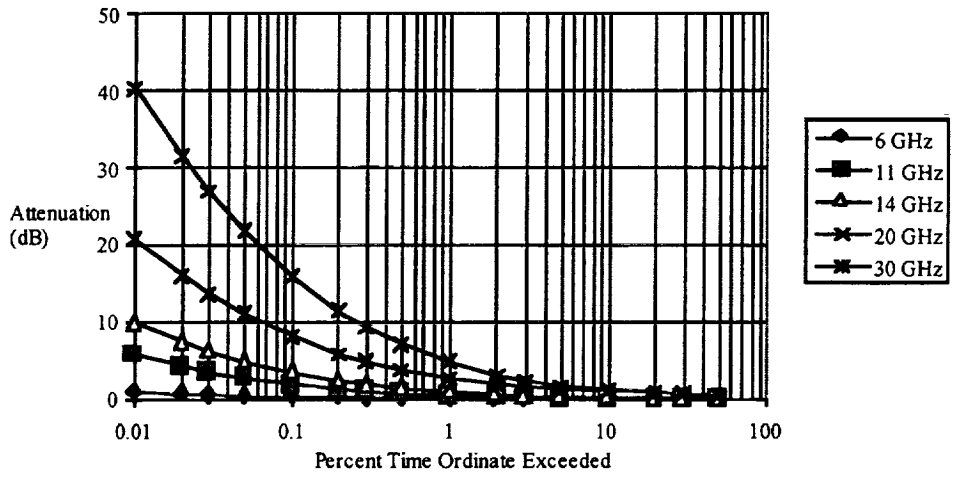

Figure 5-2. Cumulative Distribution of Rain Attenuation at Different Frequencies for a Mid-Atlantic Location; Elevation Angle 40°

5.4.2 Site Diversity

The limited horizontal extent of rain storms, and the non-uniformity of rain intensity within a storm are exploited in site diversity. In the presence of severe rain fading site-diversity has a significant advantage in improving link availability. Site diversity experiments on earth-space paths with elevation angles above about 20° have shown that diversity improvement increases rapidly as the site separation approaches, and exceeds, about 10 km, saturating beyond about 20 km. For elevation angles below 20°, the site separation requirements appear to increase proportionately. Diversity applied in the conventional sense requires two dedicated earth stations to support a single satellite link. In general, the cost involved in setting up the two earth stations and connecting them together appears to outweigh the benefits rendered.

Finite size of rain cells results in uncorrelated fading at sites separated by distances larger than the average rain cell size. In general, the average cell size is inversely proportional to the rain intensity and diversity can be highly effective in combating relatively strong fades. Improvement in link availability with the use of diversity is normally quantified as diversity gain or diversity advantage. Diversity gain is the difference between the single site attenuation and the joint attenuation between the two sites, both taken at the same probability level. The diversity gain may be predicted using the model recommended by the ITU-R [17]which requires frequency, site separation, elevation angle, and the base line orientation angle as the input parameters; the baseline orientation is the angle between the line joining the two sites and the projection of the radio path on the earth surface. Figure 5-3 and 5-4 show the predicted diversity gain at 20 and 30 GHz, respectively, as a function of single site attenuation. At the low end of the single site attenuation very little

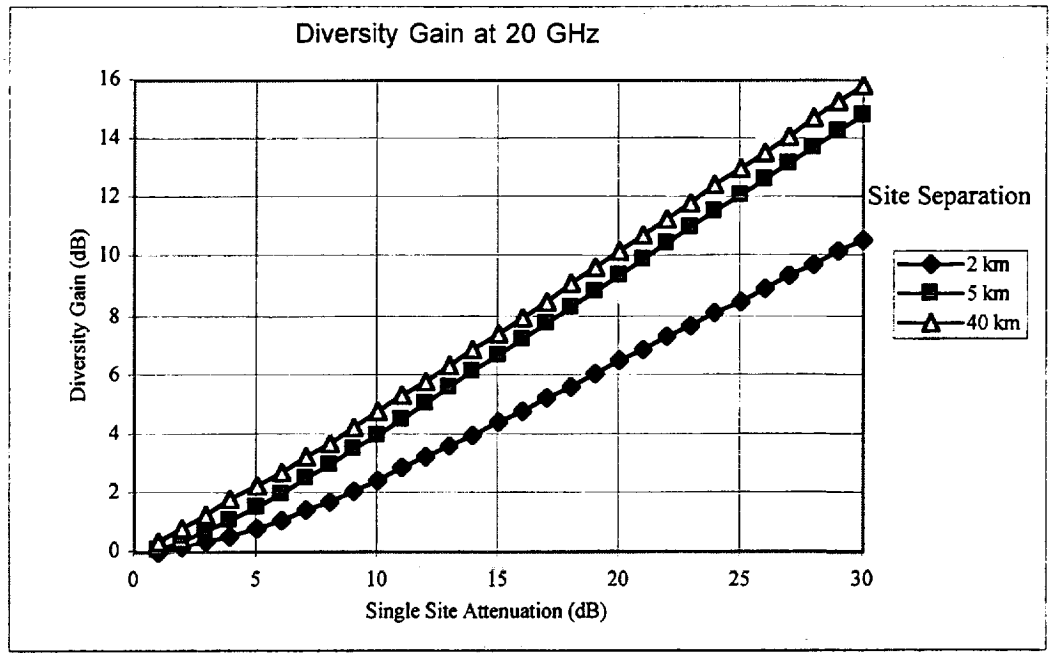

Figure 5-3. Diversity Gain at 20 GHz as Function of Site Separation

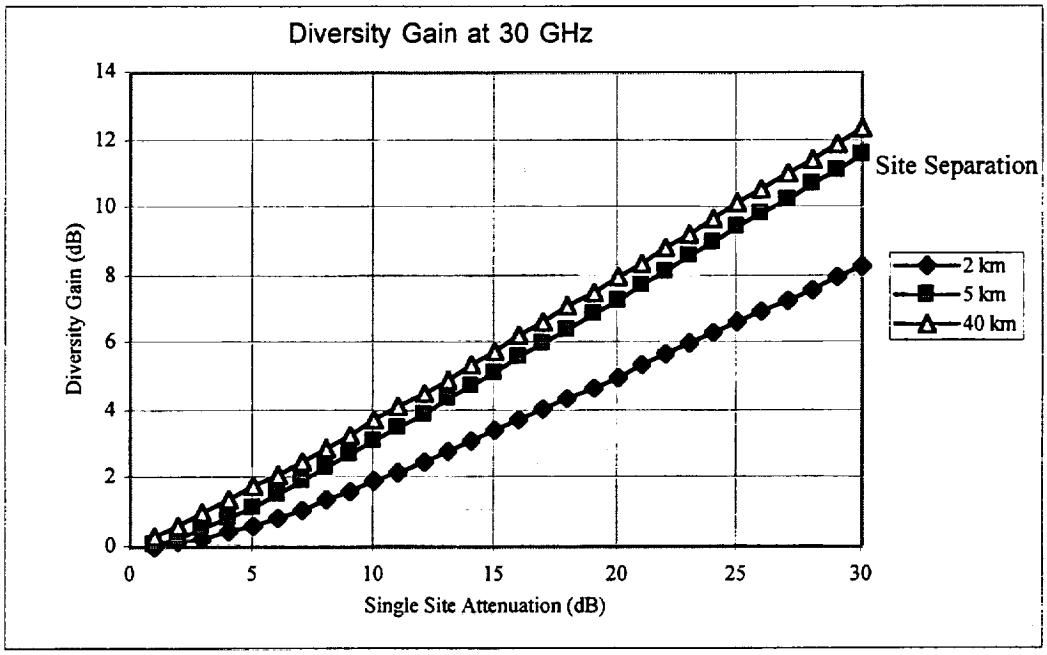

Figure 5-4. Diversity Gain at 30 GHz as Function of Site Separation

diversity gain is predicted. This is due to the fact that precipitation structures producing low attenuation levels are rather widely spread and both sites will experience similar levels of attenuation.

5.4.3 Back-up Terrestrial Network

Site diversity as described in the previous subsection requires two dedicated earth stations and an inter-link facility. As such, site diversity is not very attractive to applications involving low-cost terminals such as VSATs. However, VSATs do not normally have high activity ratios and the availability of free time on a VSAT may be gainfully employed with site diversity to overcome rain fading. VSAT terminals located in a metropolitan area can be connected together using the terrestrial network to implement traffic sharing under fading conditions. VSAT sites must have separation distances in excess of about 10 km to take advantage of site diversity. The cost of full time dedicated interconnect line is now replaced by the terrestrial network usage, which is close to the average raining time of the order of 10%. In this type of arrangement, besides rain fade mitigation, further economic benefits can be gained through sharing of ground-segment resources.

5.5 INFORMATION RATE AND FEC CODE RATE CHANGES

In communications systems, the two basic resources normally utilized to provide a specified link performance under fading conditions include carrier bandwidth and power. If the TDMA method is used, then the third resource is the time slots in a TDMA frame. In Ka-band systems, most earth stations will employ low-cost antennas with very small diameters (or very small aperture terminals (VSATs)). Therefore, it is essential that power efficient modulation and FEC techniques be used under all weather conditions (i.e., clear-sky and degraded weather). In fact, in current C-band and Ku-band systems, the use of concatenated coding (e.g., Reed-Solomon (RS) outer code and convolutional inner code) is "catching up", especially in the provision of multimedia services.

Due to operational and cost constraints, in order to mitigate the effects caused by severe rain fades, one of the simplest rain fade compensation techniques would be to keep the carrier power, transmission rate, and occupied bandwidth fixed. Thus, the information rate can be reduced by one half, and the FEC rate also reduced by one half. As an example, a clear-sky 64 kbit/s rate 3/4 FEC carrier can be switched, under rain fades, to a 32 kbit/s rate 3/8 FEC carrier. The possible additional fade margin achieved from these combined steps is at least 5 dB at a BER of 10^{-8} (i.e., 3 dB from information rate reduction by one half and more than 1 dB from FEC rate reduction from 3/4 to 3/8). In a system employing continuous carriers, it may be difficult to coordinate this switching at the transmit and receive stations, and the service may not be seamless. In a system employing TDMA carriers, the extra reserved time slots to be used by carriers suffering fades can be allocated either at the end of each burst or at the end of the frame. In the above example, in order to keep the information rate unchanged, twice the time slots will be required from the

reserved time slots. The establishment of a pool of time slots in a frame constitutes part of the frame overhead which reduces the system capacity.

Implementation of this technique in either a bent-pipe or OBP satellite depends on the traffic requirements, satellite beam configurations and parameters, earth station parameters, transmission parameters, required link performance and availability, and climate conditions at earth stations (e.g., see [34],[35] &[36]).

5.6 DOWNLINK POWER SHARING

Downlink power sharing addresses candidate methods for sharing satellite available RF power among the several downlink carriers transmitted by the satellite. Two general categories of power sharing are considered: 1) those involving linear mode high power amplifiers (HPAs) and 2) those involving HPAs operated in saturation. Candidate methods within these categories include the following.

1. Linear mode methods
   - Multiport or matrix amplifier (MPA)
   - Active transmit lens array (ATLA) antenna
   - Active transmit phased array (ATPA) antenna
2. Saturated mode amplifiers
   - Multimode amplifiers
   - Code and data rate changes

The linear mode methods and the multimode amplifier method are discussed here, in order, in sections 5.6.2 through 5.6.4 and 5.6.6. The code and data rate change method was discussed in section 5.5. A comparison of the DC power requirements of the linear mode methods is provided in section 5.6.5.

5.6.1 Preamble and System Assumptions

The satellite system for which power sharing is here considered is one which is accessable by a large number of individual and corporate users. Therefore, it is to have both high capacity and low per-user cost. In conformity with all of the current multimedia Ka-band filings with the Federal Communications Commission (FCC), the satellites of this system will serve their given coverage areas using a very large number of narrow "spot" beams, each beam covering a separate, distinct sub area.

On the average, rain occurs within any single spot beam area no more than about five percent of a year. All spot beam areas will not experience rainfall simultaneously. Also, the intensity, frequency, and time of incidence (e.g., season of the year) of the rainfall that is experienced will vary with the location of the area covered by the spot beam. These characteristics were discussed in section 3.0.

It is evident, then, that a means of sharing satellite power among spot beams is desired so that the available satellite power can be used as needed to overcome rain-induced signal attenuation. Without power sharing, the power allocated to each spot beam would be fixed and would have to be large relative to the power needed when it is not raining within the spot beam area. This fixed, large power margin would be sufficient to overcome all levels of rain-induced attenuation except those which are predicted to occur less frequently than the allowed weather-related link outage. Or, with a fixed margin, the fraction of the time, on average, that the link would be over-powered relative to link closure (at the required link quality) is equal to the advertised weather-related link availability, typically, at Ka band, between 99% and 99.9% of the time.

With power sharing, ideally, the available power generated on the satellite can be allocated as needed such that a much smaller fixed power margin is provided in each beam. The smaller margin need cover only the measurement error and the change in attenuation level which occurs during the time between fade measurement and the initiation of sharing.

5.6.2 Multiport (or Matrix) Amplifiers

5.6.2.1 Multiport Amplifier Introduction

A multiport amplifier (MPA) consists of an M x K input matrix, K individual matched linear amplifiers, and a K x N output matrix. The M channels to be transmitted arrive at separate input ports of the MPA. The N output ports connect to N separate transmit beams. The generic form of an MPA is shown in the block diagram of Figure 5-5.

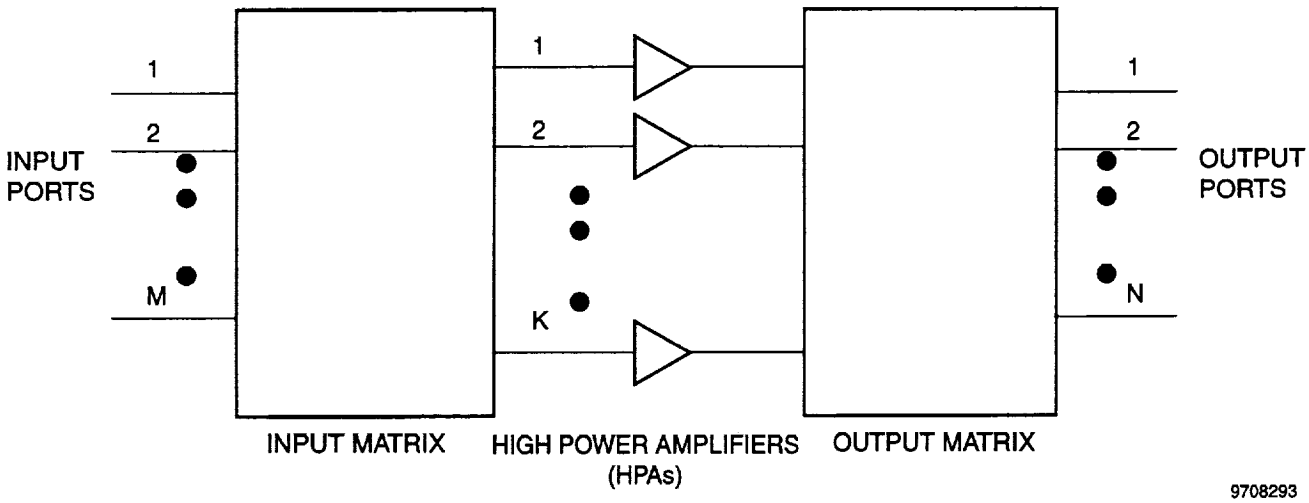

Figure 5-5. Top-Level Diagram of Multiport Amplifier

Signals in one channel arrive at one of the M input ports and are passed through a K-way, uniform amplitude power divider. Each of the K outputs of the divider are sent, via phase shifters, to the input of a separate one of the K amplifiers where it is summed with the power-divided outputs from each of the other M-1 input channels. The composite signal, all M signal units, is amplified by the corresponding amplifier. Thus, all M input signals are proportionally represented in and amplified by all K individual amplifiers. It is seen that sharing of amplifier power is easily achieved merely by setting the relative drive levels of the various signals into the multiport amplifier while maintaining linear operation of all amplifiers.

The M distinct signal units at each of the K amplifier outputs, one from each of the M input ports, are, in turn, passed through K N-way uniform power dividers. Each output of an N-way divider is then routed, via a phase shifter, to one of the output ports where it is summed with the power-divided outputs from the other K-1 amplifiers. As a result, the signal arriving at each output port consists of MK different signals, K of which originated from input port 1, K from port 2, and so on through the K which originated from port M. The K units which originated from port 1 have traversed different paths through both the input and output matrices and, therefore, may each be imparted a phase shift such that their vector sum is unity or zero. In certain implementations, this sum can be other rational numbers. In any event, the sum determines whether or not a routing connection exists between input port m and output port n. Thus, the multiport amplifier can route the signals from one of M input ports to one or more of the N output ports.

The attraction of the MPA lies in its ability to share the power of several matched amplifiers among several signals and, secondarily, to route inputs to more than a single output. If the drive level into the MPA of any one of the signals is reduced, the output level of that signal from the MPA will be correspondingly reduced. If the operation of the amplifiers is maintained at a fixed backoff from saturation to achieve linearity, the power may be shared among all the signals being amplified, from whatever input channel, merely by adjusting their relative input levels. In this regard, it is our opinion that a TWTA and linearizer, i.e., an LTWTA, optimized at, say 4 dB to 4.5 dB OBO (to achieve close to 20 dB noise power ratio (NPR)) could achieve approximately 35% to 40% efficiency.

The discussion presented here draws liberally from a 1993 report [37] by X.T. Vuong, H. Paul, and D. Cole of SAIC entitled *Matrix Amplifier and Routing System (MARS)* which was prepared for the USAF Space and Missile Systems Center (SMC). The supporting study investigated the use of matrix or multiport amplifiers in future X-band (7-8 GHz) military satellite communications payloads.

5.6.2.2 Non-Ideal Considerations

The following considerations may reduce the near-ideal sharing capability just described. First, what makes the multiport amplifier attractive in the first place may also be a limiting factor. Since each of the K individual amplifiers simultaneously amplifies all signals to be transmitted by all of the N transmit beams it must be broadband. The required width of the individual amplifier bandwidth depends on the frequency plan of the system. Usually, this will not pose any limitation as bandwidths of 1 GHz are common for 20-GHz TWTs.

The K individual amplifiers must also operate in linear mode. In this mode an amplifier is usually less efficient than in saturated mode. One might think of using a dual-mode TWTA optimized for high efficiency in both a reduced-power mode and at nominal saturation, as discussed in section 5.6.5. As noted there, however, the linearity of a dual-mode TWTA optimized for high efficiency is very nearly the same as for a single-mode TWTA at saturation. Therefore, a dual- or multi-mode TWTA cannot be used in an MPA.

Finally, the output matrix is not lossless. In addition to the insertion losses of the components of the matrix, there are combining losses. These comgining losses can be significant if the matrix is realized using microwave combiners and separate phase shifters. However, the combining losses are eliminated if the matrix is realized using a Butler or hybrid matrix where signals are combined using hybrids.

Also, the multiport amplifier does not require an output multiplexer. Since the amplifiers operate in their linear region, all multiplexing can be accomplished at low power level prior to the input matrix. That is, each of the M signals arriving at the M input ports of the multiport amplifier may originate from a corresponding single receive antenna beam or may be a multiplex of signals that individually arrived on many different receive beams. It is also possible that the multiport amplifier provide routing of signals from a single input port to more than one output port and at more than one relative power level.

5.6.2.3 Implementation Issues

The two major questions in regard to a multiport amplifier are, first, is the implementation practical at Ka band and second, how many individual amplifiers can be shared in a single multiport amplifier?

Four facets of the implementation issue are discussed by Vuong, Paul, and Cole:

1. Insertion loss of the output matrix
2. Effect of errors in amplitude and phase settings resulting from the input matrix, output matrix, and HPAs
3. Effects of HPA failure
4. Effects of HPA non-linearity

Summary discussions of these issues are given below.

Regarding the number of amplifiers, K, that can be shared, according to Vuong, Paul, and Cole: "to have the desired orthogonality among the output ports, the number of output ports N must not exceed the number of amplifiers K." That is, $K \geq N$. Other than this restriction, there does not seem to be a limit to K other than that of the obvious physical limitation of fitting K amplifiers into the spacecraft and providing the requisite input and output matrices.

As for the number of amplifiers required to serve a given number of beams, the required number K will depend upon N, the total number of beams served by the multiport amplifier; upon Y, the total number of carriers served by the MPA; upon X, the number of carriers that simultaneously experience high fades; upon P_L, the linear power contributed by each of the K amplifiers; and upon P_S, the power required from the MPA per downlink carrier in clear weather. To get a sense for the value of K, it was calculated for several values of N and X using four values of P_L and a P_S of 6.2 W (see link budget shown in Table 5-1). Further, these calculations assume a single carrier per beam (i.e., Y=N).

Table 5-2 gives the resulting values of K based on the equation

$$KP_L = (62*X + 6.2*(N-X)) \quad \text{or} \quad K = (62*X + 6.2*(N-X))/P_L,$$

where KP_L is the available linear RF power and $62*X + 6.2*(N-X)$ is the required linear RF power. Note that the power provided to each of the X carriers that experience high fades is increased by 10 dB over the clear-weather value of 6.2 W. In actual practice, the total excess power given to these X carriers could be distributed among them in any proportion, it need not be uniformly distributed.

Supposing a saturated HPA power of 120 W, the P_L values used here of 25 W, 31.6 W, 39.8 W, and 50 W correspond to HPA output backoffs of 6.8 dB, 5.8 dB, 4.8 dB, and 3.8 dB, respectively.

From Table 5-2, it is apparent that an MPA provides significant capability to counter downlink rain fades. Even for the smaller P_L values, link closure in all beams occurs when fully one third of the beams are experiencing high downlink fading. Contrast this with the probability that rain occurs in any given beam no more than about 5% of the time for most areas of the world. For the higher values of P_L, service is maintained when up to approximately 80% of the downlink beams experience high rain fades.

Table 5-1. Link Budget for Ka-band Demod-Decode/Recode-Remod Payload Transmitting 60 Mb/s per 0.6-deg Beam into 70 cm receive terminal

Ka-band budget assuming a rate 3/5, K=7 convolutional code concatenated with a rate 0.9216 R-S block code.								
On-board decoding. Required Eb/No values are taken from CyberStar filing with the FCC (9/29/95).								
Link burst (data bits) rate	0.384	60.00	Mb/s	FEC code rate=	0.55	R-S code rate=	0.92	
User terminal elev. angle	20.00	20.00	deg			Conv. code rate=	0.60	
Satellite altitude	35786.00	35786.00	km	Modulation=	QPSK	Hz/sym/sec=	1.50	
Earth radius	6378.00	6378.00	km	Uplink signal bandwidth (MHz)=			0.52	
Slant range	39554.46	39554.46	km	Downlink signal bandwidth (MHz)=			81.38	
	Uplink	**Downlink**		Total RF power radiated (assumed), W=			400	
Total xmitter power/beam	1.00	4.04	W	Tot RF pwr/bm	3.14	# active beams	128	
	0.00	6.06	dBW	Total downlink margin / beam, dB			0.00	
Tx antenna diameter	0.70	1.78	m	Array dia.=21/(f(GHz)*BW(deg)); with taper				
Tx antenna beamwidth	1.02	0.600	deg					
Antenna efficiency	60.00	55.00	%	Direct radiating elements with taper				
Transmission frequency	29.50	19.70	GHz					
Antenna peak gain	44.50	48.69	dBi					
Pointing/EOC & line loss	0.70	4.10	dB					
EIRP per User	43.80	50.65	dBWi					
Free space loss	213.79	210.28	dB					
Atmos. loss	1.00	1.00	dB	NASA Hdbk p. 6-7 for elev. angle x 1.22				
Rain loss	0.00	0.00	dB					
Path Loss	214.79	211.28	dB					
Rx antenna diameter	0.65	0.70	m					
Rx antenna beamwidth	1.10	1.52	deg					
Antenna efficiency	55.00	55.00	%					
Antenna peak gain	43.42	40.60	dBi			User rx bw (°)	1.52	
Pointing loss & polar. mis.	3.23	0.53	dB					
Gain at antenna flange	40.19	40.07	dB					
Rx clear-sky ant. noise temp.	290.00	75.48	K	**Clear Sky:**				
Rx rainy-sky ant. noise temp.	N/A	75.48	K	Ta=17.89+280*(1-10^(-Latmos/10)				
Line loss	1.00	1.00	dB	**Rainy Sky:**				
LNA+ noise figure	2.16	1.50	dB	Ta=17.89+280*(1-10^(-(Latmos+Lrain)))				
Tsys,r (in rain, at flange)	600.34	301.18	K					
G/T	12.41	15.28	dB/K					
Received signal (flange, rain)	-130.80	-120.57	dBW					
kT, in rain (if any)	-200.82	-203.81	dBW					
C/No	70.01	83.24	dB-Hz					
Link interference (C/I)	15.00	15.00	dB	Including C/IM from active antenna amplifiers				
Link interference (C/Io)	70.84	92.78	dB-Hz	C/Io = C/I+10*LOG10(Rb) in data bandwidth				
C/(No+Io)	67.40	82.79	dB-Hz					
Rain-induced crosspol (C/Xo)	200.00	200.00	dB	Circular polarization. In data rate bandwidth.				
C/(No+Io+Xo)	67.40	82.79	dB-Hz					
Link data rate (dB-Hz)	55.84	77.78						
Req'd Eb/No (w/impl. loss)	8.00	5.00	dB					
Available margin	3.56	0.00	dB					

Table 5-2. No. of Amplifiers, K, to Support 10-dB Power Increase for X of Y (=N) Carriers

a. P_L =25 W

N=20		N=30		N=50		N=60		N=80		N=100		N=120	
X	K	X	K	X	K	X	K	X	K	X	K	X	K
7	21	10	30	16	48	20	60	27	80	33	99	40	119
8	23	11	32	17	51	21	62	28	83	34	101	41	121

b. P_L =31.6 W

N=20		N=30		N=50		N=60		N=80		N=100		N=120	
X	K	X	K	X	K	X	K	X	K	X	K	X	K
9	20	13	29	22	49	27	60	36	80	45	99	54	120
10	22	14	31	23	51	28	62	37	81	46	101	55	121

c. P_L =39.8 W

N=20		N=30		N=50		N=60		N=80		N=100		N=120	
X	K	X	K	X	K	X	K	X	K	X	K	X	K
12	20	18	30	30	50	36	60	48	80	60	100	72	120
13	22	19	32	31	52	37	62	49	81	61	101	73	121

d. P_L =50 W

N=20		N=30		N=50		N=60		N=80		N=100		N=120	
X	K	X	K	X	K	X	K	X	K	X	K	X	K
16	21	24	31	40	51	48	61	63	80	79	101	95	121
17	22	25	32	41	52	49	62	64	82	80	102	96	122

Obviously, during any system implementation the linear power per amplifier would be matched to the expected broad area rain statistics such that total power per MPA is minimized.

5.6.2.3 Insertion Loss of the Output Matrix

The multiport amplifier output matrix consists of k stages of hybrids, where the number of amplifiers, K, is given by $K=2^k$. It is assumed that this output matrix would be realized in waveguide rather than, for example, squareax or a printed network. The output loss figure given here does not include the waveguide for connecting the N output ports with the N antenna beam input ports nor does it include the output zonal filters. A value of 0.4 dB to 0.5 dB per stage is estimated at 19 GHz when realized as a hybrid ring. (This compares to a 0.5-dB loss per stage estimate at X-band (7.5 GHz) given by Vuong, Paul, and Cole.)

For an MPA with 128 amplifiers, there would be 7 stages of ring hybrids, or an output matrix loss of approximately 3.0 dB. This is to be compared to an output loss, not including filter, of about 0.5 dB for either the active transmit lens array or the active transmit phased array antennas. However, as will be mentioned below, these two active antennas depend upon the use of SSPAs rather than TWTAs and would, therefore, have lower efficiency amplifiers.

5.6.2.4 Phase and Amplitude Deviations

A concern associated with MPAs is the ability to achieve nearly identical insertion phase, aside from intended phase shifts, and amplitude through the multiple paths of the input and output matrices as well as the ability to phase and amplitude match the K amplifiers themselves. Certainly, without very close phase and amplitude matching of these paths, the vector sums of the component signals at the MPA output ports will neither sum to zero at unwanted ports nor sum to unity at wanted ports. A non-zero sum at unwanted ports, i.e., in unwanted beams, reduces port-to-port isolation, I_{so}. In other words, it creates interference in frequency reuse schemes. Frequency reuse is one of the primary means of achieving high capacity in all of the Ka-band multimedia filings. A non-unity sum in wanted beams means a defacto loss, ΔC, as if an ohmic loss had been inserted after the amplifiers. In the ideal, no degradation, case, $\Delta C = 0$ dB and $I_{so} = \infty$ dB.

The tolerance on amplitude and phase tracking among the several signal paths was investigated by Vuong, Paul, and Cole in both a worst-case analysis and a Monte Carlo analysis. The worst case analysis is the easier analysis. The Monte Carlo analysis was undertaken in order to "consider the nominal system performance based upon statistically random phase and amplitude deviations that reflect the use of typical components." Also, while "worst case results may provide information that is safe to create specifications for the design of [an MPA] and its components, these specifications may be too tight to meet in a cost-effective manner."

The results of these analyses are shown in Figures 5-6 through 5-10. The worst-case analyses are summarized in Figures 5-6 and 5-7. The Monte Carlo analysis is summarized in Figures 5-8 through 5-10. In these figures, $\Delta G = 20 \log(1/(1 - \alpha))$, where α = maximum allowable amplitude deviation in relative voltage ratio and $\Delta\phi$ = maximum allowable phase deviation (degrees). Note that in voltage ratio, the maximum overdeviation allowable is the same as the maximum underdeviation allowable, which is αA (A is the nominal carrier amplitude). When converted to dB, they are no longer the same due to the nonlinear nature of the logarithmic function; the maximum overdeviation allowable becomes $\Delta G^+ = 20 \log(1 + \alpha)$ dB, and the maximum underdeviation allowable becomes $\Delta G^- = 20 \log(1/(1 - \alpha))$ dB. The values of ΔG^+ and ΔG^- are approximately the same when α is small with respect to unity.

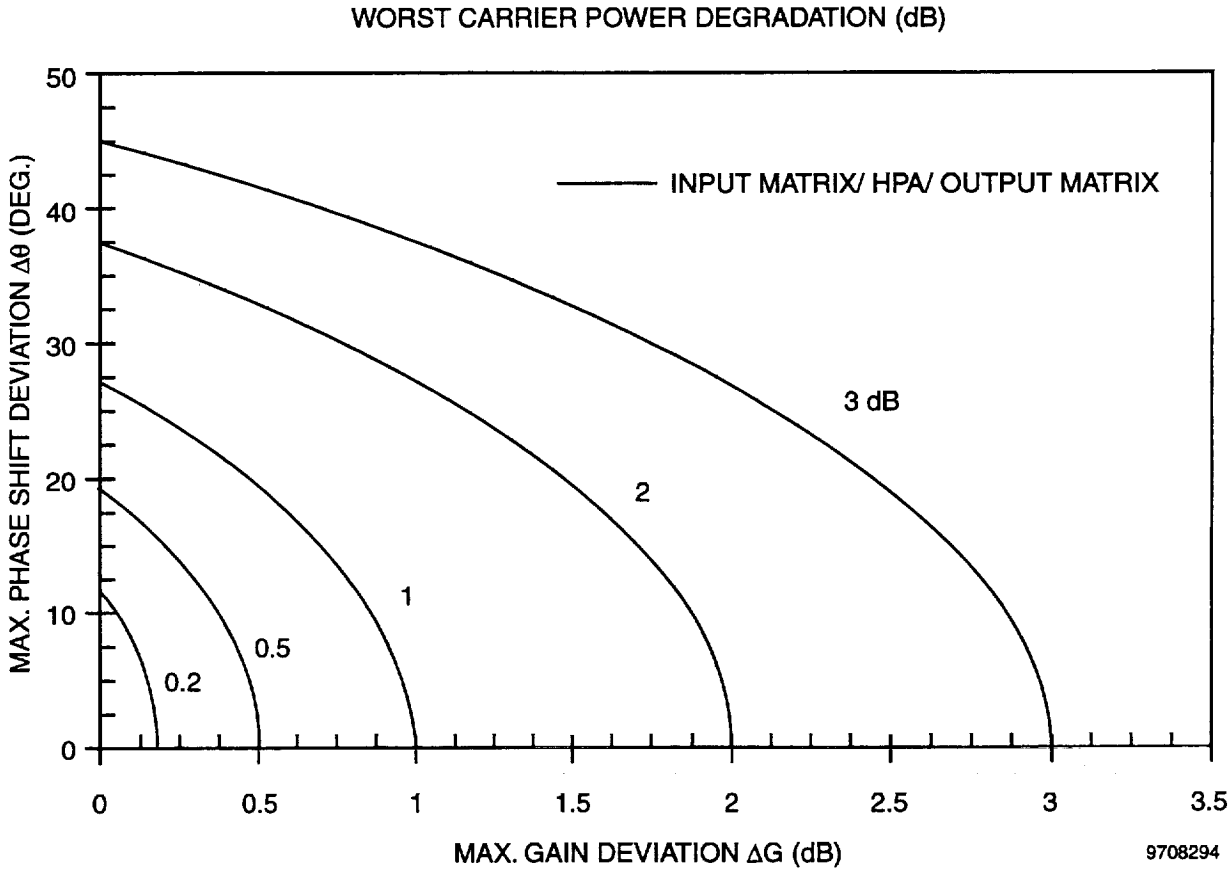

Figure 5-6. Contours of Worst-Case Carrier Power Degradation ΔC Versus Maximum Allowable Phase Deviation $\Delta\theta$ and Gain Deviation ΔG of Input Matrix, HPAs or Output Matrix

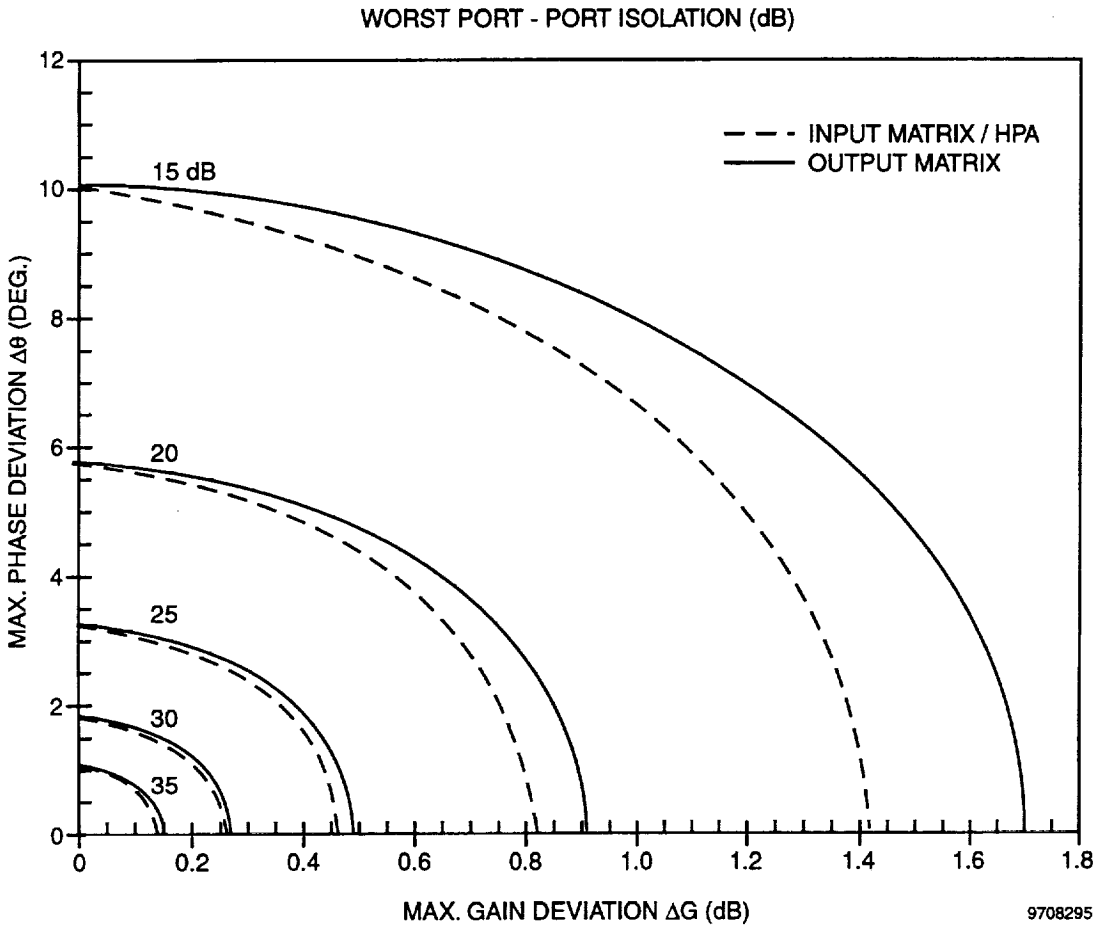

Figure 5-7. Contours of Worst-Case Port-Port Isolation I_{SO} Versus Maximum Allowable Phase Deviation Δθ and Gain Deviation ΔG of Input Matrix, HPAs or Output Matrix

Vuong, Paul, and Cole generated worst-case port-to-port isolation results for K=4, 8, and 16 and found them to be identical. They state, therefore, that "It is reasonable to extrapolate that the same worst case results are also expected for any K= power of 2. No attempts have been made, however, to prove mathematically that the worst case port-port isolation results are indeed indentical for any K= power of 2."

5.6.2.5 Providing Redundant HPAs

If no redundancy were provided, HPA failures would reduce the power available at the "wanted" port and decrease the isolation of the "unwanted" ports. The power at the wanted port is the sum of K vectors, all aligned in phase. Therefore, the reduction in power from failure of L out of K HPAs is given by:

$$\Delta C = 20 \log10(K/(K-L)) \qquad dB$$

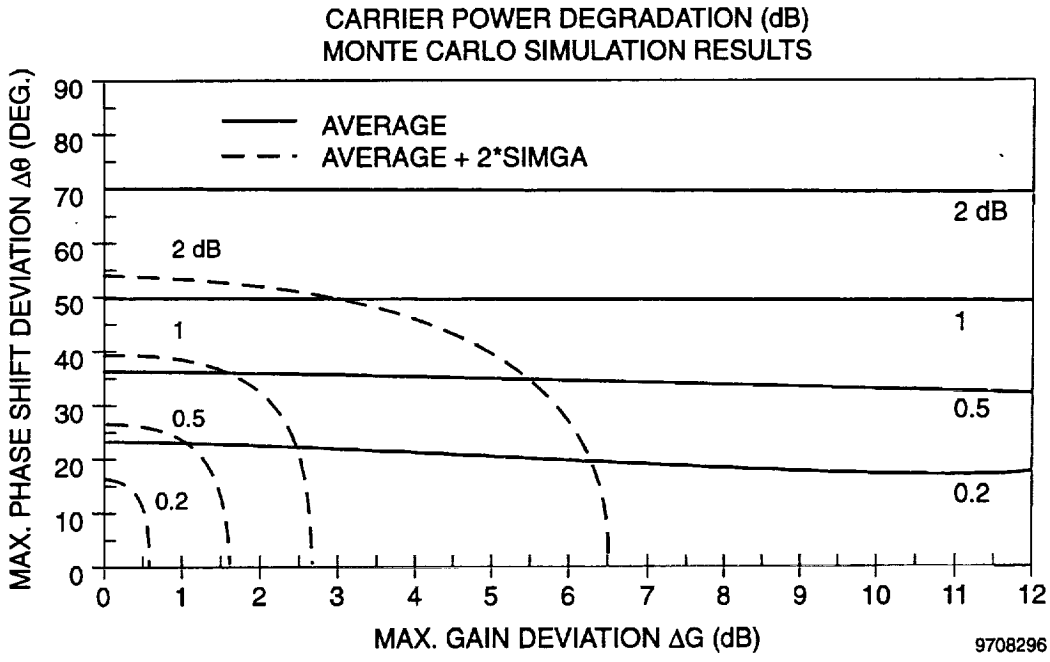

Figure 5-8. Contours of Average and (Average +2 x Sigma) of Carrier Power Degradation ΔC Due to Random Deviations in Characteristics of Input Matrix, HPAs or Output Matrix (K = 8 and # Monte Carlo Cycles = 20,000)

The isolation at unwanted ports depends upon pairwise cancellation of the K vectors. In the best case, the L failed HPAs would be paired such that the remaining K-L vectors would still cancel except when L is odd, in which case a single vector would remain uncancelled. In the worst case, L vectors would remain uncancelled and be aligned. The associated isolations, which establish the upper and lower bounds, are:

$$I_{so}\ \text{(best case)} = 20\log_{10}(K-L)\ \text{dB}\quad \text{where L is odd}$$
$$= \infty\ \text{dB}\quad \text{where L is even}$$
$$I_{so}\ \text{(worst case)} = 20\log_{10}((K-L)/L)\ \text{dB}$$

A table of values of ΔC and I_{so} taken from Vuong, Paul, and Cole showing their dependence upon K and L is given in Table 5-3. Note that for large K and for ideal input and output matrices (i.e., phases set according to ideal MPA theory), both the worst-case reduction in power and the worst-case isolation are probably acceptable. Nevertheless, it would be prudent to provide redundant amplifiers. Care must used in how the associated switching is accomplished so that the desired phase relations among output vectors are not perturbed when redundant units are brought into use.

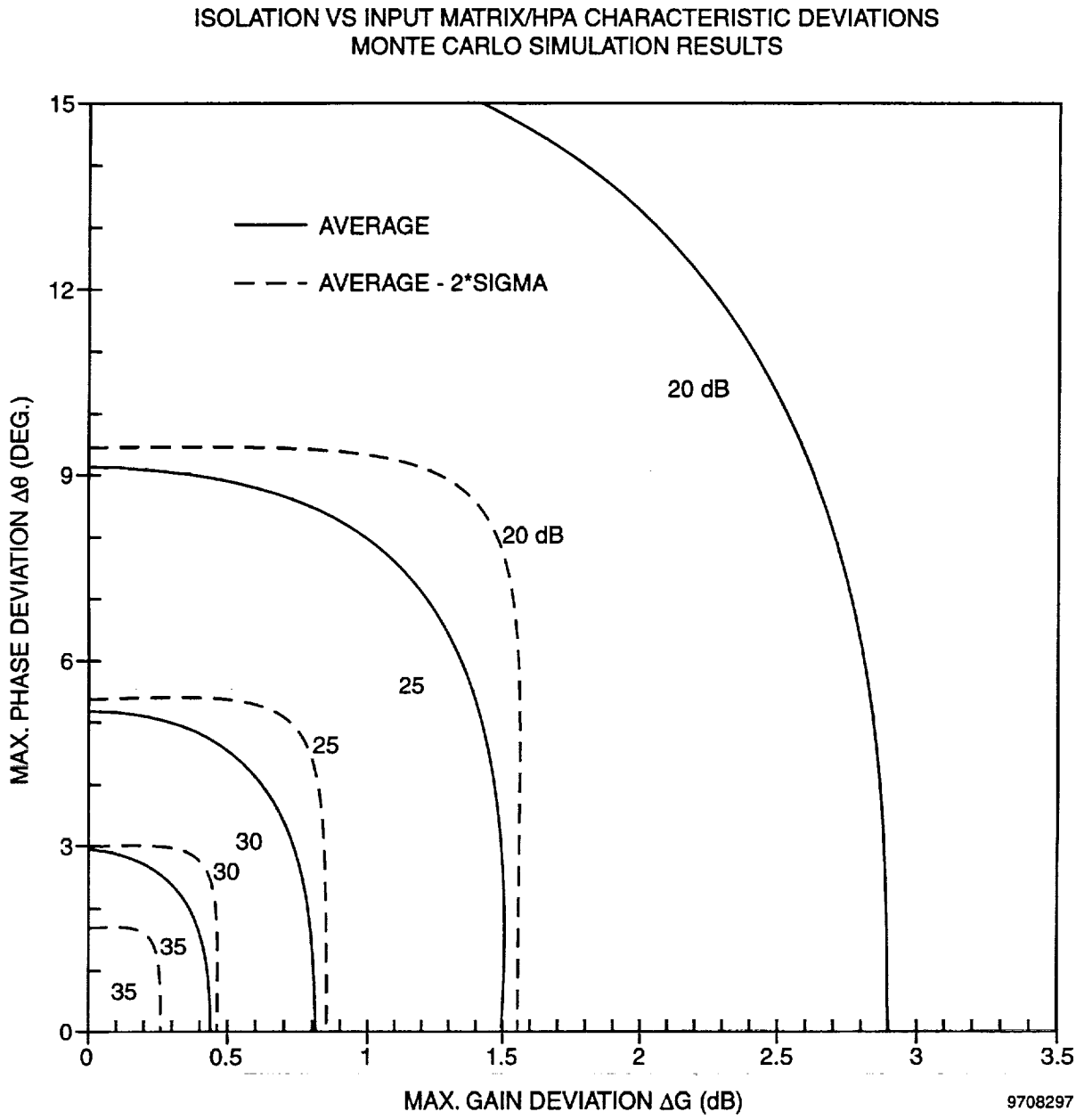

Figure 5-9. Contours of Average and (Average +2 x Sigma) of Port-Port Isolation I_{SO} Due to Random Deviations in Characteristics of Input Matrix or HPAs (K = 8 and # Monte Carlo Cycles = 20,000)

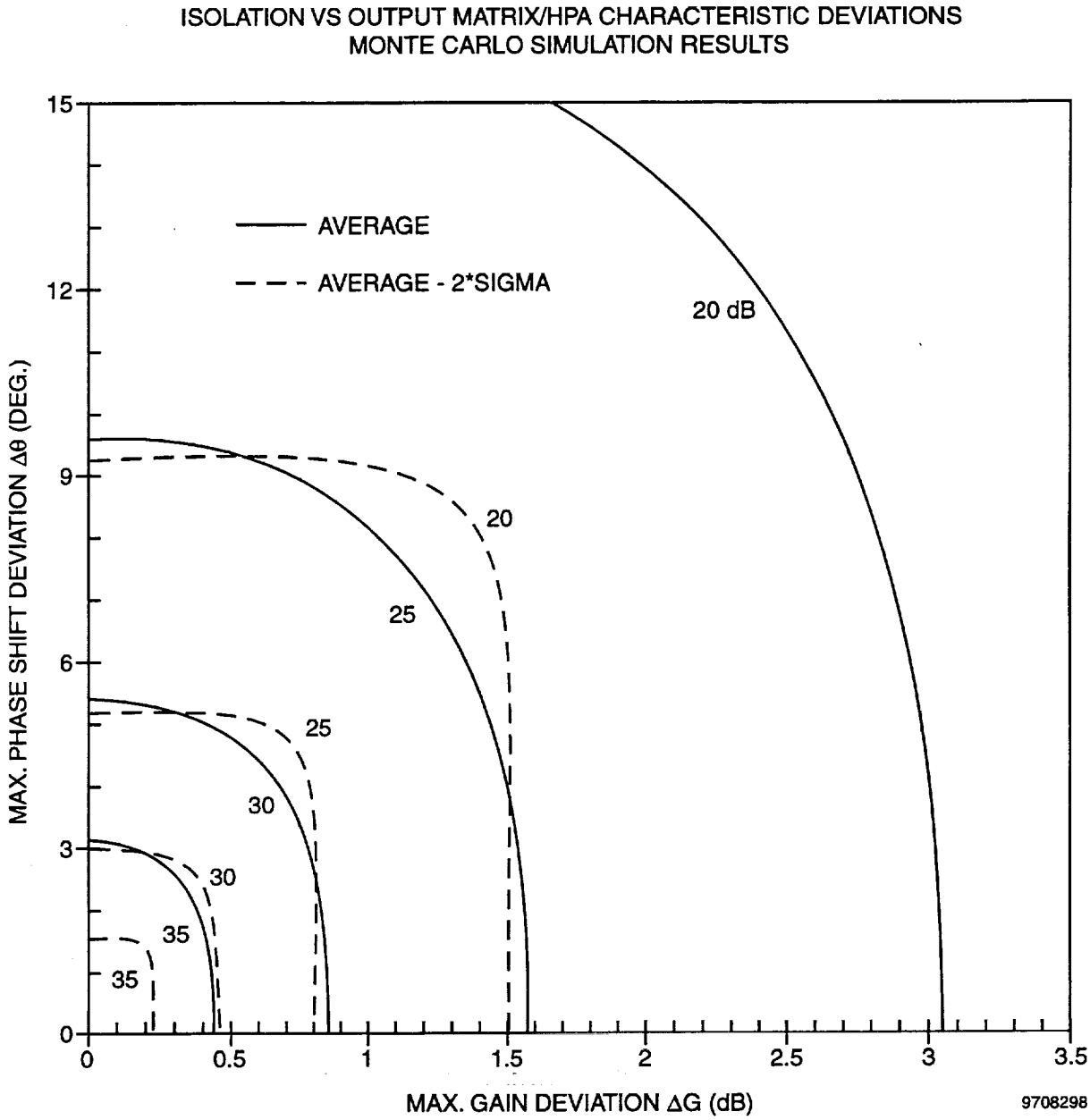

Figure 5-10. Contours of Average and (Average +2 x Sigma) of Port-Port Isolation I_{SO} Due to Random Deviations in Characteristics of Output Matrix or HPAs (K = 8 and # Monte Carlo Cycles = 20,000)

Table 5-3. Effects of HPA Failure on Carrier Power and Port-to-Port Isolation

L, No. of Failed HPAs	K, No. of Original HPAs	ΔC (dB)	Min. I_{so} (dB) (worst case)	Max. I_{so} (dB) (best case)
1	4	2.5	9.5	9.5
2	4	6.0	0.0	∞
1	8	1.2	16.9	16.9
2	8	2.5	9.5	∞
3	8	4.1	4.4	14.0
4	8	6.0	0.0	∞
1	16	0.6	23.5	23.5
2	16	1.2	16.9	∞
3	16	1.8	12.7	22.3
4	16	2.5	9.5	∞
1	32	0.3	29.8	29.8
2	32	0.6	23.5	∞
3	32	0.9	19.7	29.2
4	32	1.2	16.9	∞
1	64	0.1	36.0	36.0
2	64	0.3	29.8	∞
3	64	0.4	26.2	35.7
4	64	0.6	23.5	∞

5.6.2.6 Effects of HPA Nonlinearity

The effects of HPA nonlinearity can be summarized in the following statements, per Vuong, Paul, and Cole:

(1) When frequency reuse is not employed, the MPA intermodulation noise performance is better than that of conventional amplifiers operated at similar output backoffs.

(2) When frequency reuse is fully employed, the MPA intermodulation noise performance is worse than that of conventional amplifiers, but approaches their performance as the number of carriers in the system becomes large.

(3) When the number of carriers per MPA output (or channel) is small (i.e., 1, 2, or 3), the intermodulation noise for a conventional amplifier system is negligible. By contrast, the MPA intermodulation noise may not be negligible due to the existence of inter-port intermodulation products.

5.6.3 Active Transmit Lens Array

An active transmit lens array (ATLA) antenna has four major sections, three of which comprise the RF lens. The fourth is a feed array. These sections, shown in an artists sketch of a proof of concept antenna in Figure 5-11, are:

(1) A flat array of radiating elements launches the far-field spot beams.

(2) A corresponding array of power modules, one for each radiating element, supplies signal power to the radiating array. Each power module contains an amplifier and a delay line. Collectively, the delay lines of the modules constitute the center portion of the lens.

(3) Signals arrive at the modules from individual receive elements at their inputs.

(4) The receive elements are space fed, in turn, from an array of feed horns that is physically separate from the lens. Each far-field beam is created by the signals transmitted from a single feed horn. The beam direction is fixed by the location of the feed horn in the feed array.

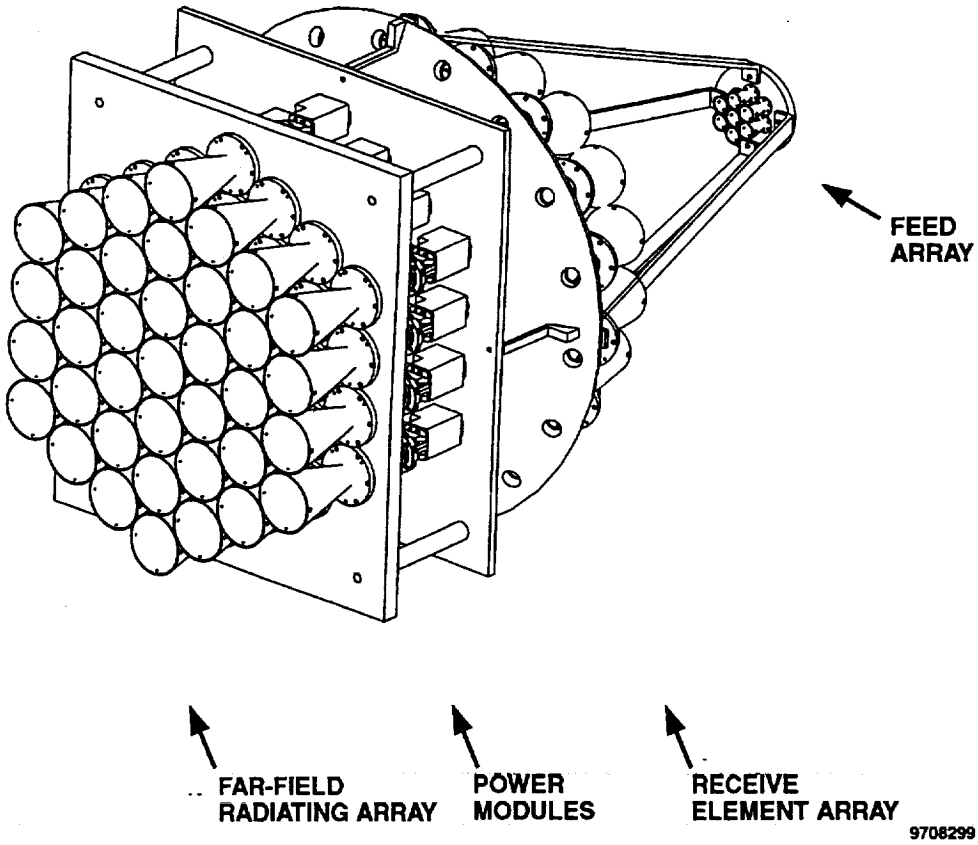

Figure 5-11. Active Transmit Lens Array Antenna Concept

The attraction of the ATLA is that no beam forming networks, per se, are required. Thus, in principle, a major difficulty encountered in the ATPA concept is avoided. The beam forming network is the lens which forms all beams simultaneously with directions determined by the geometry of the feed array and lens structure.

Both the ATLA and the ATPA lend themselves to solid state power amplifiers (SSPAs); thus heat dissipation remains a common challenge. For large arrays, creating several tens of beams each transmitting carrier data rates in the 60 to 100 Mb/s range, the power dissipation problem is acute.

These two similarities of the ATLA and the ATPA mean that their weights are comparable. As such, the above ATPA weight estimate, to a first order, applies to the ATLA also. A closer look at weight would likely show that the ATLA weighs slightly less than the ATPA because it does not have the multiple beam forming networks.

As with the ATPA, a major impediment to the ATLA technology is cost of the lens itself and, specifically, of the several hundred power modules. At Ka band, as noted above, a large number of modules is indicated for two reasons. First, the small size of the corresponding radiating elements means that a large number of such is required to create the desired narrow beamwidths. Second, the relatively small power available in Ka-band SSPAs means that tens of high-power beams require a large number of modules to achieve the total power.

5.6.4 Active Transmit Phased Array

Based on work done for Globalstar and on engineering work for an active transmit phased array (ATPA) antenna at Ka band (20 GHz) [38], it is known that the use of ATPAs for more than a relatively few beams from the same aperture is not practical. The difficulty arises in creating the beam forming networks (BFNs), one for each beam, in a physically small space. Each BFN must have the same number of outputs as there are antenna elements. Furthermore, an output from each BFN must be summed with corresponding outputs from all other BFNs to feed each one of the antenna elements. As the number of beams and antenna elements grows, the physical task becomes overwhelming just from a topological viewpoint. Globalstar achieves 16 beams. It is believed that Iridium also achieves 16-beams (from the FCC filing for Iridium, 48 beams per satellite are created in three separate phased arrays). The FCC filing for M-Star states that up to 32 beams are created in a single phased array. Although not a clear confirmation of the limited beam capacity, these are certainly indicative. In terms of the numbers of beams which are indicated in the current Ka-band multimedia filings, shown in Table 5-4, 16 beams is small. Even 32 beams (note that this antenna is only conceptual at this juncture; it has not been built) is fewer than is shown for all but one of the systems.

Table 5-4. Representative Ka-band Systems with Number of Beams per Satellite

System	Astrolink	CyberStar	NetSat 28	Spaceway	Teledesic	Volce Span
Company	L-M	SS/L	NetSat 28	HAC	Teledesic	AT&T
No. Beams	192	27	1000	48	64	64

5.6.5 Comparison of Total DC Power

The results of a first-cut analysis of total required DC power for the three sharing approaches (ATLA antenna, ATPA antenna, and MPA) for 128 beams and a required 60 Mb/s per beam into a 70-cm ground receive terminal are shown in Table 5-5. For each sharing approach, the per-carrier EIRP of 50.65 dBW is taken from Table 5-1. The number of active elements (i.e., SSPA transmit modules) for the active phased array and the active lens array are shown in Table 5-6. For the multiport amplifier, there is an active amplifier, which is assumed to be a TWTA, for each of the 128 beams.

Table 5-5. Total DC Power for Three Transmit Power-Sharing Approaches (assumes required EIRP of 50.65 dBW, 128 0.6-deg spot beams with 48.7 dBi peak gain)

Parameter	ATLA	ATPA	MPA
Loss to EOC	3.0 dB	3.0 dB	3.0 dB
Output loss (w/filter)	1.1 dB	1.1 dB	3.7 dB
Antenna peak gain	48.7 dBi	48.7 dBi	48.7 dBi
Req'd RF pwr per beam at HPA output	6.05 dBW (4.03 W)	6.05 dBW (4.03 W)	8.65 dBW (7.33 W)
Total Req'd RF pwr (=128 x above line)	515.8 W	515.8 W	938.2 W
HPA linear mode efficiency	14%	14%	45%
Total DC Power	**3685 W**	**3685 W**	**2085 W**

Table 5-6. Number of Active Transmit Modules (or Elements) for Three Sharing Technique

Parameter	ATLA	ATPA	MPA
Rated RF power per transmit module, assumed	1.0 W	1.0 W	25 W
HPA OBO, assumed	4.09 dB	4.09 dB	5.33 dB
RF power per transmit module	0.39 W	0.39 W	7.33 W
Number of active transmit modules	1323 (=515.8/0.39)	1323 (=515.8/0.39)	128 (=no. of beams)
Diameter of array, approximate at 19.2 GHz (see Appendix B)	43 antenna elements 69 inches (at 2.6λ spacing)	43 antenna elements 69 inches (at 2.6λ spacing)	N/A

The power dissipated and the size of the corresponding radiator for each sharing technique is indicated in Table 5-7 based on plausible efficiencies for the SSPA and TWTA units. This power is the sum of the power dissipated in the output loss and the power dissipated by the transmit modules themselves. The radiator size shown assumes a radiator capacity of 60 W/ft^2. A value of 45 to 50 W/ft^2 would be reflective of current capability.

What can be concluded from the above comparison? First, the power required for a large array-type sharing technique is about twice that required for an MPA technique. That is, of the two primary contributors to DC power differences, i.e., HPA efficiency and output circuit losses, the lower efficiency of the SSPAs dominates. Therefore, even with nearly a 4-dB output circuit loss, the MPA power, for the same EIRP per beam, is half that of the array techniques. Second, the additional power dissipation of the array-type techniques also requires larger solar arrays to generate the increased power and larger radiators to reject the heat.

An estimate of the increased weight associated with the larger power subsystem and the larger radiators, not to mention the increased difficulty of integrating the radiators into the spacecraft configuration, may be obtained. A current nominal value for Watts per pound for solar-power subsystems on large geosynchronous satellites with 12 year lifetimes is about 10 W per pound of total power subsystem weight. In the above comparison, the array-type techniques must generate 1600 W more DC power than the MPA technique. This would, nominally, translate into a power subsystem weighing 160 lbs more.

For the radiator panels (heat pipes embedded in aluminum honeycomb with face skins and optical solar reflectors (OSRs)), a nominal weight is 5 gm/in^2, or 1.6 lb/ft^2. Therefore, the weight difference occasioned by the larger radiators is approximately 44 lbs (=1.6 x 4.6 x 6). The total weight difference arising from these considerations is approximately 200 lbs. A

Table 5-7. Power Dissipated and Radiator Size for the Three Sharing Techniques

Parameter	ATLA	ATPA	MPA
Total DC power (per Table 5.6-2)	3685 W	3685 W	2085 W
Power dissipated at transmit module	3169 W	3169 W	1147 W
Power dissipated in output loss	116 W (=516 x (1-10$^{-0.11}$))	116 W (=516 x (1-10$^{-0.11}$))	538 W (=938 x (1-10$^{-0.37}$))
Total RF power dissipated	3285 W	3285 W	1685 W
Required radiator area	55 sq. ft. (=3285/60)	55 sq. ft. (=3285/60)	28 sq. ft. (=1685/60)
Dimensions of two radiator panels	4.6 x 6 ft. (two)	4.6 x 6 ft. (two)	4.6 x 3 ft. (two)

complete comparison of mass should include the array antennas themselves versus the multiple beam reflector antenna postulated for use with the MPA. It is believed that this comparison favors the reflector antenna.

Another consideration is the cost of the systems. Active arrays are much more expensive than are reflector antennas. The cost difference would be magnified for arrays with 50 to 100 beams compared to a reflector multiple beam configuration. It would be magnified even further to make good on the promise of arrays of beam steering and shaping. The cost of the input and output matrices for the MPA would not narrow the difference appreciably.

5.6.6 Multimode Amplifiers

A multimode amplifier is designed so as to achieve near maximum efficiency when operated at saturation as well as when operated at selected output power levels below this saturation level. Thus, if it is not raining in the area of a given spot beam, the amplifier for that beam could be run at reduced output power while still operating near peak efficiency. The DC power required to run the amplifier would be reduced in the same proportion (assuming no loss in overall efficiency) as is the output power and would be available for application to an amplifier connected to a beam whose area is experiencing rain. In this manner, the total DC power allocated to the satellite HPAs can be shared and could be much less than without this sharing, as discussed above.

This technology would be ideal for reflector multiple beam antennas (MBAs) where each beam is fed, typically, by a single HPA. It allows redundant amplifiers to be provided in the usual fashion, does not require large beam forming or switching networks to accomplish power sharing, is straight-forward and relatively simple to implement. However, while the multimode feature drops the output power level with very little loss in efficiency, it also drops the gain and has very little effect on the linearity. In other words, a multimode TWTA cannot be used for linearity enhancement. Therefore, the multimode amplifier would be used only in systems with a single carrier per HPA.

In almost all instances, the HPA of choice for this architecture would be a traveling wave tube (TWT) amplifier (TWTA). Especially at Ka band, TWTAs are capable of much greater power output and much higher efficiency than are solid state power amplifiers (SSPAs). High capacity, one of the required system characteristics for the target system, translates directly into high power HPAs. Thermal control considerations on the satellite also favor the higher efficiency TWTAs.

One might suggest that reduced output power of the HPA be achieved by merely backing off the drive level. However, because amplifier operating efficiencies fall drastically with reduced drive levels, this approach is not practical. The necessity for multimode operation

is seen by noting the approximate tube efficiencies for representative output power levels of a single-mode tube shown in Table 5-8. These efficiencies assume a 20-GHz TWT operated with a single carrier.

As a result of this loss of efficiency, even though the power consumption of a single-mode TWTA decreases, the dissipated power stays relatively constant.

In addition to a TWT efficiency loss, two other effects accompany reduced output levels in a single-mode TWTA and contribute to the attraction (at least in theory) of multimode TWTAs. First, the gain of the TWT increases. Although not a problem, a calibration would be required to determine the input backoff corresponding to a given desired reduction in output power level. Second, the efficiency of the electronic power conditioner (EPC) for the TWT would also drop. EPC efficiency varies with the processed power level. Typical EPC efficiencies for saturated TWT loads are in the range of 92% to 94%. At large values of OBO, where the total power consumption is reduced, the EPC efficiency will drop to as low as 86% to 88%.

It should be noted, however, that other effects also must be considered when contemplating use of a multimode TWTA. For output power reductions achieved by adjusting the operating voltages (a multimode TWTA), the adjusted voltages cause a decrease in cathode current in the TWT which, in turn, reduces the output power. The reduction in effective current density through the tube reduces the gain per inch in the TWT circuit. For any given physical geometry, the gain continues to drop as the current density is reduced. For a 10 dB output power range, the gain of a single-mode TWT would drop by at least 30 dB. [Below a certain threshold, usually around 30 dB, the TWT efficiency will basically fall off a cliff because the tube requires a certain minimum gain level in order to operate properly.] This change would have to be offset in the drive circuits and would likely seriously perturb the phase of the signal being transmitted. It would need to be determined whether the ground receiver could track through this perturbation. Also, the statement made above regarding reduced efficiency of the EPC for a single-mode TWT applies to a multimode TWT as well. When the processed power level drops, whether in a single-mode or a multimode TWT, the EPC efficiency will drop.

Table 5-8. Representative Single-Mode TWT Efficiencies at Several Output Backoff (OBO) Levels

TWT Operating Point	Approximate TWT Efficiency
0 dB OBO (saturation)	58%
3 dB OBO	40%
10 dB OBO	15%
20 dB OBO	2% or less

To date, multimode TWTAs with the necessary span in output power have not been realized. To offer significant rain fade mitigation at Ka band independent of other approaches, a power level difference of at least 10 dB is desired. It is our opinion that a 10-dB output power range using commandable voltage steps is completely impractical. While dual and triple mode tubes for space have been achieved (none of which were built using modern technology), the span in output power levels has not exceeded 6 dB. For example, an L-band triple-mode TWTA was baselined for and flew on Marisat with nominal, 0 dB, 3 dB, and 6 dB OBO modes. Marisat was a very successful program.

Apparently, the number of power levels is not the efficiency driver. Rather, TWT efficiency is a function of the span of the power range. Over an output power range of 3 dB, very little loss of efficiency will occur. Over 6 dB, expect an efficiency drop of from 15% to 25%. The resulting efficiency can be increased, theoretically, by increasing the complexity of the EPC so that more than just the anode voltage is adjusted. This has, to our knowledge, never been successfully implemented. One might envision separate EPCs in parallel, one for each mode. However, EPCs and tubes must come on-line together and must be cycled through a warm-up period prior to coming on line. The typical turn-on period is about 3 minutes. The consequent disruption to the transmitted signal would likely be unacceptable. Also, this multiple EPC approach would be much heavier. These considerations, to date, have meant that a multimode TWTA is almost never used because the perceived benefits do not offset the added complexity and mass.

For example, in the ACTS program, a 1988 study [39] "compared the spacecraft resources required for an operational system employing either dual-power TWTAs or fixed power TWTAs using [then current] technology." The study found that "the ACTS dual-power system ... offer[ed] no major advantages compared to a conventional ... fixed-power system."

It should be stated that perturbations to the transmitted signal will be experienced not only when changing the EPC, as mentioned earlier, but also when changing modes in a multi-mode TWTA. For a very large power change (>6 dB), the carrier would likely have to be taken down. It might also be necessary to turn off all high voltage in the EPC. At this point, the warm-up cycle would be initiated and the overall downtime would be about 3 minutes.

In summary, the multimode TWTA for large (>6 dB) changes in output power appears to be infeasible. For changes less than 6 dB, a multimode TWTA might be used in conjunction with data and code rate changes to provide up to 16 dB of rain fade mitigation by halving the data rate and simultaneously introducing rate one-half forward error correction coding. Note, however, that development for such a multimode tube at Ka band was not successful during the ACTS development and has not been reinitiated.

5.6.7 Conclusions for Downlink Power Sharing

It is concluded that the multiport amplifier (MPA) offers significant promise for downlink power sharing of many tens of downlink beams. In contrast, the active transmit lens array (ATLA) and the active transmit phased array (ATPA) antennas would find application only for relatively smaller numbers of total beams. This is not to say that the MPA will, after considered engineering design effort, prove feasible at Ka band (20 GHz). Nevertheless, it is believed to be feasible at this time. Vuong, Paul, and Cox concluded that an MPA was feasible at X band (7.5 GHz). As discussed in section 5.5, power sharing by code and data rate changes, is also feasible. The advantage of the MPA is there is no disruption to data rate nor need for synchronization of code and data rate changes at the transmitter and at the receiver.

SECTION 6 — FADE COMPENSATION FOR ATM'S ABR TRAFFIC

To limit the impact of congestion on performance of ATM connections, the ATM Forum is in the process of adopting several feedback control mechanisms for the ABR traffic. This section evaluates these mechanisms for satellite links which use the information rate reduction and code rate change technique to compensate for rain attenuation during bad-weather conditions. The feedback controls considered are end-to-end binary feedback, explicit rate feedback, and virtual source and destination feedback. This section also discusses the system configuration for implementing fade compensation, using the COMSAT ATM Link Accelerators (ALAs).

6.1 ATM OVERVIEW

ATM was initially developed as a transfer mode solution for Broadband Integrated Services Digital Networks (B-ISDN) operating at bit rates of 155 Mbps and higher, but soon it was realized that it could be employed in the local area as well. Indeed, one of the major advantages of ATM is that it represents an opportunity to integrate in a seamless manner the wide-area, metropolitan-area, and local-area domains.

Common to all technologies which bear the name or associate themselves with ATM is the notion of cell relay. A cell is just a fixed-size, fixed-format packet. The ATM cell, as shown in Figure 6-1, is 53-bytes long, of which the first five bytes are headers and the remaining bytes are referred to as payload. Among the advantages of such a rigid packet structure are:

(1) Ease and low cost of implementation of cell processing in VLSI chips,

(2) Higher per-packet processing speed,

(3) Lower per-packet queuing delay, and

(4) Easier buffer allocation.

The disadvantages are bandwidth inefficiency (i.e., an unavoidable 9.4 percent overhead in ATM) and processing overhead for many types of traffic (e.g., bulk data transfer) which are more suited to larger, variable-size frames. The relatively small size of the ATM cells contributes to lower and less variable network latency and easier allocation of bandwidth, but exacerbates the disadvantages mentioned above for some traffic types.

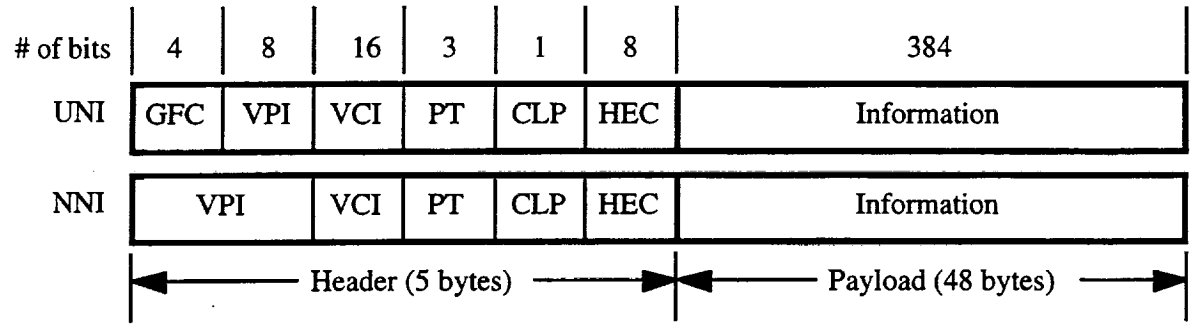

UNI:	User Network Interface	VCI:	Virtual Channel Identifier
NNI:	Network Node Interface	PT:	Payload Type
GFC:	Generic Flow Control	CLP:	Cell Loss Priority
VPT:	Virtual Path Identifier	HEC:	Header Error Control

Figure 6-1. ATM Cell Format

There are numerous proposals on how ATM cells might be relayed: over shared or dedicated media; in a ring, dual-bus, or star topology; over synchronous or asynchronous transmission infrastructure; etc. An emerging paradigm appears to be switch-centric with dedicated media connecting data terminal equipment in a star topology to a local switch optimized for local area networking; the local switches are connected to wide-area ATM switches; and these switches are interconnected in a relatively arbitrary topology. The local connections to a switch are typically via either a synchronous or asynchronous transmission protocol, and the inter-switch connections via a synchronous protocol.

ATM cells are multiplexed contiguously in a sequence and transmitted in a transmission link. To identify and route each cell, a label which contains routing information is carried in the cell header. When an ATM switch receives a cell, switching is performed by reading the label and consulting the routing table to determine the outgoing path. The routing table must be set up in advance, either pre-assigned or dynamically allocated. This requires an end-to-end connection to be established prior to actual transmission of ATM cells. Associated with each connection, a virtual channel identification (VCI) is assigned, the traffic usage parameters are specified, and the quality of service (QoS) parameters, such as allowable cell loss ratio (CLR), etc. are determined.

In ATM, the type of service will be negotiated with an ATM provider when the connection is established. At that time, the user will provide a description of the service desired and the constraints within which the user is willing to accept (e.g., average data rate and maximum data rate). Once a connection is established, there is an agreement that the network will provide the desired service as long as the user stays within his constraints. This sounds fairly simple in concept, but the details of how the user-network agreement is

reached, what happens if any of the parties fail to live up to their end of the agreement, how agreements are coordinated across possibly many switches, how the switch can help shape terminal traffic, etc. are complex, numerous, and contentious. The ATM Forum, in its User-Network Interface (UNI) specification, has taken the first steps in providing some definitions in this area, but there is a great deal more to do.

6.1.1 ATM Service Categories

The ATM Forum currently defines five service categories [40]:

(1) Constant Bit Rate (CBR),

(2) Real-Time Variable Bit Rate (rt-VBR),

(3) Non-Real-Time Variable Bit Rate (nrt-VBR),

(4) Available Bit Rate (ABR), and

(5) Unspecified Bit Rate (UBR)

ATM service categories may be arranged into two groups: those supporting real-time applications and those which do not. Real-time service classes are CBR and rt-VBR. The non-real-time service classes are nrt-VBR, ABR, and UBR. Table 6-1 provides the attributes of the ATM service categories [41].

Table 6-1. Attributes of ATM Traffic Categories

Service Category	Typical Traffic Type	Cell Switching Priority	Bit Rate	Delay Sensitivity	Target CLR for CLP=0
CBR	Voice or video	High	Constant	Yes	1.7 E-10
rt-VBR	Image or compressed video	Medium	Bursty	Yes	1.0 E-7
nrt-VBR				No	
ABR	Data	Low	Bursty	No	1.0 E-7
UBR	Data (email, fax, file transfer)	Low	Bursty	No	No target

6.1.1.1 Constant Bit Rate

The CBR service supports leased line connections and real-time applications such as voice and video by providing end-to-end timing recovery. The traffic can be characterized by a constant cell arrival rate, which corresponds to a peak cell rate (PCR), and therefore, it requires a predefined dedicated capacity equivalent to its PCR. Cells conforming to this traffic pattern are guaranteed a QoS. A CBR contract typically specifies the cell loss ratio (CLR), cell delay variation (CDV), and maximum cell transfer delay (CTD) as the QoS parameters.

6.1.1.2 Variable Bit Rate

The VBR service supports bursty applications which can benefit from statistical multiplexing. Based on traffic delay requirements, the VBR service is further divided into two sub-categories, referred to as rt-VBR and nrt-VBR. The rt-VBR service is intended for real-time applications with variable bit rate such as packetized voice and video applications. The nrt-VBR service is intended for non-real-time applications such as data services. In contrast to CBR, where a constant amount of capacity equivalent to PCR is pre-reserved, VBR requires an average capacity which is equal to the sustainable cell rate (SCR). The rt-VBR traffic contract specifies an acceptable CLR, CTD as well as CDV. Compared to the CBR and rt-VBR service categories, the nrt-VBR category does not place stringent requirements on the network for CDV and CTD, and only a mean CTD is ensured.

6.1.1.3 Available Bit Rate

Similar to nrt-VBR, the ABR service category is suitable for data applications such as e-mail, fax transmission, file transfers, and Telnet. The main difference is a guarantee for a minimum throughput, known as minimum cell rate (MCR), as opposed to the VBR's average cell rate SCR. In addition, the ABR service is designed to support applications which cannot effectively characterize their traffic behavior at connection establishment but can adapt their traffic following a feedback flow control protocol. For example, ABR transmission rates may be reduced due to a congestion indication from the network. In the ABR service, if the source behaves in a certain way in response to feedback flow control , then no packets will be intentionally dropped.

6.1.1.4 Unspecified Bit Rate

The UBR service category is intended for applications which are tolerant to delay and do not require non-real-time response. Furthermore, no guarantees on the CLR are offered, thus leaving it to the end-system applications to handle. With this service, the user is willing to tolerate whatever capacity and cell loss the network can provide at the instant the cell goes through the network. Therefore, UBR is ideally suited to low-cost and low-priority services such as electronic mail or low-tariff file transfers. Practically, large buffers are used to minimize cell loss at the expense of delay.

6.1.2 ATM Adaptation Layer

To support the multiplicity of user information within a common ATM cell structure, the ATM adaptation layer (AAL) is defined for five classes of user information:

(1) Type 1: intended to provide connection-oriented, CBR traffic.

(2) Type 2: intended to provide connection-oriented, rt-VBR traffic.

(3) Type 3/4: intended to provide connection-oriented and connectionless, nrt-VBR, ABR, and UBR traffic.

(4) Type 5: This protocol grew out of concerns about the complexity for Type 3/4. Its original name was Simple and Efficient AAL (SEAL), and it performs a subset of AAL Type 3/4 functions.

The primary purpose of the AAL is to map user information into ATM cells in the most suitable form for a desired application. The AAL functions include segmentation, reassembly, sequence numbering, error protection, and transmission of timing information.

6.1.3 ATM Layer

The ATM layer provides for the transparent transfer of ATM service data units (SDU) over already existing virtual circuits among communicating users. All ATM SDUs are simply 48 bytes of data. The functions performed by the ATM layer include:

(1) Multiplexing of ATM connections

(2) Cell relay and routing

(3) Cell delineation

(4) Payload type discrimination

(5) Selective cell discarding

(6) Cell rate shaping

(7) Enforcement of traffic contract.

6.1.4 Physical Layer

The physical layer provides ATM cells transportation services to the ATM layer. It consists of two sublayers: the Physical Medium (PM) sublayer and the Transmission Convergence (TC) sublayer. The PM sublayer performs physical medium dependent functions such as specifying the physical medium, the transmission characteristics, and the insertion and extraction of timing information. The TC sublayer performs cell delineation, cell rate decoupling, Header Error Check (HEC) generation and verification, and mapping the cells received from the ATM layer into frames of the transmission system. The HEC field is used for cell header single-bit-error correction and multiple-bit-error detection. Cells with uncorrectable errors in the cell header are discarded.

Currently, there are two major groupings of physical layer protocols for ATM:

(1) Based on Plesiochronous Digital Hierarchy (PDH)

(2) Based on Synchronous Digital Hierarchy (SDH).

PDH is basically the existing digital telephony transmission system. There are five levels in the PDH, though the bit rates associated with these levels vary with geological region. In the U.S., the levels of the hierarchy are DS-0 (64 kbit/s), DS-1 (1.544 Mbit/s), DS-2 (6.312 Mbit/s), DS-3 (44.736 Mbit/s), and DS-4 (139 Mbit/s). The ATM Forum has defined a way for the DS-1 and DS-3 framing structures to carry ATM cells.

SDH is a flexible synchronous time division multiplexing transmission system defined by the ITU-T to carry data streams at rates higher than those defined in PDH. SDH was derived from Synchronous Optical Network (SONET). SONET defines a set of framing formats, transmission speeds, and multiplexing standards. The first level of the SONET framing hierarchy is STS-1 (51.84 Mbit/s). When the STS-1 structure is carried over fiber optic medium, the resulting service is called OC-1. Higher synchronous rates (STS-N) are achieved by multiplying the basic rate by N (e.g., OC-3 (155.52 Mbit/s), OC-12 (622.08 Mbit/s), OC-48 (2488.37 Mbit/s)). To transport ATM cell streams over SDH/SONET, the TC sublayer performs the mapping of the ATM cell into the SDH/SONET frames. All timing and synchronization functions are performed by the SDH/SONET transmission systems.

6.1.5 ATM Traffic Management

The ATM layer defines a comprehensive set of ATM service categories controlled by a sophisticated set of traffic management functions and procedures. The challenge is to balance a high quality service with maximum network utilization. For example, a low network utilization is expected if capacity is reserved for PCRs of every connection to achieve a high service quality. This option is uneconomical to operate because all connections do not continually operate at full capacity. Another option is to allocate resources in a way in which there are always more connections than available capacity. In this case, the network utilization will be high, but the QoS will be unacceptable during peak usage periods. Therefore, effective traffic management requires end-to-end participation of all network elements. Traffic management functions and procedures at an ATM node are typically distributed among interface modules, switch fabric, and a control module. The four traffic management building blocks are:

(1) Traffic parameter descriptors,

(2) Quality of Service parameters,

(3) Connection admission control (CAC),

(4) Conformance monitoring and enforcement, and

(5) Congestion control.

6.1.5.1 Traffic Parameter Descriptors

A traffic descriptor defines the bandwidth guidelines to which a connection within a service category must adhere. Traffic descriptors are required to ensure proper resource allocation and guarantee the QoS across an ATM network. A traffic descriptor has two key elements: Source Traffic Descriptor and Cell Delay Variation Tolerance (CDVT).

The Source Traffic Descriptor is a set of parameters which describes the expected bandwidth utilization which the connection needs. These parameters are PCR, SCR and Maximum Burst Size (MBS), and MCR. The set of traffic descriptors conveyed at connection set up varies depending on the connection's service category. A sustained bi-directional connection has a set of connection traffic descriptors for each direction. Note that the descriptor sets need not be the same for each direction. Source traffic descriptors can specify CLP_0 cell traffic, or the aggregate CLP_0+1 traffic.

The CDVT is a network descriptor that provides a measure of the jitter in the cell inter-departure pattern of a given connection. Jitter is typically caused by the multiplexing effect of placing several virtual circuits on a single connection.

6.1.5.2 Quality of Service Parameters

ATM QoS is measured and specified in terms of the following parameters:

(1) Cell Delay Variation (CDV),
(2) Maximum Cell Transfer Delay (Max CTD),
(3) Cell Loss Ratio (CLR),
(4) Cell Error Ratio (CER),
(5) Severely Errored Cell Block Ratio (SECBR), and
(6) Cell Misinsertion Rate (CMR).

Of these six QoS parameters, only CDV, max CTD, and CLR are specified on a per-connection basis. CER, CMR, and SECBR take default values which the network guarantees to meet for all connections. Specification of individual QoS parameters is currently supported by the ATMF UNI Signaling 4.0. In addition, the ATMF UNI Signaling 4.0 provides mechanisms for the negotiation of CDV, max CTD, and CLR between the user and the network.

The traffic descriptors and QoS parameters are the main components of a traffic contract representing a mutual agreement between the user and the network provider. The user specifies its connection descriptors and a set of QoS parameters in each direction, and the network agrees to provide the QoS level specified in this contract.

6.1.5.3 Connection Admission Control

Connection Admission Control (CAC) is the set of actions taken by the network during the connection set-up phase in order to determine whether a connection request can be accepted or denied, and to ensure that existing connections are not affected when a new one is established. CAC involves determining the bandwidth/capacity required by each connection along the path to support the traffic descriptors and the QoS requirements included in the traffic contract. If a connection request is accepted, the network allocates certain bandwidth capacity to the connection. The end-systems and all intermediate ATM nodes are active participants of CAC. Each node along the path can reject the connection request if it can not meet the defined QoS parameters.

The set of traffic descriptors and QoS parameters indicated for a connection request depends on the ATM service category. Therefore, the computation of the required bandwidth is different for each category. The simplest CAC algorithm allocates bandwidth equivalent to the PCR for each connection. Although this is appropriate for CBR connections, it proves to be overly conservative for VBR connections. Service providers can take advantage of significant statistical multiplexing gains in VBR using the lower SCR parameter, rather than PCR. Service providers prefer powerful CAC algorithms which take into account SCR, as well as PCR, for accepting or refusing a connection request. This optimizes utilization of network resources for VBR traffic and ensures that the network meets the required QoS of the new connection, as well as maintaining the agreed QoS of the existing connection.

For CAC to be credible, the algorithm needs to factor in all of the standard traffic descriptors. In addition, a unique algorithm is required for each of the five service categories: CBR, rt-VBR, nrt-VBR, ABR and UBR. Ensuring that each of these algorithms is optimal will result in efficient allocation of network bandwidth. Thus, how refined these algorithms are will determine how efficiently bandwidth is allocated.

6.1.5.4 Conformance Monitoring and Enforcement

When a network carries an ATM connection, it commits to provide the agreed QoS to all the cells conforming to the theoretical generic cell rate algorithm (GCRA). The GCRA has been selected by both the ITU-T Recommendation I.371 and ATM TM 4.0 specification to define conformance with respect to the source traffic descriptors and the CDVT. To achieve this objective, the network polices the traffic of the connection to detect non-conforming cells, and takes appropriate action on these cells to prevent them from affecting the QoS of the conforming cells of other connections. The compliance enforcement is done by a Usage Parameter Control (UPC) process at the UNI and optionally by a Network Parameter Control (NPC) process at the NNI (Network-to-Network Interface).

The CAC and UPC/NPC functions must work together to protect the network from congestion while meeting the network performance objectives of all current connections. The CAC uses the traffic descriptors of the connections to allocate bandwidth/capacity, while the UPC/NPC polices the network connections, making sure the traffic conforms to the traffic descriptors. In this way, users are isolated from one another, and are not affected by any "misbehaving" users.

A UPC/NPC process implements one or more leaky bucket algorithms to police each connection. Each leaky bucket mechanism has two parameters: the increment parameter corresponds to the inverse of the compliant rate (fill rate of the bucket) and the limit parameter corresponds to the number of cells that can burst at a higher rate (size of the bucket). When more than one traffic descriptor is used (for example, PCR and SCR) for a connection, multiple leaky buckets are cascaded, with the highest rate being policed first. For example, ATM connections carrying frame relay service may actually define three traffic descriptors and thus require three leaky buckets: PCR0, PCR1 and SCR0.

6.1.5.5 Congestion Control

There are two general categories of congestion control: preventive control and reactive control. As indicated by their names, a preventive control technique prevents congestion by taking appropriate actions before it actually occurs. In a reactive control technique, the network is monitored for congestion. When congestion is detected, sources are requested to slow down or stop transmission until the end of congestion.

Early Packet Discard (EPD) and Partial Packet Discard (PPD) are preventive congestion examples. A network can quickly experience a state of congestion as increasing levels of cell loss generate more and more packet re-transmission requests. EPD fixes the problem of flooding the network with re-transmissions by discarding cells on a packet level rather than a cell level. This drastically reduces useless traffic caused by the transfer of corrupted data packets which have to be re-transmitted by the sender. EPD and PPD are applied to ABR and UBR traffic of AAL Type 5 connections, which are used especially for this packet traffic.

Feedback flow control mechanisms are considered reactive control techniques which can be used to guarantee the QoS of existing connections in case network capacities run low. The objective is to reduce the overall traffic in a way that the network never reaches an undesirable state of congestion. As mentioned previously, the ATM network informs the traffic sources of impending congestion; on receiving this information, the traffic sources stop increasing or slow down their traffic. Table 6-2 indicates that implementation of a feedback flow control mechanism is mandatory for the ABR service category and optional for the other services. Section 6.2 provides a summary of several feedback flow control mechanisms.

6.2 ABR FEEDBACK FLOW CONTROLS IN RAIN FADE COMPENSATION

ATM has essentially been designed for use over very stable transmission media with low error rates such as those provided by optical fiber cables. Satellite networks are inherently noisier than terrestrial wired systems and often suffer from added impediments such as rain fades. These impediments reduce the performance of satellite links. To improve performance of satellite links, non-adaptive approaches such as coding and built-in link margins are often used in satellite links. However, these techniques may not be economically attractive for satellite links which experience severe rain attenuation. This is because significant satellite resources must be reserved for bad-weather operations, and therefore wasted during clear weather condition. To improve satellite resource utilization, adaptive fade compensation approaches such as information rate reduction, code rate change and uplink power control have been proposed for use in satellite links which may otherwise be severely degraded.

The use of the information rate reduction and code rate change technique to compensate for rain fades with no feedback mechanisms to dynamically control the source rate can lead to severe cell loss. Thus, this fade compensation technique requires an adaptive adjustment of source information rates for active ABR connections over a fading satellite link to maintain an acceptable performance. The ABR feedback control mechanisms will provide this adaptive rate adjustment capability.

Table 6-2. Feedback Controls for ATM Traffic

Service Category	Service Guarantee	Feedback Control
CBR	Capacity for PCR, Max CTD and CDV	Optional
VBR	Capacity for SCR, Max CTD and CDV for rt-VBR, Mean CDV for nrt-VBR	Optional
ABR	Capacity for MCR	Mandatory
UBR	Nothing	Optional

6.2.1 ABR Feedback Flow Control Mechanisms

There are essentially three mechanisms [40], where feedback controls enable each participating ABR source to adapt its information rate to a satellite channel condition. The activation of a feedback control mechanism is assumed triggered by a notification message originated from the earth station's fade compensation equipment. This is different from the typical terrestrial implementation, where the feedback congestion controls are based on switch buffer thresholds. The notification message is then relayed to a switch with ABR traffic being sent to the earth station for transmission over the satellite. At the switch, certain cells are appropriately marked that will be used by their ABR sources to adjust the information rates. The processing of rate adjustment requests can also be accomplished at the earth station. However, this would require a system configuration that integrates satellite networks with ATM. Section 6.3.2 discusses the integrated system configuration in greater detail.

6.2.1.1 End-to-End Binary Feedback

Binary feedback is a flow control mechanism where a network element marks the Explicit Forward Congestion Indication (EFCI) bit in the Payload Type Indicator (PTI) field of the data cell header as "congestion experienced" until the end of a congestion duration. The destination end-system which receives data cells with EFCI=1 may notify the source end-system of congestion (e.g., to inform the traffic sources that the satellite link is attenuated). The source notification is accomplished through the use of Resource Management (RM) cells which are turned around by the destination.

Figure 6-2 depicts the binary feedback control of ABR traffic over a satellite link. Under the clear-weather condition, a source end-system sends all of its data cells with the EFCI bit set to zero and inserts RM cells at a frequency proportional to the number of data cells sent. Once rain fades are detected and compensation is activated, the transmit earth station sends a fade notification message to the switch supporting the active ABR connection. The switch responds by setting the EFCI bit to one for all data cells.

Upon reception of a forward RM cell, the destination end-system turns the RM cell around with the direction (DIR) bit changed to backward. The congestion indication (CI) bit of the backward RM cell is set to one if the last "N" consecutive received data cells had their EFCI bits equal to one. The destination end-system may use this information to lower its transmission rate. Note that the destination may generate backward RM cells without having received a forward RM cell. The rate of these backward RM cells is limited to 10 cells/sec per connection [40].

When a backward RM cell with CI=1 is received, the source cell transmission rate is reduced by a rate decrement factor (RDF). The RDF factor is a negotiated parameter during the signaling phase. The simplified flow diagram of this procedure is shown in Figure 6-3.

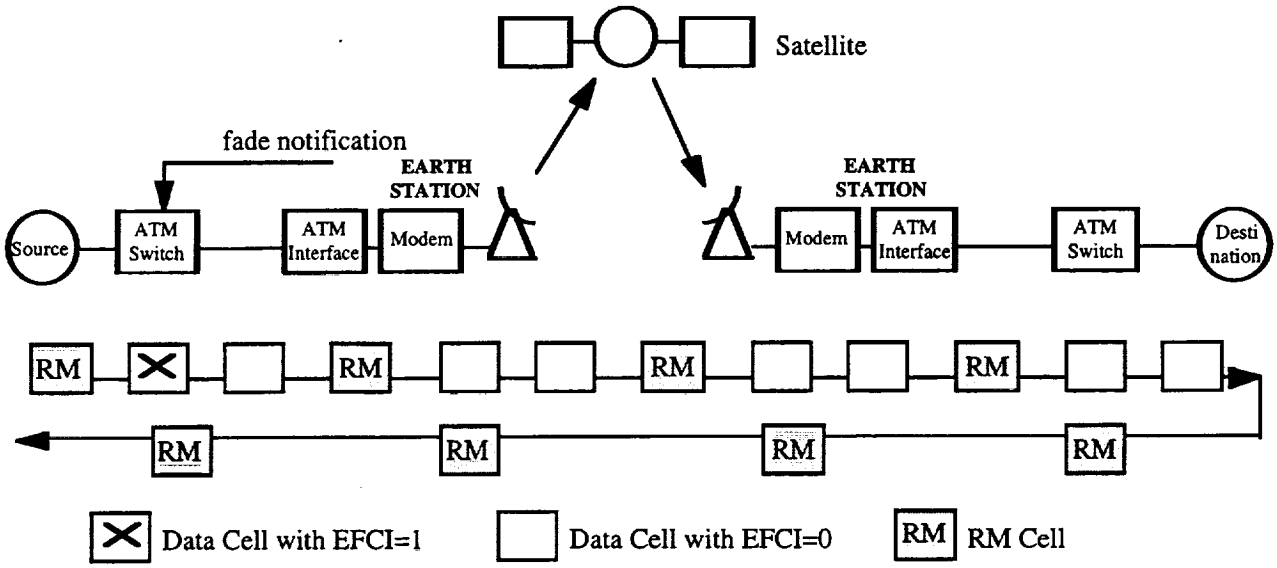

Figure 6-2. End-to-End Binary Feedback Flow Control

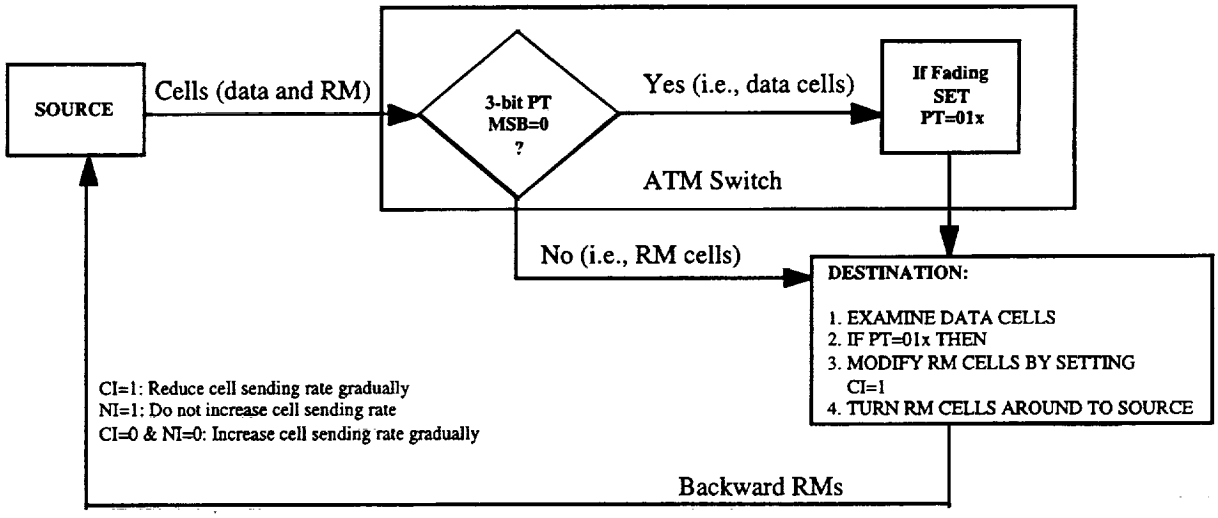

Figure 6-3. Simplified Flow Diagram of End-to-End Binary Feedback Control

6.2.1.2 Explicit Rate Feedback

Because of a gradual rate adjustment dictated by the end-to-end binary feedback, the explicit rate feedback mechanism allows for any network element to request ABR sources to transmit cells at any desired rate (i.e., between MCR and PCR). Hence, this mechanism is adaptive to network conditions since ABR sources can react effectively to congestion status along their paths. Specifically, each end-system periodically generates RM cells and injects them into the connection. Any intermediate network element along the ABR path can have access to forward and backward RM cells to modify explicit cell rate (ECR) values based on available capacity and impending congestion condition. However, no network element should ever increase the ECR value since this would result in the loss of information if a more stringent congestion situation is encountered somewhere along the path.

Figure 6-4 depicts an over-the-satellite ABR connection using the explicit rate feedback as a flow control mechanism. A transmit earth station detects rain fades and activates compensation by reducing the information rate on the satellite link. A fade notification message is sent by the earth station to the switch supporting the active ABR connection. The switch responds by inserting feedback control information into RM cells (setting the CI bit and ECR field) when they pass in the forward and backward direction. Upon receiving a backward RM cell with CI=1, the source end-system adjusts its cell transmission rate to the value in the ECR field. Similarly, the destination end-system adjusts its transmission rate to the value in the ECR field of a forward RM cell with CI=1. The simplified flow diagram of this procedure is shown in Figure 6-5.

6.2.1.3 Virtual Source and Destination (VS/VD) Feedback

VS/VD is essentially the explicit rate feedback flow control mechanism for an ABR connection segmented at several intermediate network elements. The first ABR segment is sourced by the source end-system. Each adjacent ABR control segment is sourced by a virtual source, which assumes the behavior of the source end-system. Each ABR control segment, except the last, is terminated by a virtual destination, which assumes the behavior of the destination end-system. Forward RM cells received by a virtual destination are turned around and not forwarded to the next segment of the connection. The DIR bit of the forward RM cell is changed from "forward" to "backward." When congestion occurs, the CI field is set to one and the ECR field is set to an appropriate value. Backward RM cells received by a virtual source are removed from the connection.

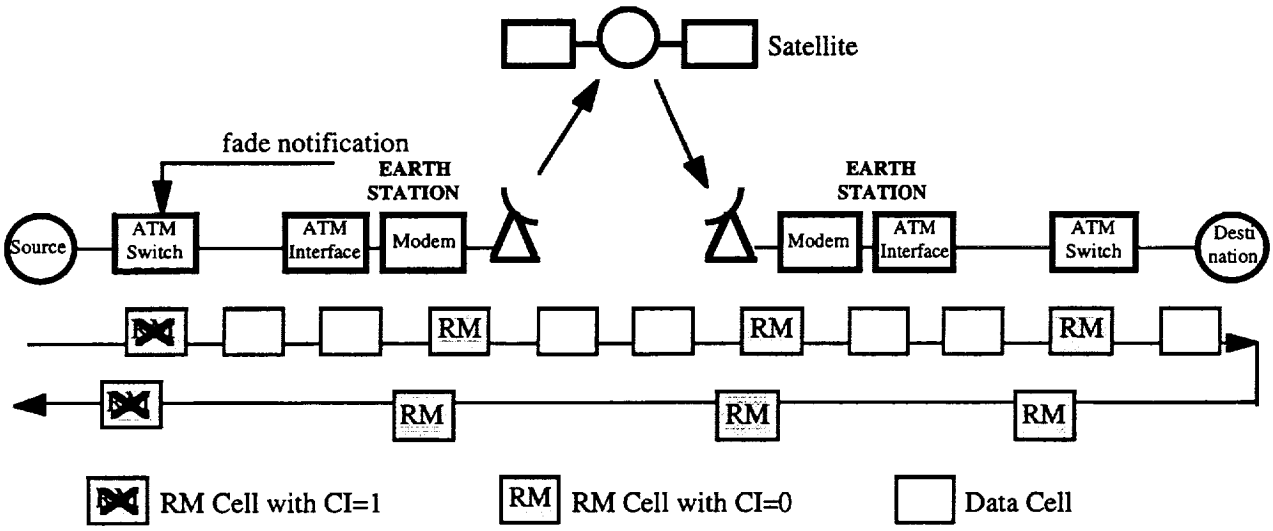

Figure 6-4. Explicit Rate Feedback Flow Control

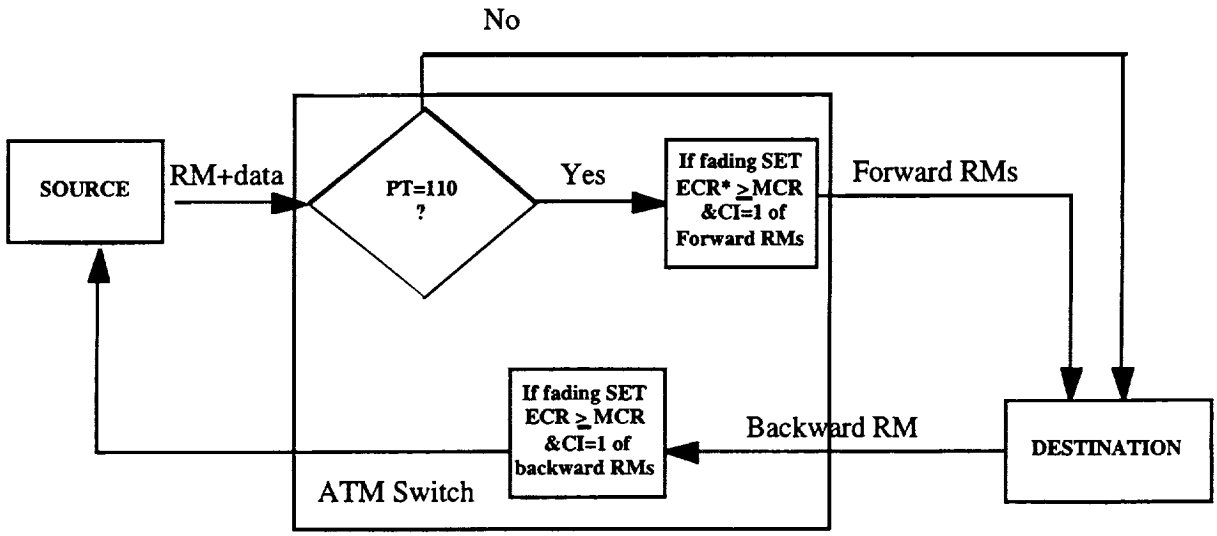

Figure 6-5. Simplified Flow Diagram of Explicit Rate Feedback Control

Figure 6-6 depicts an over-the-satellite ABR connection using the VS/VD feedback as a flow control mechanism. The ABR connection is divided into three separately controlled ABR segments. The ATM Switch 1 becomes the virtual destination for the source end-system, and the ATM Switch 2 becomes the virtual source for the destination end-system. A transmit earth station detects rain fades and activates compensation by reducing the information rate on the satellite link. The earth station then sends a fade notification message to Switch 1. Upon receiving the notification message, Switch 1 modifies the CI bit and ECR value for RM cells that are not terminated by Switch 1 (i.e., RM cells turned around to the source end-system and RM cells transmitted over the satellite). Switch 2 examines the CI and ECR fields of RM cells coming from Switch 1 and sets RM cells destined for the destination end-system accordingly. Upon receiving RM cells with CI=1, the source and destination end-systems set the cell transmission rates equal to the value specified in the ECR. The simplified flow diagram of this procedure is shown in Figure 6-7.

6.2.2 Assessments

Table 6-3 compares the feedback flow control mechanisms using criteria such as response delay, cell rate adjustment method, and reliability. The response delay refers the elapsed time beginning when the earth station decides to compensate for fading until the source end-system of a particular ABR connection receives a "congestion notification" message. The rate adjustment method criterion assesses a given feedback control mechanism to request the transmission rates explicitly or relatively. The last criterion refers to the reliable arrival of the congestion notification message at the source. An evaluation of the feedback flow control mechanisms is provided in the following paragraphs.

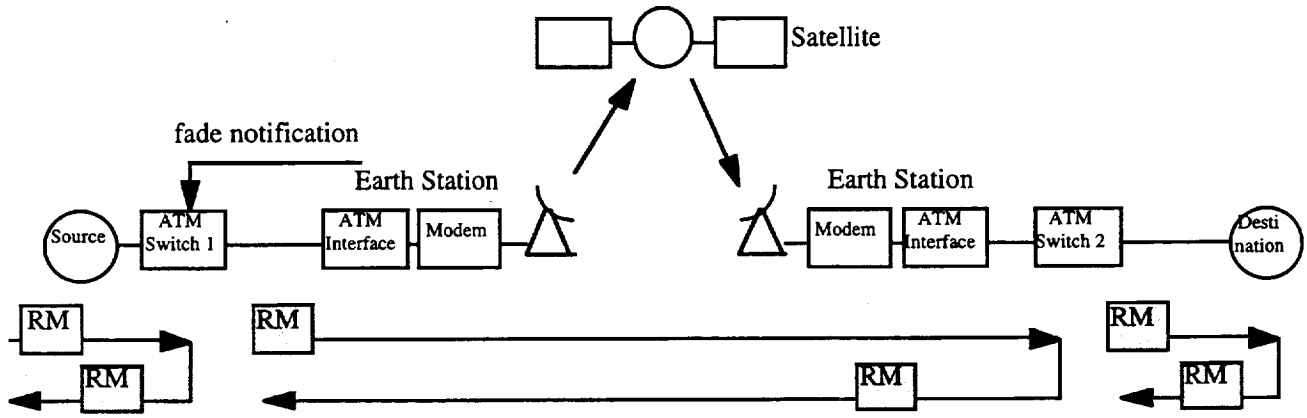

Figure 6-6. VS/VD Feedback Flow Control

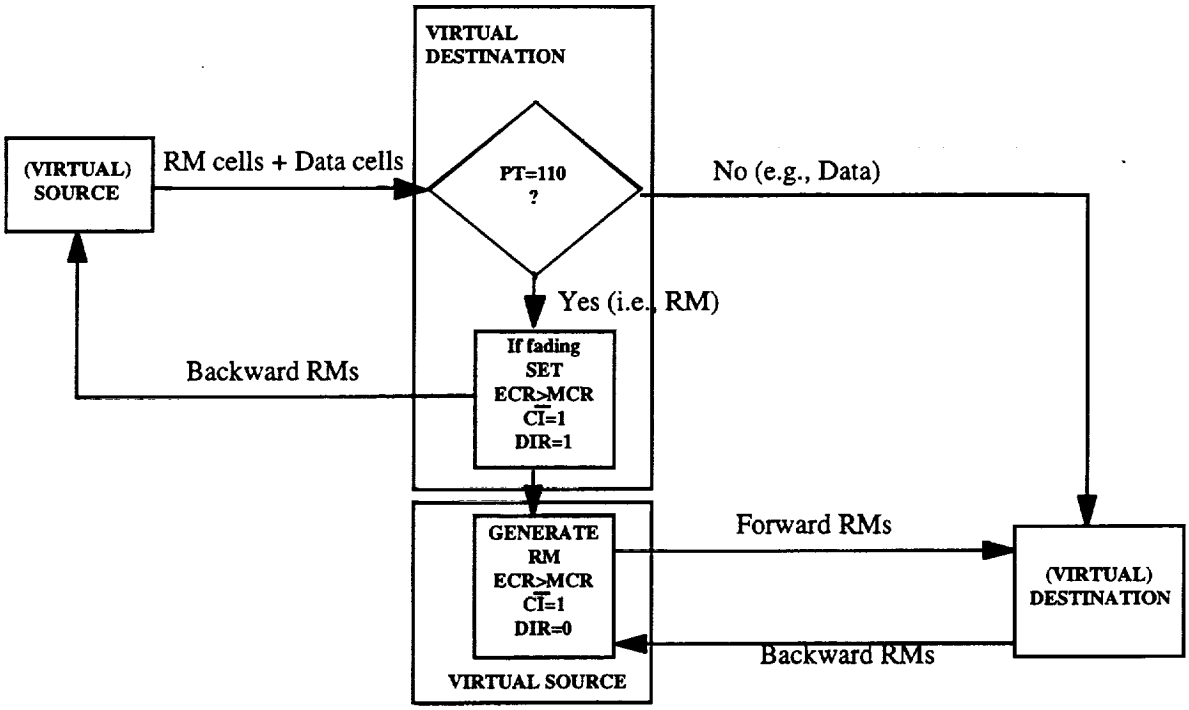

Figure 6-7. Simplified Flow Diagram of VS/VD Feedback Control

Table 6-3. Assessments of ABR Feedback Flow Controls

Criteria	Binary Feedback	ECR Feedback	VS/VD Feedback
Source Response Delay	Two satellite hops	Negligible	Negligible
Destination Response Delay	One satellite hop	One satellite hop	One satellite hop
Rate Setting	Gradual	Actual	Actual
Reliability	Low (ES waits for data/RM cells, some of which may be lost or corrupted)	Low (ES waits for RM cells some of which may be lost or corrupted)	Better (ES generates RM cells to notify ABR source and destination)

6.2.2.1 Response Delay

For the end-to-end binary feedback, the time it takes a data cell with EFCI=1 to arrive at the destination end-system from transmit earth station is a single satellite hop propagation delay (approximately 240 ms). Delays due to processing and terrestrial propagation are assumed negligible. If the destination reacts upon receiving this data cell, the source end-system would receive a backward RM cell marked with CI=1 one satellite delay later. Therefore, the response delay of the end-to-end binary feedback is two satellite hop propagation delays.

In the explicit rate feedback, the destination response delay is the same as the binary feedback, as shown in Figure 6-2. However, the source is much faster in adapting its rate to the current state of the link since the delay of backward RM cells from the transmit earth station to source is insignificant.

Similar to the explicit rate feedback, the time to request an ABR source end-system to transmit cells at any desired rate is almost immediately. As shown in Figure 6-6, this is accomplished by the turned-around RM cells in the first loop of the ABR path. The delay of feedback control information to the destination end-system from the transmit earth station is the same as the other two feedback mechanisms.

6.2.2.2 Rate Adjustment Method

As mentioned previously, the binary feedback control mechanism uses the gradual transmission rate decrease approach. It is therefore not effective against short term fading since rate reduction delays may exceed the fade duration. The explicit rate and VS/VD feedback mechanisms however allow for the actual specification of desired transmission rates on any ABR connections based on the satellite link capacity under different fading conditions.

6.2.2.3 Reliability

The binary feedback mechanism is less reliable since feedback control cells must successfully propagate through the satellite twice before reaching the source end-system. The explicit rate feedback control mechanism is more reliable than the binary feedback, but backward RM cells transported by a faded return satellite link must survive. The VS/VD feedback mechanism therefore appears to be more favorable, since the source end-system adjusts its transmission rate based on information contained in feedback control cells transported by a terrestrial link in the first loop (i.e., not transported by the satellite link experiencing rain fades).

6.2.2.4 Recommendation

Practical considerations play an important part in implementing a given feedback mechanism in satellite networks, where the propagation delays are large compared to terrestrial networks. From the above discussions, the end-to-end binary feedback mechanism is unacceptable due to its long source response delay and gradual transmission rate decrease approach. The explicit rate feedback mechanism is acceptable from the viewpoint of its response delay and explicit rate specification. However, since this mechanism depends on the arrival of backward RM cells in a critical time, it is not reliable while the satellite link is degraded. Similar to the explicit rate feedback, the VS/VD feedback mechanism accomplishes a negligible response delay and explicit rate transmission request. It is superior to the explicit rate feedback for the ability that the request to reduce source transmission rate is reliably transmitted to the source via terrestrial links and that the request can be generated by the source's virtual destination.

6.3 SYSTEM CONFIGURATION FOR IMPLEMENTING FADE COMPENSATION

COMSAT Laboratories manufactures an ATM Link Accelerator™, model ALA-2000™ [42], which facilitates the transmission of ATM traffic over satellite systems. The ALAs perform rate adaptation and signal conditioning functions to output data at rates of up to 8.448 Mbit/s but do not implement any of the ABR feedback flow control mechanisms. As shown in Figure 6-8, modified versions of ALA-2000 units will be required. The ABR sources are connected to the switches through physical links running at standard rates such as 51.84 Mbit/s over OC-1 lines. The switches are interconnected via links running at 155.52 Mbit/s (STS-3). The ALAs are connected to the switches via links running at 44.736 Mbit/s over DS-3 lines. Another possible system configuration would make use of the interface proposed in [43].

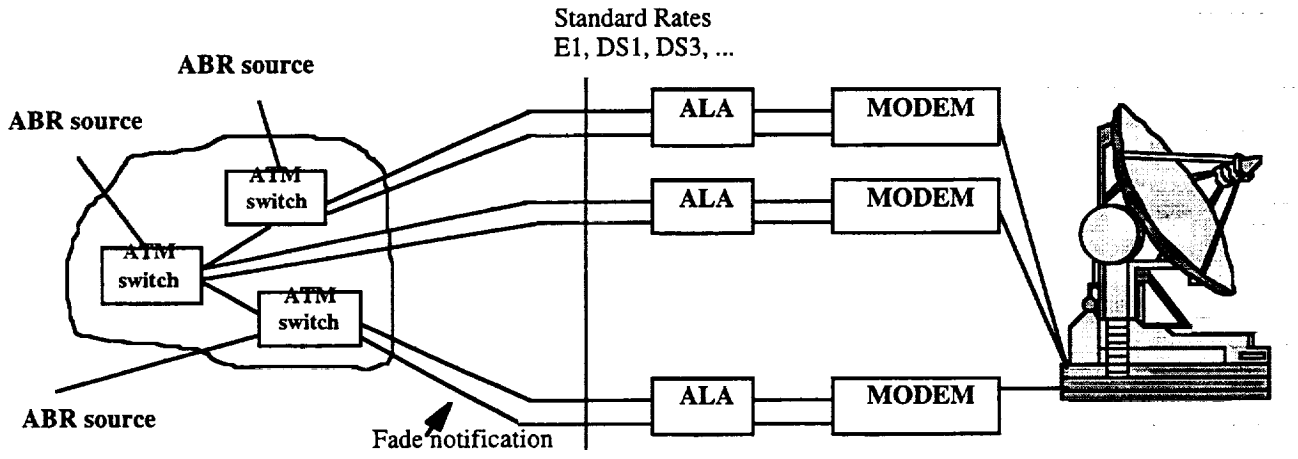

Figure 6-8. System Configuration for Implementing Fade Compensation

SECTION 7 — SYSTEM REQUIREMENTS

In order for the selected fade mitigation schemes to operate successfully consideration must be given to several system related aspects. These include system margin, setup time required to invoke the mitigation scheme, fade compensation range, and size of the common resource pool required for fade compensation. Most of these issues cannot be addressed adequately without defining the overall system requirements. An outline of a general approach to selecting the system parameters that affect fade mitigation is given below.

7.1 SYSTEM MARGIN

System margin is directly related to the service availability requirements. This in turn is largely a function of the rain climate in which the service is to be provided and the elevation angle. When implementing fade mitigation the system margin may be considered in terms of a fixed component and a dynamic component. The fixed allocation essentially takes care of the clear-sky conditions and the dynamic margin is the portion available through the fade compensation schemes being implemented. The clear-sky margin must allow for clear-air signal attenuation, measurement inaccuracies associated with the link quality measurement, and the time required for invoking the fade compensation.

Link quality estimation was discussed in Section 6 and typical measurement errors associated with different measurement techniques were presented. Some of the techniques pertain to measuring the link quality at one frequency (up-link or down-link) and scaling this value to the other frequency. In this approach, errors are introduced in the frequency scaling process and this must be factored into the clear-sky margin. Figure 7-1 shows statistical behavior of frequency scaling from the down-link to the up-link. In this figure the fade ratio between the up- and down-link fade is plotted against the down-link fade; the results have been derived from ACTS beacon measurements at Clarksburg, MD. It is seen that the estimation error is proportional to the down-link fade and for down-link fades around 5 dB the estimation error is of the order of ±0.5 dB. Most compensation techniques have some overheads associated with them (signaling delays). During the time period allocated for the overhead the link must stay intact, and to ensure this an appropriate margin must be allowed. Assuming a fade rate of 0.5 dB/s and an overhead of 2 s, the additional margin required is 1 dB. Another factor that must be accounted for in applying fade compensation is the time duration for which the compensation is invoked. The time duration must be significantly larger than the time associated with the overhead to ensure adequate utilization of resources. This can be handled by including an implementation margin of around 0.5 dB together with a suitable wait time after the fade has ceased. The implementation margin provides a hysteresis around the clear-sky threshold to avoid very short duration fades which may cause the fade compensation to

kick-in and out. The clear-sky margin may be assigned using typical values to account for the following factors:

- gaseous absorption (~ 1 dB)
- link-quality measurement error (~1 dB)
- time delay in applying compensation (~ 1 dB)
- frequency scaling error within the clear sky margin (~ 0.5 dB)
- fade compensation implementation margin (~ 0.5 dB)

A contribution from each factor can be added together to arrive at the fixed margin required under worst case conditions; e.g. 4 dB. Clear-sky margin has a direct impact on the overall system cost, and as such an overly pessimistic value should be avoided. On the other hand, a very low value can cause the fade compensation to kick-in too frequently and tie-up valuable resources. A trade-off between the two opposing requirements must be made in selecting the fixed margin.

The dynamic component of the link margin, which is available through the fade compensation schemes must be determined on the basis of rain and other propagation impairments. Figure 7-2 and 7-3 show up-link fade (30 GHz) and down-link degradation (20 GHz) cumulative distributions for different rain climates for an elevation angle of 20°; a system noise temperature of 200 K is assumed in the down-link degradation calculation.

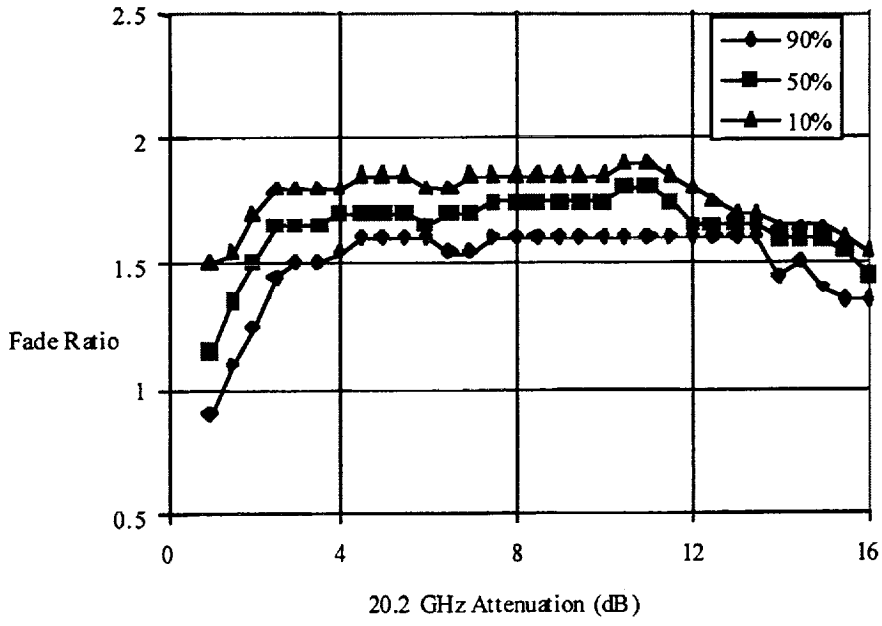

Figure 7-1. Distribution of the Fade Ratio Between 27.5 and 20.2 GHz

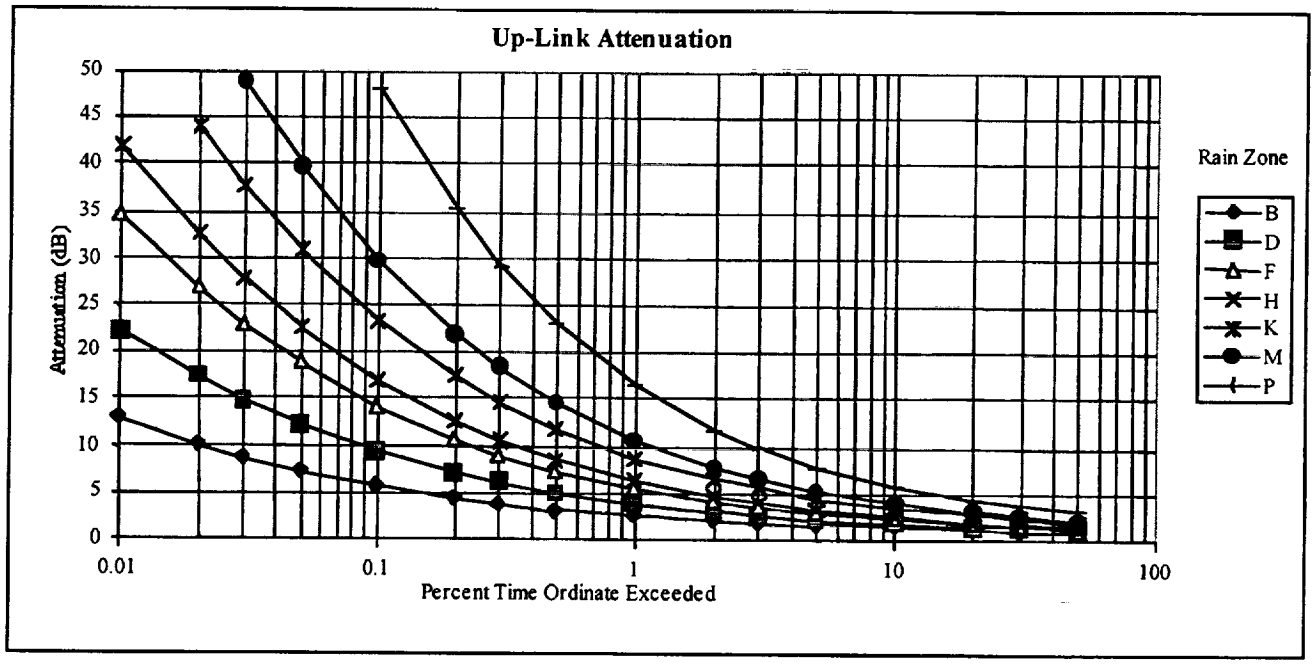

Figure 7-2. Attenuation Distributions at 30 GHz for Different Rain Zones; Elevation Angle 20°

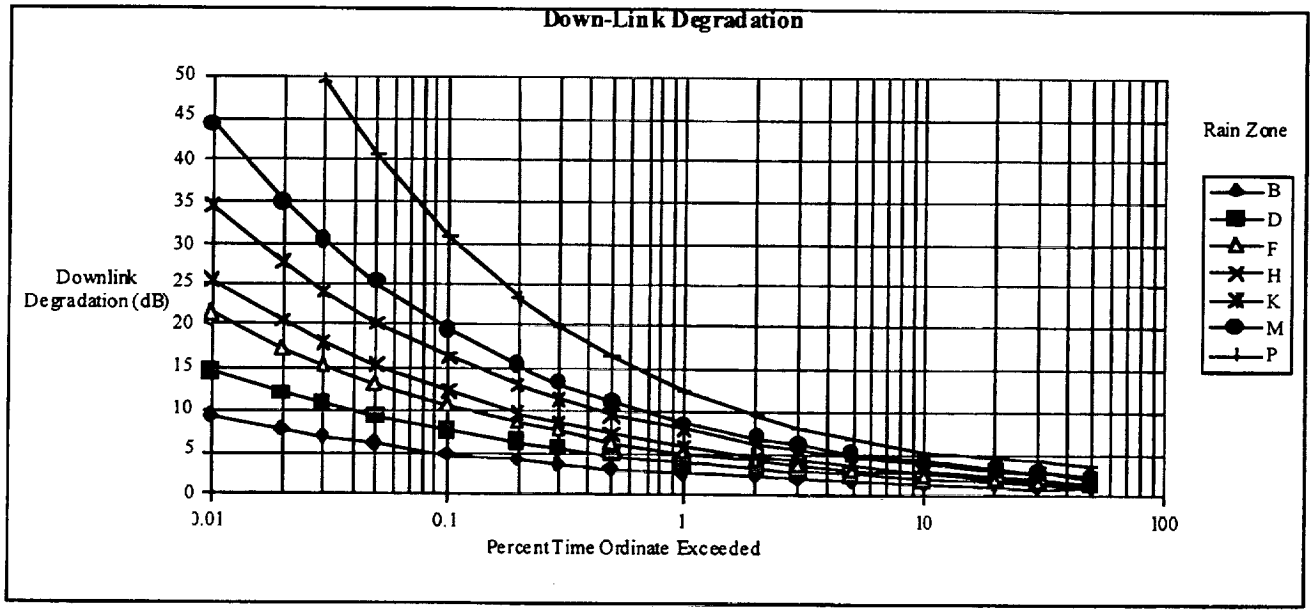

Figure 7-3. Down-Link Degradation Distributions at 20 GHz for Different Rain Zones; Elevation Angle 20°.

The calculation is based on the ITU-R attenuation prediction model errors and include gaseous absorption and tropospheric scintillation; an antenna diameter of 0.6 m is assumed for the scintillation calculation. Attenuation and down-link degradation distributions for the ITU rain regions B, D, F, H, K, M, and P are shown in the figures.

Table 7-1 shows the total margin required for three availability levels; 99%, 99.5%, and 99.7%. Most Ka-band systems are not expected to operate at elevation angles below about 20°, and the calculations shown can be considered to be the worst case. Assuming a clear sky margin of 4 dB and approximately 10 dB of compensation, it is seen that rain climates up to about region K can be accommodated even at 99.7% availability level. Operation in heavier rain climates such as region P may require either additional clear-sky margin or reduced service availability.

7.2 RESPONSE TIME

The response time for fade compensation is a function of the signaling and synchronization time required for the selected fade compensation method. Power control implemented in an open loop fashion has the smallest response time (of the order of milliseconds) since the response time is essentially determined by the measurement and processing time required for the determination of the fade level at the point where the power control is applied. Closed-loop power control on the other hand will suffer a minimum delay of two satellite hops. Most other techniques also require setting-up times of the order of one to several seconds. During the setting-up time the satellite link must stay intact, and the time delay factor included in the clear-sky margin must be adjusted to meet the set-up time requirements.

Table 7-1. Link Margins Required for Availability Times of 99%, 99.5%, and 99.7%

Rain Zone	Up-link Margin (dB)			Down-link Margin (dB)		
	99%	99.5%	99.7%	99%	99.5%	99.7%
B	2.5	3.2	3.8	2.6	3.1	3.6
D	3.9	5.0	6.1	3.9	4.7	5.5
F	5.4	7.2	9.0	5.1	6.3	7.4
H	6.4	8.6	10.7	5.7	7.2	8.5
K	8.7	11.8	14.6	7.8	9.7	11.4
M	10.6	14.5	18.3	8.7	11.1	13.3
P	16.5	23.0	29.3	12.4	16.3	20.0

7.3 COMPENSATION RANGE

The fade compensation range is determined by the cost and the capability of the fade compensation being selected. As an example the compensation range available for up-link power control is a function of the high power amplifier (HPA) capacity at the earth station. The HPA capacity in turn is a function of its cost. Fade compensation range available for data rate reduction, on the other hand, is a function of the reduction ratio, and has very little cost impact on its implementation. Referring to Table 7-1, and assuming a clear-sky margin of 4 dB, it is seen that for heavy rain climates the required fade compensation may not be handled by any of the compensation techniques described in Section 6. In such situations, recourse may be made to increasing the clear-sky margin to provide acceptable levels of service availability.

SECTION 8 — EXPERIMENTS AND ESTIMATED COSTS

Three experiments have been planned as part of this study. The first two experiments focus on low cost hardware modifications which will enable small Ka-band terminals to achieve higher average availability by reducing service outages caused by rain attenuation. The fade measurement experiment compares the performance of three rain fade measurement techniques which can be implemented with a relatively low cost impact on a small terminal. The second experiment is a rain fade compensation experiment. Fade compensation consists of staged power control and convolutional code rate changes coupled with information rate reductions to improve link availability. The final experiment demonstrates a mechanism for dynamically reducing the information rate of an ATM traffic stream thereby enabling fade compensation utilizing code and information rate changes to occur on satellite links carrying ATM traffic. This experiment will demonstrate the transmission of ATM traffic over the compensated satellite link of experiment two. Each experiment is described, a plan for conducting the experiment is presented and an estimate of the cost associated with the conduct of each experiment is shown in the following three sections.

8.1 FADE MEASUREMENT EXPERIMENT – OVERVIEW

The fade measurement experiment compares the relative accuracy, implementation cost and response time of three low-cost fade measurement techniques. Beacon power, bit error rate from channel coded data and signal to noise fade measurement techniques have been selected for this experiment. This selection is based upon the analysis of Section 4 and suitability of the technique for low-cost, independent, user premises terminals. The performance of the three fade measurement techniques can be compared by implementing the techniques and allowing them to run simultaneously under identical conditions.

The proposed fade measurement experiment setup is shown in Figure 8-1. The experiment is best described by starting at the signal source, the Link Evaluation Terminal (LET) at Lewis Research Center (LeRC). The LET is fed a power controlled, QPSK modulated carrier which is generated by a satellite modem. The modem input is a 384 kbit/s pseudo-random bit sequence generated by the bit error rate test set. Uplink power control based upon the NASA Ground Station (NGS) 27 GHz uplink beacon is provided by the power controller developed by COMSAT under contract NAS 326402 [28]. This uplink power control system is expected to provide less than 0.5 dB signal level variation at the satellite for 90% of the experiment duration.

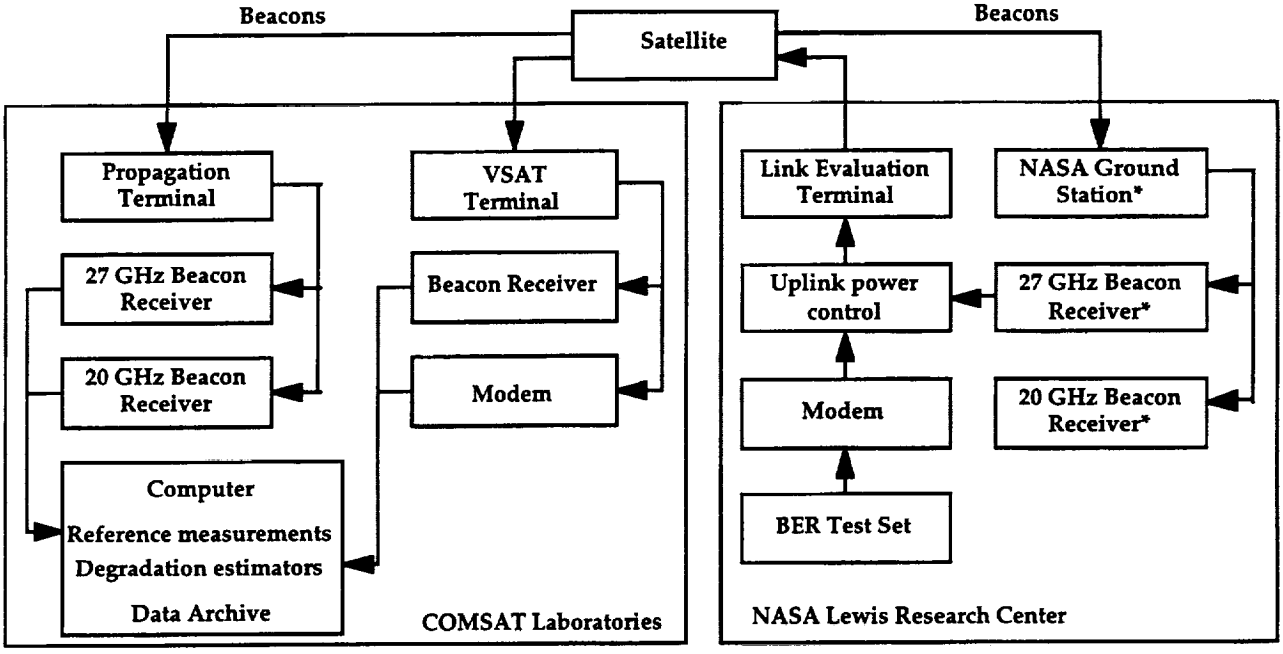

* Propagation conditions at LeRC are monitored and recorded on a continuous basis. NGS equipment performing this function is not included in experiment cost and requirements.

Figure 8-1. Fade Measurement Experiment Block Diagram

The signal transmitted by the LET is received by the ACTS satellite in HBR mode, switched at IF by the microwave switch matrix into the E-08 spot beam which is directed towards the VSAT site in Clarksburg, Maryland. Propagation conditions are monitored on the downlink path to the VSAT site by the co-located propagation terminal which will monitor both the uplink and downlink beacon. Meteorological conditions including instantaneous rain rate, temperature and wind speed, at the VSAT site will also be monitored. The LNB output from the VSAT terminal is split and provided to the low cost beacon receiver and a modem performing simultaneous BER from coded data and SNR fade measurements. Each of the three fade measurement systems will run independently. A computer at the VSAT site will:

- Read beacon signal measurement results from the low-cost beacon receiver.
- Read BER from channel coded data results from the modem and calculate received E_b/N_o from each reading.
- Read SNR results from the modem and calculate received E_b/N_o from each reading.
- Maintain a table of hourly clear-sky baselines for each fade measurement technique and calculate the downlink degradation estimated from each technique on a continuous basis.

- Read downlink and uplink fading reference measurements from the co-located propagation terminal.
- Maintain a record of measurement results, parameters used in calculations and degradation estimates for each fade measurement technique.
- Read the current time from a WWV receiver and append time stamps to data records to allow propagations effects on the uplink from LeRC to be correlated with NGS generated propagation data.
- Read and record meteorological parameters at the VSAT site.

The experiment should run for sufficient time to establish reliable clear-sky baseline data for each fade processing algorithm and should encompass several rain events following the baseline establishment phase. The cost estimates assume that the duration of the data collection phase is between 2 and 3 months. The collected data will be analyzed to determine the relative performance of the three fade measurement techniques. Although the fade measurement utilizes existing equipment and resources whenever possible, there still remains significant development effort which must be undertaken to perform the experiment. The following text describes the required development effort and suggests a method to achieve the required development at reasonably low cost.

8.1.1 Fade Measurement Experiment – Low Cost Beacon Receiver

Beacon receivers are designed to provide control signals to antenna positioning systems and tend to be far to expensive for application in a VSAT terminal priced to sell around $2K. A beacon receiver which sacrifices some performance, in terms of accuracy, acquisition time and features, must be developed for fade measurement applications in VSAT terminals. Preliminary specifications have been established for the low cost beacon receiver. These performance parameters are shown in Table 8-1.

Table 8-1. Low Cost Beacon Receiver Performance Requirements

Parameter	Requirement
Accuracy	±0.80 dB
Acquisition bandwidth	50 kHz
Acquisition time	3 seconds
Input frequency range	1385±.05 MHz
Input beacon level	-20 to -40 dBm
Beacon modulation types	BPSK
Threshold C/N_O	40 dB/Hz

A beacon receiver link budget is shown in Table 8-2. The beacon receiver sensitivity threshold of 43 dB/Hz allows operation through 10 dB fades. During fades in excess of 10 dB at 20 GHz the receiver will lose lock and will re-acquire when the signal returns from the fade. The selection of this threshold is based upon the conclusion that no more than 10 dB of uplink compensation is reasonable in a low cost terminal and the beacon receiver will provide meaningful beacon power measurements whenever acquisition of the communications link is possible.

Table 8-2. Beacon Receiver Link Budget at Threshold

Carrier Frequency, F	20.19	GHz
20 GHz Beacon EIRP	18.50	dBW
Modulation Loss	1.20	dB
Single tone EIRP	17.30	dBW
Satellite Slant Path Range, S	38,500	km
Path Loss, Lp	210.31	dB
Clear Sky Attenuation	0.95	dB
Rain Attenuation, Lr	10	dB
Rain Temperature, Tm	280	K
Flux Density at Earth Terminal	-203.96	dBW/m^2
Antenna Gain, Gr	45.18	dB
Antenna Noise Temperature, Tant	257.74	K
Pointing Loss	0.10	dB
Feed loss, L	0.20	dB
Feed Transmission, a	0.95	
LNA Noise Temperature, Tlna	145.00	K
Ambient Temperature, To	290.00	K
System Noise Temperature, Ts	404.19	K
G/T	19.11	dB/K
C/No	43.55	dB-Hz
VSAT terminal phase noise	71.70	dB-Hz
C/No total	43.55	dB
C/No required	43.00	dB
Margin	0.55	dB

A block diagram of the beacon receiver which was used for generation of the cost impact estimates of section 4.1.3 is shown in Figure 8-2. The L-band synthesizer is set to a fixed frequency to bring the downconverted beacon (RF unit LO = 18.8 GHz) at 1350 MHz to a nominal 70 MHz. The second phase-locked loop is a tracking filter which is estimated to have a 5 kHz loop bandwidth. The loop signal to noise ratio, calculated using Equation (8-1), at downlink fading of 10 dB, is 3 dB which is just adequate for acquisition. The frequency of the beacon signal must be known to within 6 kHz to be acquired without additional acquisition circuitry. This level of performance should be achievable for periods of several months with the ACTS beacon and existing VSAT terminal.

$$(SNR)_L = \frac{P_S}{P_N} \cdot \frac{B_i}{2B_L} \qquad (8\text{-}1)$$

P_S = signal power

P_N = noise power at PLL input

B_i = PLL input bandwidth, (2 MHz)

B_L = PLL bandwidth, (5 kHz)

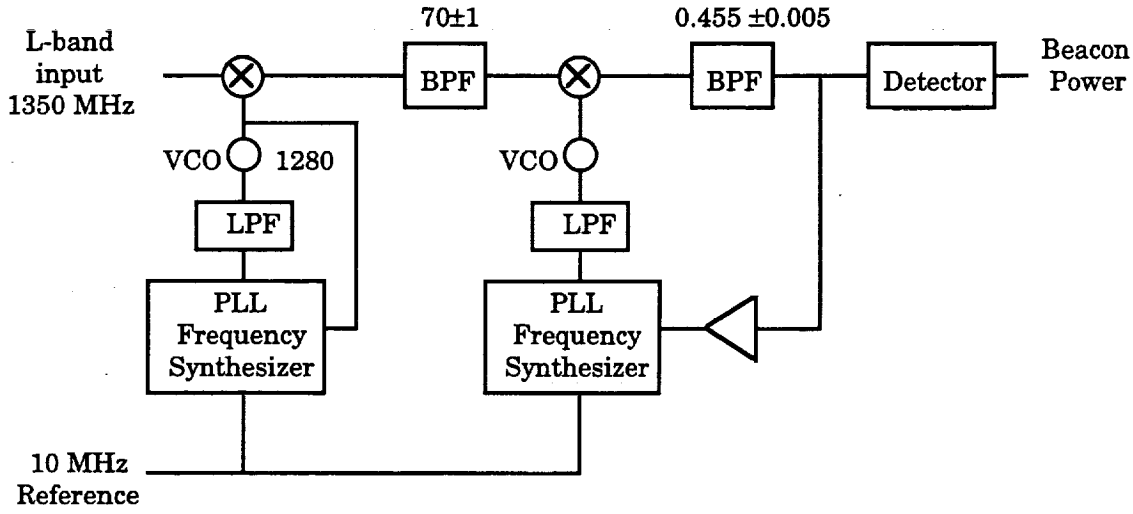

Figure 8-2. Low Cost Beacon Receiver Block Diagram

8.1.2 Fade Measurement Experiment – Modem Modifications

A modem capable of performing simultaneous BER from channel coded data and SNR fade estimates must be obtained. A search of commercially available satellite modems has found no modems which measure link quality by the SNR technique. Modems are readily available which provide the BER from channel coded data signal quality measurement. Therefore it is necessary to procure a modem with the BER fade measurement capability and modify it to perform simultaneous SNR measurements. The alternative approach of running two modems in parallel, one measuring fades by the BER from channel coded data and the other measuring fades from SNR measurements, was deemed to be less desirable because there is no guarantee that the modems are in fact estimating fades from identical data samples. Differences in the implementation and performance of the analog, A/D converter, carrier recovery and symbol timing circuits between the two modems may distort the experiment results.

The circuitry required to implement SNR fade measurement is shown in Figure 4-7. Modem firmware must also be modified to meet the additional data handling requirements. These requirements include the reporting of BER from channel coded data and SNR data statistics to the experiment computer.

8.1.3 Fade Measurement Experiment – Link Budgets

Table 8-3 shows the link budget for the LET to VSAT link carrying a 384 kb/s information rate. The modulator is assumed to perform framing channel coding and modulation consistent with the European Telecommunications Standards Institute's digital broadcasting system for sound and data services.[44] The coding includes a rate 3/4 convolutional code with Reed-Solomon, (204,188) outer block code. The symbol rate after QPSK modulation is approximately 274 ksymbols/s. The VSAT terminal performance parameters are applicable to COMSAT's VSAT terminal which was manufactured by NEWTEC CY of Antwerp, Belgium. The required carrier to noise density of 61.8 dB provides E_S/N_O of 4.4 dB for the 274 ksymbol/s channel data rate with QPSK modulation and is expected to provide $BER_i < 10^{-10}$.

8.1.4 Fade Measurement Experiment – Cost Estimate

A cost estimate for the fade measurement experiment is provided for planning purposes in Table 8-4. This estimate is based upon modifications to a modem which is currently in production (COMSAT Laboratories CL-107). The modifications required were described in section 8.1.2. All hardware modifications required to perform both the fade measurement and compensation experiments are included in this estimate. Software and firmware modifications required to implement the fade compensation experiment are not included. In addition to the modem data handling firmware, software must be written for the

Table 8-3. Fade Measurement Experiment Communications Channel Link Budget

Uplink		
Carrier Frequency, F	29.00	GHz
LET EIRP	75.00	dBW
Backoff	42.00	dB
Pointing loss	0.50	dB
Single tone e.i.r.p.	32.50	dBW
Distance to satellite, S	38,000	km
Path Loss, Ls	213.29	dB
Clear Sky Attenuation, Lc	0.50	dB
Rain Attenuation, Lr	0	dB
Polarization loss, Lp	0.50	dB
G/T	23.10	dB/K
Transponder bandwidth, B	900.00	MHz
Received C/No	69.91	dB

Downlink		
Carrier frequency, [F]	19.28	GHz
Fixed beam e.i.r.p. at saturation	65.00	dBW
Backoff	26.00	dB
Satellite pointing loss	0.22	dB
e.i.r.p.	38.78	dBW
Distance to VSAT, [S]	38,500	km
Path loss, [Lp]	209.85	dB
Clear sky attenuation, [Lc]	0.50	dB
Rain attenuation, [Lr]	0.00	dB
Clear sky noise temperature, [Ts]	275	K
Rain fade, [Lf]	0.00	dB
Polarization loss	0.13	dB
Antenna gain	45.58	dB
Pointing loss	0.50	dB
Downlink C/No	77.59	dB-Hz
VSAT downconverter phase noise	71.57	dB-Hz
Combined C/No	67.23	dB-Hz
C/No required (CBER=10E-4)	61.80	dB-Hz
Margin	5.43	dB

Table 8-4. Cost Estimate for Fade Measurement Experiment

DEVELOPMENT COST	
Beacon Receiver	40 K
Modem Modifications	46 K
EQUIPMENT COST	
Modem (2+0 spare)	48 K
Beacon Receiver	4 K
EXPERIMENT COST	
Experiment design	8 K
Design reviews	8 K
Testing	10 K
Data collection	10 K
Data analysis and reporting	6 K
TOTAL	$180 K

computer to collect data, store data, implement the clear-sky baseline algorithms and implement the degradation calculations for both fade measurement techniques. These costs are included in the experiment design, testing and data collection categories.

8.1.5 Fade Measurement Experiment-Schedule

The schedule for the Fade Measurement Experiment is shown in Figure 8-3. The duration of the experiment is expected to be approximately ten months.

8.2 FADE COMPENSATION EXPERIMENT – OVERVIEW

The fade compensation experiment utilizes experiment hardware from the fade measurement to implement a fade compensation technique suitable for low cost VSAT terminals. Low cost VSAT terminals tend to be limited on transmit EIRP at Ka-band due to the fact that solid state power amplifiers cost increases rapidly with output power. It is not cost effective to counteract fading entirely with uplink power control. Bandwidth can be held in reserve, either in the form of unused time slots or frequency slots, to accommodate additional channel capacity which would be required if code rates are changed to compensate for rain attenuation. Due to the requirements for coordination between transmitting and receiving terminals during code rate changes it is desirable to limit the frequency of transitions between code rates. This experiment demonstrates the effectiveness of code rate changes, combined with limited (4 dB) uplink power control employed to limit the rate of code rate transitions, in achieving high satellite link availability with reduced margin.

Allocation of reserved bandwidth while maintaining a fixed symbol duration on the satellite channel requires the existence of a TDMA, FDMA, FDM or TDM system with

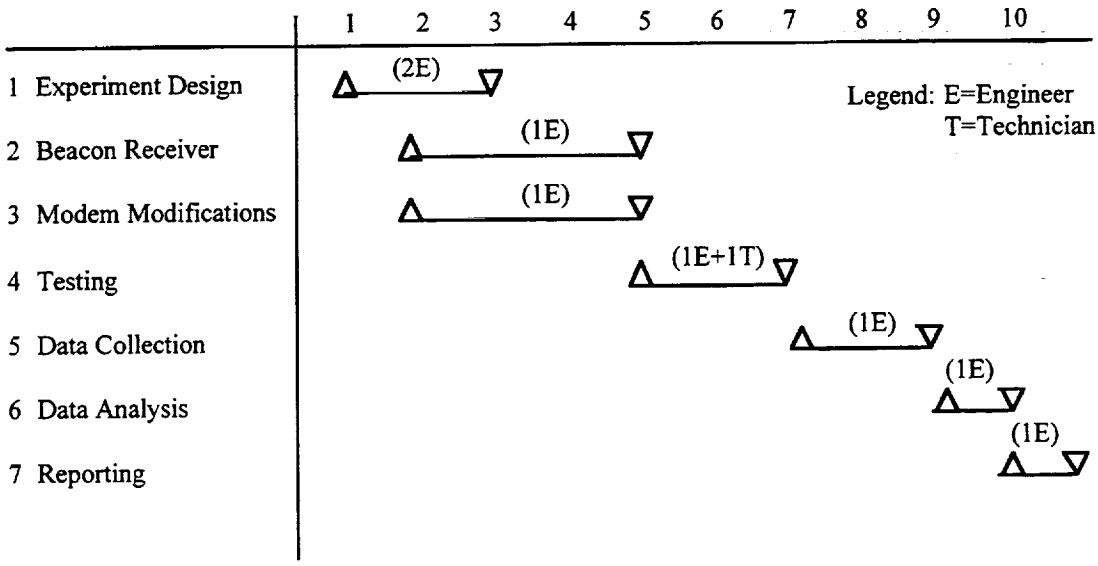

Figure 8-3. Schedule for Fade Measurement Experiment

reserved capacity. To limit the cost of the experiment by not requiring a bandwidth management system, the code rate transitions will be performed in conjunction with information rate reductions. This allows the compensation system to be evaluated, including the effect of propagation delay, without the additional complexity and cost of demonstrating bandwidth management.

The fade compensation experiment will achieve approximately 8.5 dB of degradation compensation with the combination of 4 dB of uplink power control, rate 3/4 to rate 3/8 code rate transitions providing approximately 1.5 dB of compensation and information rate transitions contributing 3 dB compensation. Code rate and power control transition signaling will be performed over the information carrying channel allowing the experiment to be run with two continuous-mode modems. Fade measurements will be performed by either the low cost beacon receiver, BER from Channel Coded Data or SNR fade measurement circuits.

Figure 8-4 is a block diagram of the fade compensation experiment. The hardware is very similar to the fade measurement experiment except the uplink power controller is absent and a computer is required at the LET site in Cleveland. The duplex link between the VSAT site and ACTS operates with a margin of only 4 dB and achieves high availability through 9.5 dB of fade compensation. Operation of the compensation experiment is best described by starting at the LET site in Cleveland. The LET-modem provides clock to the BER test set at 384 kB/s when code rate compensation is not in effect. The BER test set provides a pseudo-random sequence of data bits to the LET-modem. The LET-modem frames, multiplexes in a low rate (160 b/s) signaling channel and performs randomization and coding compliant with the Digital Video Broadcasting Specification, ETS 300 421.[44] Details of the multiplexing, signaling and coding are provided in following sections. The modulator output feeds the LET upconverter. The ACTS space segment is identical to that described for the fade measurement experiment.

The signal received by the VSAT is split and fed to the low cost beacon receiver and VSAT-modem. The beacon receiver measures beacon power and outputs measurement results to the computer. The VSAT-modem demodulates the data and may also measure fading by either the BER from channel coded data or SNR techniques. The computer performs all functions required by the fade measurement experiment except it may only calculate degradation estimates based upon one fade measurement system. The computer also outputs fade compensation commands. These commands include:

- ULPC commands to the VSAT-modem.
- DLPC commands to be sent by the VSAT-modem to the LET-modem.
- Code rate transition commands to the VSAT-modem.

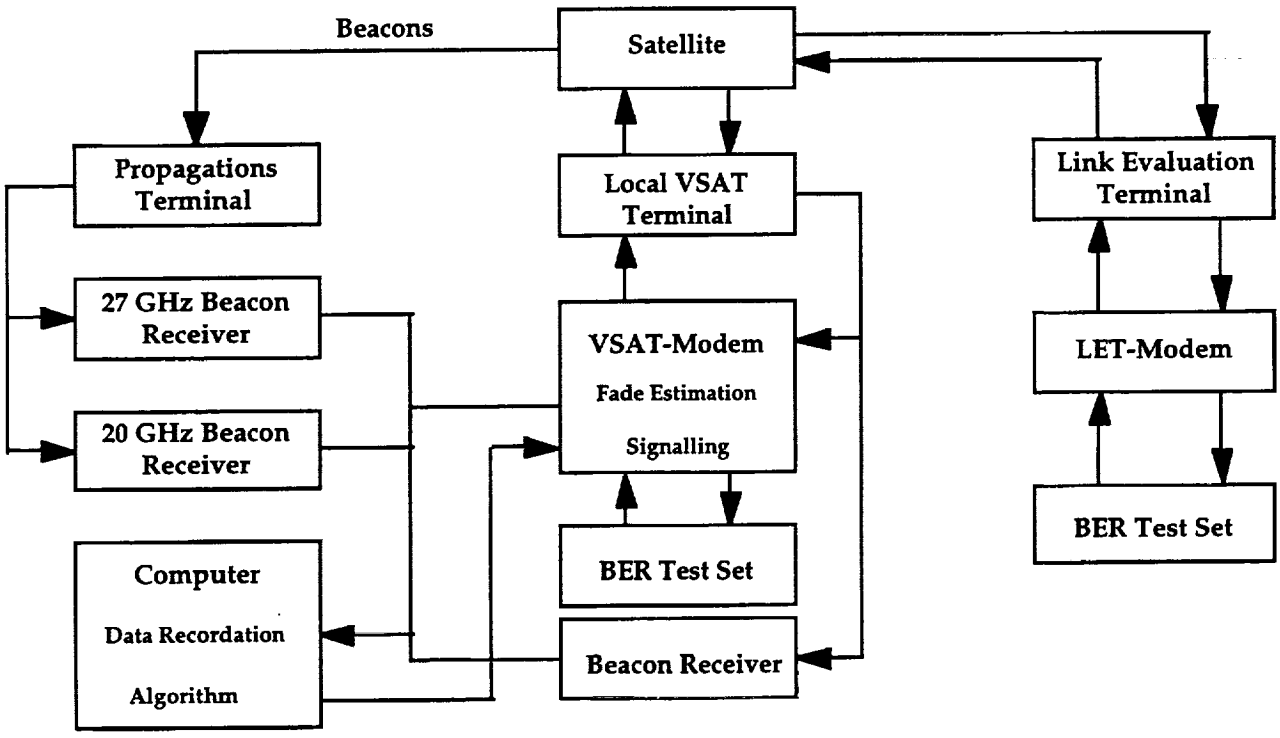

Figure 8-4. Fade Compensation Experiment Block Diagram

The VSAT-modem implements ULPC, signals DLPC commands to the LET-modem and implements the code rate transition algorithm as described in section 8.2.2. The recovered and demultiplexed data from the VSAT-modem is routed to the BER test set for channel performance monitoring. The BER test set also sources a pseudo-random sequence, synchronous with the VSAT-modem recovered clock, to be multiplexed with the VSAT-modem generated signaling traffic and returned to the LET site. Fade estimates are also being generated at the LET site based upon either beacon receiver or one of the two communications channel fade measurement techniques. The VSAT-to-LET channel data will also be demodulated, demultiplexed and monitored for errors at the LET site. The fade compensation algorithm is also implemented by the computer at the LET site to provide compensation for rain at Cleveland. Return channel BER and signaling channel activity are also recorded by the computer in Cleveland.

8.2.1 Fade Compensation Experiment – Multiplexing and Coding

Multiplexing and coding of the signaling and information channels is performed by each modem. The multiplexing of signaling and information streams is shown in Figure 8-5. The MPEG-2 transport multiplex packet utilized by ETS 300 421 consists of an eight-bit sync byte followed by 187 eight-bit data bytes. The sync byte is inverted on every eighth packet creating what shall be called, for purposes of this report, a master frame. Five

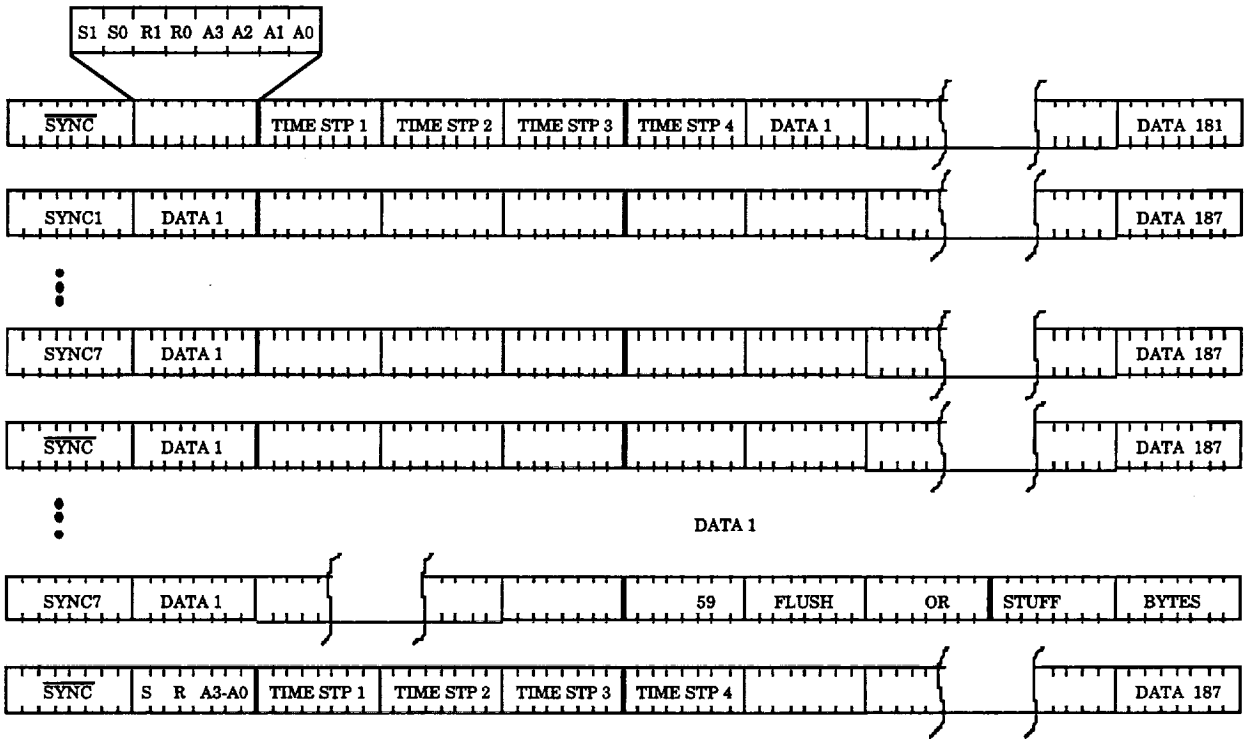

Figure 8-5. Signaling and Information Channel Multiplexing

signaling bytes will be sent every eight master frames. These bytes consist of one byte for code rate and power control and four bytes for each time stamp. Since errors in the code rate bits can create extended sequences of errors in the information channel through inadvertent code rate transitions, they are provided a 3 dB additional margin by transmitting each bit twice. The demodulator will average the values for bits S0 and S1 to determine the value of S. The S-bit marks the current master frame as a signaling master frame. Similarly, the demodulator will average the values for bits R0 and R1 to determine the value of R. The R-bit is an indication of the desired code rate (3/4 or 3/8) for successive frames. Bits A0 through A3 provide 4 bits of power control settings to the modem.

At 0.5 dB for the least significant bit, this provides 7.5 dB of power control range. The attenuator setting bits are not sent twice but are protected by constraining attenuator setting transitions to sequential half-decibel steps. Details on the use of signaling the channel for code rate and power control transitions are provided in section 8.2.2.

The coding process is shown in Figure 8-6 for the link operating with rate 3/4 convolutional coding. The randomization, convolutional interleaving, Reed-Solomon encoding and convolutional encoding are compliant with ETS 300 421 except that rate 3/8 coding, as used during deep fades, is not specified in ETS 300 421. The optional interleaver is included to reduce the impact of VSAT downconverter phase noise which is significant for low bit rate systems.

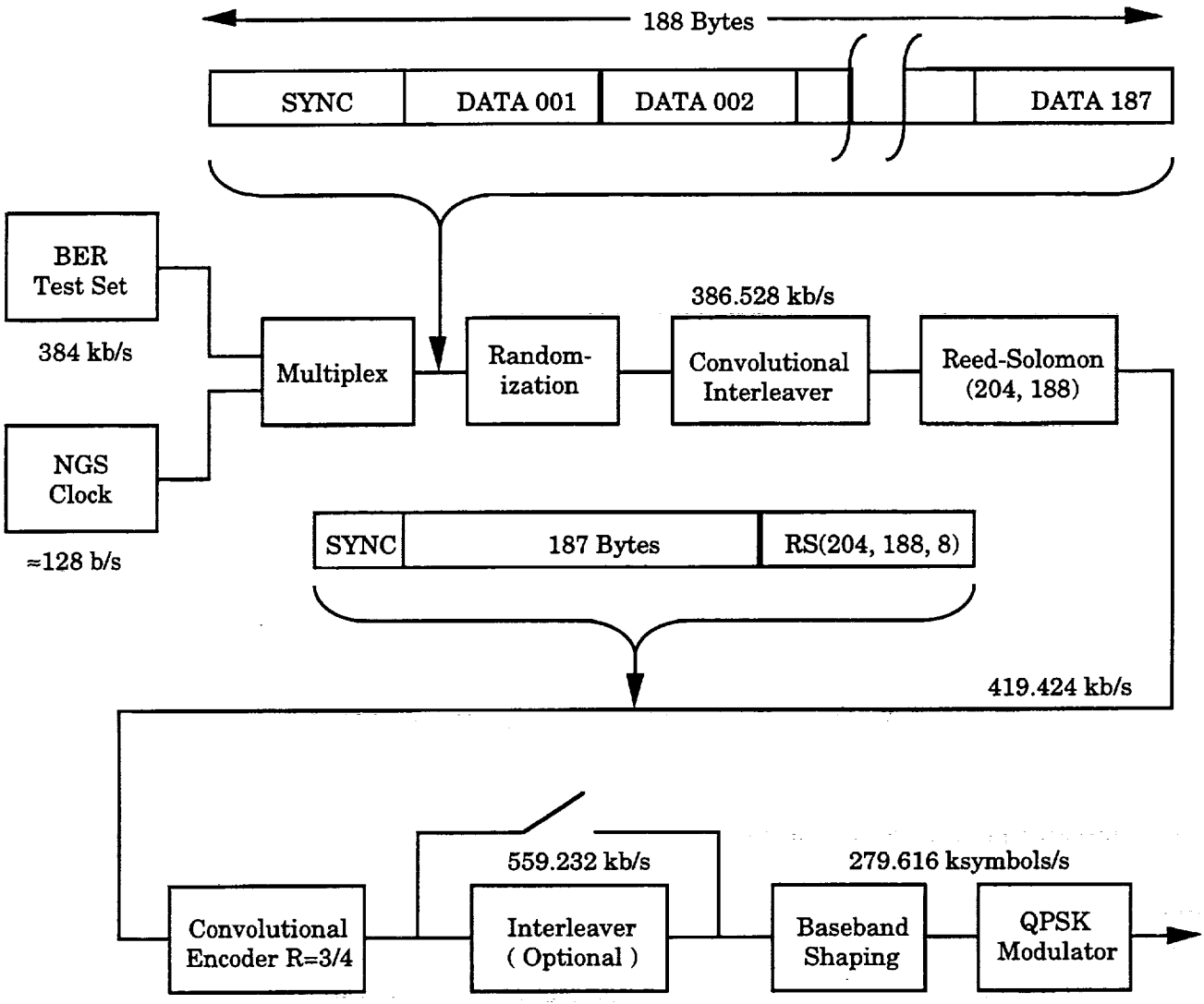

Figure 8-6. Channel Coding Process

A 257 frame/s frame rate is chosen because it is the lowest integral frame rate which provides in excess of 384 kb/s information capacity. The information capacity is 257*187 = 48,059 data bytes/s or 384.472 kb/s. The five signaling bytes per eight master frames occupies 160.625 b/s leaving approximately 311 b/s excess capacity. Prior to each code rate transition the modulator must transmit seven bits to empty the convolutional encoder and approximately 160 bits to flush out the Viterbi decoder in the remote demodulator. The selected frame rate and multiplexing format will therefore allow one code rate transition per second.

8.2.2 Fade Compensation Experiment – Fade Compensation Signaling

Fade compensation algorithms and signaling in an actual VSAT system would be implemented by a microprocessor within the modem. For this experiment, these functions are performed by the computers to limit modem modifications and thereby reduce experiment cost. Fade compensation is continuously performed by both computers. Power control is used to maintain link margin through shallow fades of up to 4 dB. When the margin is no longer maintained with full transmit power then a code rate transition is initiated. This process is shown in Figure 8-7 for a rain event at Clarksburg. The VSAT processor algorithm has determined that a code rate transition is required. It signals the new code rate to the VSAT modem, CR=R_i. Each modem maintains two parameters, its current transmit code rate, R_{tx} , and its current receive code rate, R_{rx} . The VSAT-modem sends the next signaling frame at the prior code rate with code rate bits, R0 and R1 set to the new code rate. The LET-modem receives this frame, the subsequent 6 master frames of

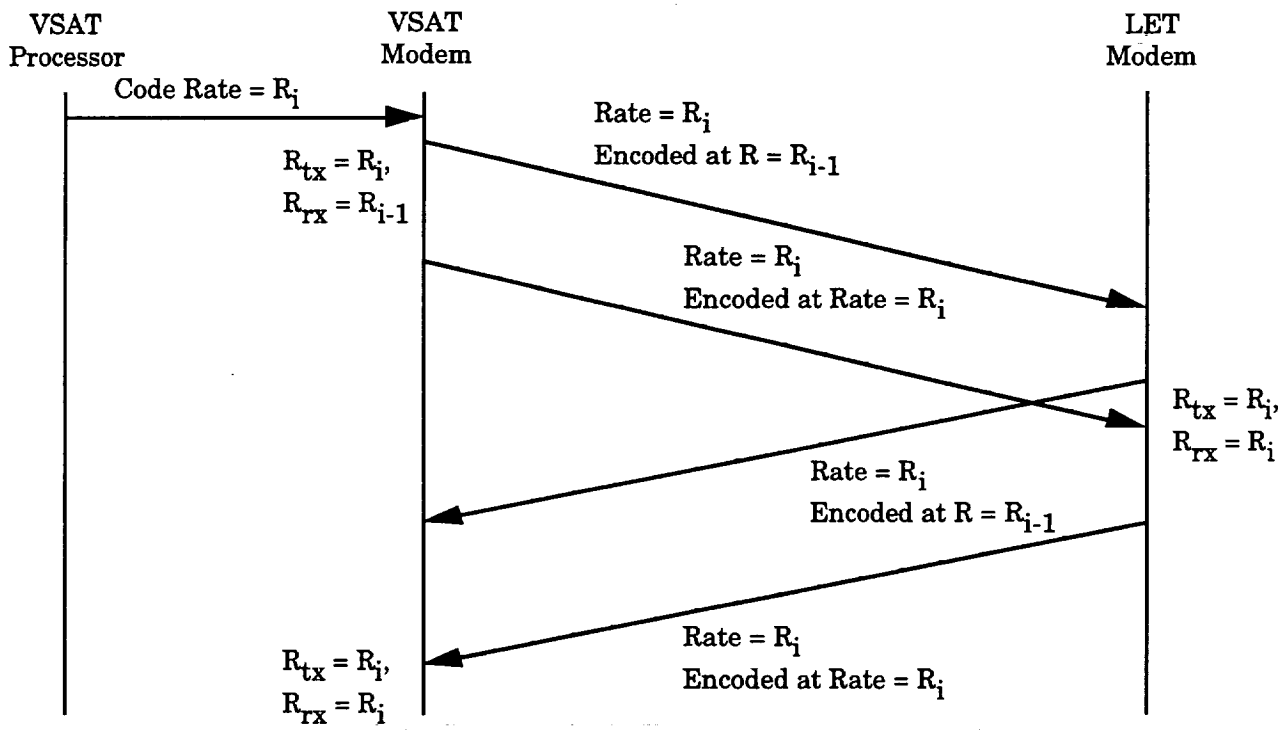

2 * (propagation delay) + Signalling frame period ≤ Delay ≤ 2 * (propagation delay) + 3 * (Signalling frame period)

750 ms ≤ Delay ≤ 1,250 ms

Figure 8-7. Code Rate Transition Sequence

data and prepares for the code rate transition by flushing out its' Viterbi decoder at the end of the 7th master frame. Meanwhile, the LET-modem returns the new code rate signaling bit to the VSAT-modem at its first signaling master frame but continues to transmit at the prior code rate. The VSAT-modem prepares for the new code rate which will occur at the first signaling frame following receipt of the new code rate indication. Since the modems are providing clock to the BER test sets, they will reduce the clock rate by one-half as they change code rate. The delay between the request for new code rate and the completed transition to the new code rate is between 750 ms and 1,250 ms for the signaling frame rate of 4 signaling frames/s and a space segment propagation delay of 250 ms. A state transition diagram for this process is shown in Figure 8-8. The variable CR is the code rate desired by the computer at the site suffering fading.

8.2.3 Fade Compensation Experiment – Link Budgets

Link budgets for the LET to VSAT and VSAT to LET links are shown in Tables 8-5 and 8-6. They reflect the performance of the LET, ACTS and NEWTEC CY VSAT terminal which is available at Clarksburg. The link budgets include no modem implementation margin and use the theoretical C/N_O threshold applicable to the modulation, coding and 3.576 μs QPSK symbol duration utilized.

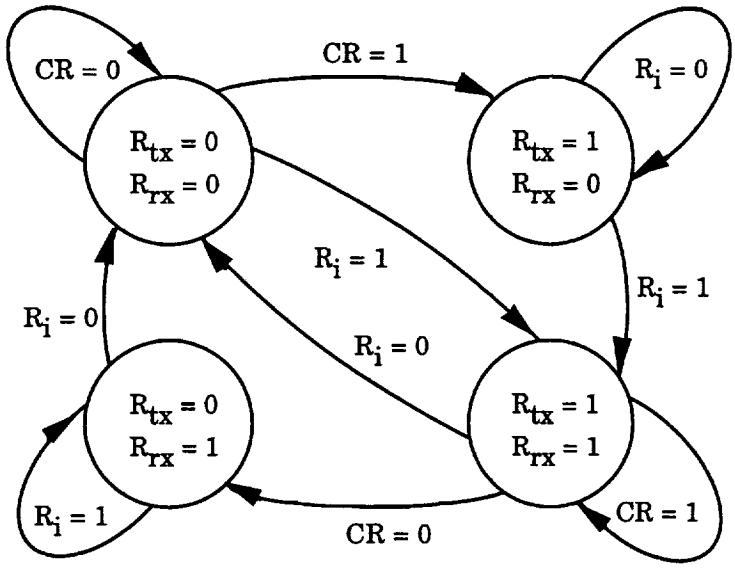

Figure 8-8. Code Rate Transition State Diagram

Table 8-5. LET to VSAT Link Budget

Uplink		
Carrier Frequency, F	29.00	GHz
LET EIRP	75.00	dBW
Backoff	42.00	dB
Pointing loss	0.50	dB
Single tone e.i.r.p.	32.50	dBW
Distance to satellite, S	38,000	km
Path Loss, Ls	213.29	dB
Clear Sky Attenuation, Lc	0.50	dB
Rain Attenuation, Lr	0.00	dB
Polarization loss, Lp	0.50	dB
G/T	23.10	dB/K
Received C/No	69.91	dB-Hz

Downlink		
Carrier frequency, [F]	19.28	GHz
Fixed beam e.i.r.p. at saturation	65.00	dBW
Backoff	26.00	dB
Satellite pointing loss	0.22	dB
e.i.r.p.	38.78	dBW
Distance to VSAT, [S]	38,500	km
Spreading loss, [Ls]	209.85	dB
Clear sky attenuation, [Lc]	0.50	dB
Rain attenuation, [Lr]	0.00	dB
Clear sky noise temperature, [Ts]	275	K
Downlink Degradation	0.00	dB
Polarization loss	0.13	dB
Antenna gain	45.58	dB
Pointing loss	0.50	dB
Downlink C/No	77.59	dB-Hz
VSAT phase noise	71.70	dB-Hz
Combined C/No	67.28	dB-Hz
C/No required (BER=10E-9)	61.80	dB-Hz
Margin	5.48	dB

Table 8-6. VSAT to LET Link Budget

Uplink		
Carrier Frequency, [F]	29.00	GHz
VSAT terminal e.i.r.p.	40.01	dBW
Backoff	5.00	dB
Pointing loss	0.50	dB
e.i.r.p.	34.51	dBW
Distance to satellite, [S]	38,500	km
Path loss, [Ls]	213.40	dB
Clear sky attenuation, [Lc]	0.50	dB
Rain attenuation, [Lr]	0.00	dB
Polarization loss, [Lp]	0.50	dB
G/T	20.00	dB/K
Uplink C/No	68.71	dB-Hz

Downlink		
Carrier frequency, [F]	19.28	GHz
Fixed beam e.i.r.p. at saturation	65.00	dBW
Backoff	18.49	dB
Satellite pointing loss	0.22	dB
e.i.r.p.	46.29	dBW
Distance to LeRC, [S]	38,000	km
Path loss, [Lp]	209.74	dB
Clear sky attenuation, [Lc]	0.50	dB
Rain attenuation, [Lr]	0.00	dB
Clear sky noise temperature, [Ts]	1260.00	K
Rain fade, [Lf]	0.00	dB
Polarization loss	0.13	dB
Pointing loss	0.50	dB
Downlink C/No	90.57	dB-Hz
Combined C/No	68.68	dB-Hz
C/No required (BER=10E-9)	61.80	dB-Hz
Margin	6.88	dB

8.2.4 Fade Compensation Experiment – Cost Estimate

A cost estimate for the Fade Compensation Experiment is shown in Table 8-7. This estimate makes similar assumptions to those of the Fade Measurement Experiment cost estimate. This cost estimate also assumes that the Fade Measurement Experiment has been performed and that all hardware modifications to the modems were performed at that time. A second beacon receiver may be required for this experiment. Modem modifications include the firmware revisions allowing the modem to respond to and initiate signaling channel commands, perform error-free code rate transitions, respond to code rate commands sent by the local computer and report operational parameters to the local computer for archiving. Significant additional software is required within the computers to initiate code rate transitions, monitor and record experiment data.

8.2.5 Fade Compensation Experiment-Schedule

The schedule for the Fade Measurement Experiment is shown in Figure 8-9. The duration of the experiment is expected to be approximately ten months.

8.3 ATM EXPERIMENT

The purpose of this experiment is to demonstrate the use of the VS/VD feedback flow control mechanism in Ka-band satellites to compensate for link attenuation due to rain fades. Quantitative measurements are response delays, cell transmission rates, and cell loss ratios (CLR). These measurements are useful metrics to assess the effectiveness of the feedback flow control mechanism in the satellite environment where the propagation delays are large compared to terrestrial networks. It is important that these parameters are collected for each fade duration. To control the CLR, large buffers are needed since there are a large number of cells in transit due to the large propagation delay in geostationary satellite communications.

Table 8-7. Cost Estimate for the Fade Compensation Experiment

DEVELOPMENT COST	
Modem modifications (firmware)	38 K
Software design (algorithms)	20 K
EQUIPMENT COST	
Beacon receiver	4 K
EXPERIMENT COST	
Experiment design	25 K
Design reviews	12 K
Testing	26 K
Data collection	10 K
Data analysis and reporting	12 K
TOTAL	$150 K

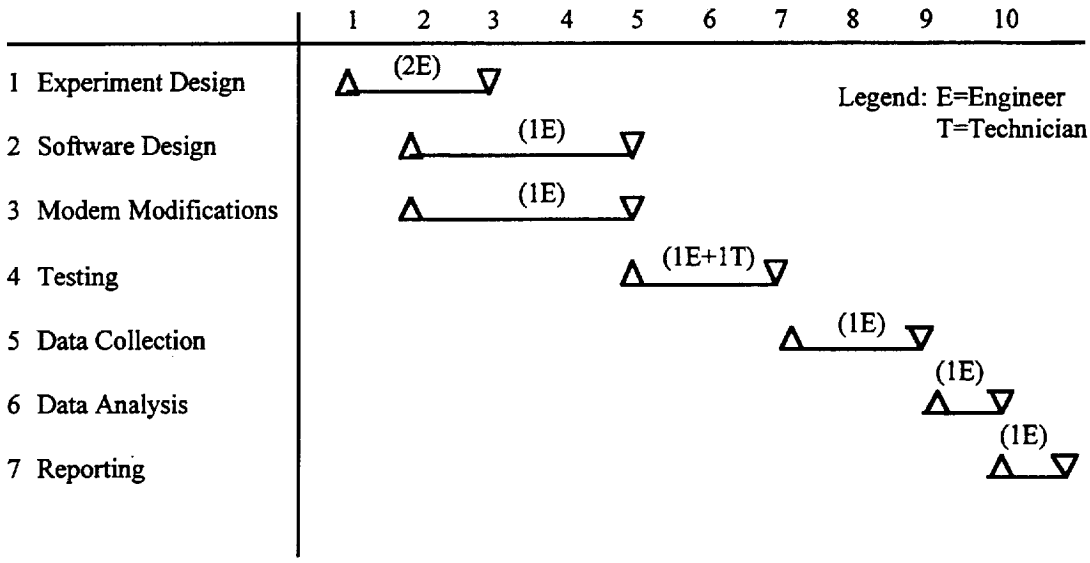

Figure 8-9. Schedule for Fade Compensation Experiment

8.3.1 Description

Figure 8-10 illustrates the test configuration. The ABR end-to-end connection under test is segmented at ALA equipment into three separate loops as indicated by the ellipses. In the first loop, the ABR traffic generator is the source end-system and the local ALA is the virtual destination. In the middle loop, the local and remote ALAs are the virtual source and the virtual destination, respectively. In the third loop, the remote ALA behaves as a virtual source and the ABR traffic analyzer as the destination end-system. RM cells generated by the source end-system (or a virtual source) are turned around by its virtual destination (or the destination end-system) and not forwarded to the next loop of the connection.

It is preferable that RM cell generation rates are the same in all three loops. In each loop, the RM cell generator is required to stamp the creation time and termination time on each RM cell in order to compute their full-loop delays. The response delays, estimated at about one-half full-loop delays, are recorded for RM cells with CI=1 by their generators.

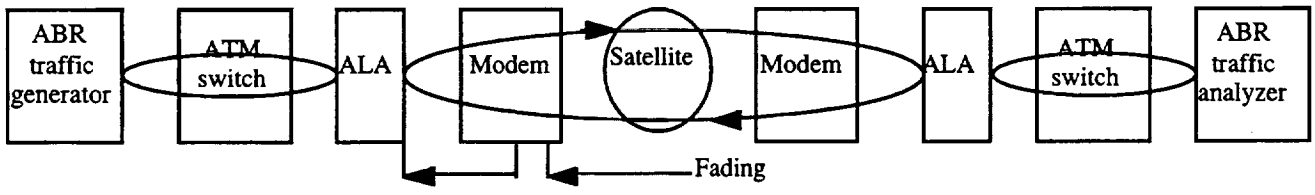

Figure 8-10. ATM Experiment Configuration

Data cells generated by the ABR traffic generator are processed by the ABR traffic analyzer. The VS/VD loops for RM cells are however transparent to data cells. The transmission rate of data cells determined by the reciprocal of measured inter-cell departure times is recorded by the ABR traffic generator. The desired cell transmission rate during fade compensation is one-half of the clear-weather rate.

The measurement and recording of the CLR for data cells are accomplished by the ABR traffic analyzer. The ALAs also record statistics of the number of cells in their buffers, including maximum, mean, and variance. The product of transmission rate and response delay should be used to determine the buffer requirement.

This experiment will make use of equipment setups in Experiments 1 and 2, including earth stations, modems, and fade measurement and compensation equipment. When the satellite link encounters attenuation, the fade detectors will trigger a rate reduction and code rate change in the transmit and receive modems. The modems then provide clock information to their ALAs. The ALAs then process and/or generate RM cells based on the current clock rate. These RM cells contain feedback information which enables an ABR source to adapt its transmission rate.

8.3.2 Development

The experiment configuration shown in Figure 8-10 shows that the needed test equipment includes an ABR traffic generator, ATM switches, ALAs, modems, and earth stations. To perform this experiment, the following development is needed for the test equipment.

The workstations must be equipped with controllers capable of generating and receiving traffic at different rates. Also, the workstations must have ATM adapters to interface with an ATM switch. The workstation functioning as an ABR traffic generator must have software which accomplishes:

(1) Generation of ABR data traffic with rate control,

(2) Recording and plotting output cell rate,

(3) Generation, insertion, and time-stamping forward RM cells,

(4) Searching for backward RM cells,

(5) Time-stamping and computing the response delays of RM cells,

(6) Adjusting data output rate according to information specified in backward RM cells, and

(7) Terminating backward RM cells.

The workstation functioning as an ABR traffic analyzer must have software which accomplishes:

(1) Turning around forward RM cells,

(2) Adapting to incoming traffic rate, and

(3) Analyzing received data.

At present, ALAs provide limited capability such as cell insertion and signal conditioning. RM cell processing and generation capabilities are not available. Therefore, ALAs must be modified to perform the following functions:

(1) Differentiate cell types,

(2) Acquire modem clock,

(3) Turn-around forward RM cells,

(4) Forward data cells,

(5) Generate and time-stamp RM cells,

(6) Time-stamp and terminate backward RM cells,

(7) Compute the response delays, and

(8) Collect buffer usage statistics.

8.3.3 Cost Estimate

The cost breakdown for this experiment is shown in Table 8-8. Specifically, the total cost is approximately $265K for developing ABR traffic generation and analysis, modifying ALAs, and implementing the ALA/modem interface. The equipment cost is approximately $111K for two ALAs, two workstations, two ATM adapters, and two ATM switches and associated software. The experimental cost estimate is $96K for a detailed test procedure, equipment setups, testing, and data analysis. Summing these estimates results in a total of $472K. These estimates are preliminary and subjected to change as information becomes available.

8.3.4 Experiment Schedule

The milestones for this experiment are shown in Figure 8-11. The timeline is estimated in terms of the number of months to complete each task. The number of engineering staff involved is also indicated for each task.

Table 8-8. Preliminary Cost Estimate for ATM Experiment

DEVELOPMENT COST	
ALA modification	170 K
ABR traffic generation and analysis	80 K
ALA-modem interface	15 K
EQUIPMENT COST	
ALAs (2 @ 9 K/Unit	19 K
ATM adapters (2 @ 1 K)	2 K
Workstations (2 @ 5 K/Unit)	10 K
ATM switches and management software	80 K
EXPERIMENT COST	
Design reviews	30 K
Setup	22 K
Testing	22 K
Data collection and analysis	22 K
TOTAL	472 K

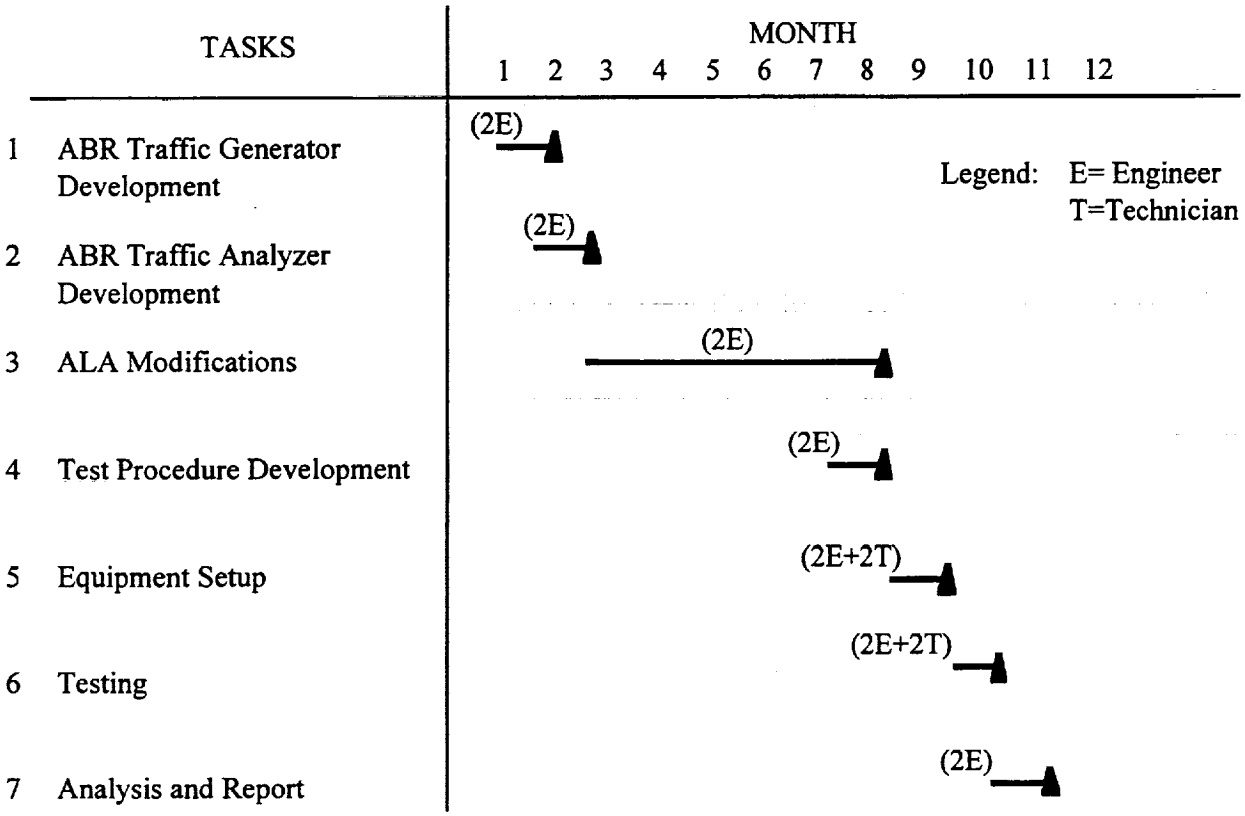

Figure 8-11. ATM Experiment Schedule

As shown in Figure 8-11, the experiment effort encompasses several tasks: (1) ABR traffic generation, (2) ABR traffic analysis, (3) ALA modifications, (4) test procedure design and review, (5) equipment setup, (6) testing, (7) data analysis and reporting. The time to complete Tasks 1 and 2 is approximately 2.7 months by two full-time software engineers familiar with ATM technology and protocols. These engineers then proceed with Task 3 that can be accomplished in approximately 5.8 months. While the software engineers working on Tasks 1, 2, and 3, two systems engineers develop and finalize detailed test procedures (i.e., Task 4) in about one month. Task 5 is followed upon completion of the first four tasks and can be accomplished in two weeks by two technicians and two test procedure development engineers. Tasks 6 and 7 take approximately two weeks and one month, respectively. Experiment report generation is expected to require approximately 1 month.

SECTION 9 — SUMMARY AND CONCLUSIONS

Following a detailed review and evaluation of the Ka-band rain fade characteristics, a study has been performed to evaluate a number of practical rain fade compensation alternatives for possible implementation in recently proposed commercial Ka-band communications satellite systems. Three experiments have also been proposed to assess the implementation issues related to these techniques. The first experiment deals with rain fade measurement techniques while the second one covers the rain fade compensation techniques. A feedback flow control technique for the ABR service (i.e., for ATM-based traffic) is addressed in the third experiment.

The evaluated rain fade characteristics, which directly affect the rain fade compensation techniques, include rain attenuation or fade depth, rain and ice depolarization, tropospheric scintillation, fade duration, inter-fade interval, fade rate, frequency scaling of fade, correlation of fades within a 1-GHz bandwidth, simultaneity of rain events over extended areas, and antenna wetting. The evaluated fade measurement techniques include satellite beacon power, modem AGC, pseudo bit error ratio, bit error ratio from channel coded data, bit error ratio from known data pattern, and signal-to-noise ratio. The evaluated fade compensation techniques include built-in link margin, overdriven satellite transponder, uplink power control, diversity techniques (i.e., frequency diversity, site diversity through routing, and back-up terrestrial network), information rate and FEC code rate changes, downlink power sharing (i.e., active phased array, active lens array, matrix or multiport amplifier, and multimode amplifier), and ABR feedback flow control technique for varying the information rate from the source.

Based on the evaluation criteria of measurement accuracy and time, and implementation complexity, the three measurement techniques which were selected for further evaluation in the first two experiments are beacon power, bit error ratio from channel coded data, and signal-to-noise ratio. The two compensation techniques which were selected for further evaluation in the second experiment are uplink power control, and information rate and FEC code rate changes. Implementation of the ABR feedback flow control technique is carried out in the third experiment. For each experiment, preliminary details are provided on the experiment setup, development phases covering the system engineering, hardware, and software aspects, and high-level cost estimates.

In particular, the following conclusions can be made:

(1) Due to severe fading in Ka-bands in a number of rain zones, sufficient system margins should be allocated for all carriers in a network. In a Ka-band satellite system, for the link from earth station A to earth station B, the system margin

generally consists of a fixed clear-sky margin and an additional margin which is dynamically allocated through the rain fade compensation technique being implemented. The fixed clear-sky margin must include clear-sky attenuation (i.e., gaseous absorption), fade measurement accuracy, frequency scaling error, and additional incremental change in fading at the time the fade compensation system is activated (i.e., carrier power being increased or decreased). This margin is typically in the range of 4-5 dB.

The dynamically allocated margin depends on several factors such as required high link availability, earth stations located in heavy rain zones (e.g., rain zones M and P), etc.; and directly impacts the system costs (e.g., earth station HPAs and antenna sizes, and satellites with high downlink EIRP's). It is not uncommon to provide more than 15 dB in the dynamic range of a typical uplink power control system in moderate and heavy rain zones.

(2) In order to provide a high system margin, it is desirable to combine the uplink power control technique and the technique which implements the source information rate and FEC code rate changes. The use of the second technique alone will contribute about 3 to 4.5 dB toward the dynamic part of the system margin; and will, therefore, reduce the size of the earth station HPA.

(3) The three proposed experiments are intended to assess the feasibility of the selected fade measurement and compensation techniques, and ABR feedback flow control technique. The first experiment, planned for a ten-month period, will compare the beacon power, bit error ratio from channel coded data, and signal-to-noise ratio techniques in terms of implementation issues such as measurement accuracy and reliability, stability of measured data, and ease of operation. The second experiment, also planned for a ten-month period, will address the implementation issues related to the uplink power control technique and the technique which implements the source information rate and FEC code rate changes, and the combination of both techniques. The third experiment, planned for a twelve-month period, will address the implementation issues related to the ABR feedback flow control technique.

SECTION 10 — REFERENCES

[1] T. Inukai, "Ka-Band Satellite Communications Systems Proposed by U.S. Corporations," Proceedings of Fifth ESA International Workshop on Digital Signal Processing Techniques Applied to Space Communications, Barcelona, Spain, 25-27 September 1996, pp. 7.1-7.11.

[2] P. P. Nuspl et al. , "On-Board Processing for Communications Satellites: Systems and Benefits," International Journal of Satellite Communications, Vol. 5, No. 2, April-June 1987, pp. 65-76.

[3] T. Inukai, F. Faris, and D. Shyy, "On-Board Processing Satellite Network Architectures for Broadband ISDN," 14th International Communication Satellite Systems Conference Record, Washington, DC, March 22-24, 1992, pp. 1471-1484.

[4] G. Chiassarini, G. Gallinaro and A. Vernucci, "Digital Signal Processing Exploitation Trends for Future On-Board Processing Satellite Systems," Proceedings of Fifth ESA International Workshop on Digital Signal Processing Techniques Applied to Space Communications, Barcelona, Spain, 25-27 September 1996, pp. 6.1-6.16.

[5] F. Gargione et al., "Advanced Communications Technology Satellite (ACTS): Design and On-Orbit Performance Measurements," International Journal of Satellite Communications, Vol. 14, No. 3, May-June 1996, pp. 133-159.

[6] P. L. Bargellini, Editor, "The INTELSAT IV Communications System," COMSAT Technical Review, Vol. 2, No. 2, Fall 1972, pp. 437-572.

[7] W. L. Morgan and G. D. Gordon, *Communications Satellite Handbook.* New York: J. Wiley & Sons, Inc., 1989, pp. 371-399.

[8] M. P. Brown et al., "INTELSAT VI Transmission Design and Computer System Models for FDMA Services," COMSAT Technical Review, Vol. 20, No. 2, Fall 1990, pp. 373-399.

[9] J. C. Fuenzalida, O. Shimbo, and W. L. Cook, "Time-Domain Analysis of Intermodulation Effects Caused by Nonlinear Amplifiers," COMSAT Technical Review, Vol. 3, No. 1, Spring 1973, pp. 89-143.

[10] O. Shimbo, L. N. Nguyen, and J. P. A. Albuquerque, "Modulation-Transfer Noise Effects among FM and Digital Signals in Memoryless Nonlinear Devices," Proceedings of the IEEE, Vol. 74, No. 4, April 1986, pp. 580-599.

[11] S. J. Campanella et al., "SS-TDMA System Considerations." COMSAT Technical Review, Vol. 20, No. 2, Fall 1990, pp. 335-371.

[12] B. A. Pontano, A. I. Zaghloul, and C. E. Mahle, "INTELSAT VI Communications Payload Performance Specifications," COMSAT Technical Review, Vol. 20, No. 2, Fall 1990, pp. 271-308.

[13] N. A. Mathews, "Performance Evaluation of Regenerative Digital Satellite Links with FEC Codecs," Proceedings of the Third Tirrenia International Workshop on Digital Communications, Tirrenia, Italy, 14-16 September 1987, pp. 213-223.

[14] CyberStar, FCC File Numbers 187-SAT-AMEND-95, 188/189-SAT-P/LA-95, 109-SAT-P/LA-95, and 110-SAT-P-95.

[15] Galaxy/Spaceway, FCC File Numbers 174-SAT-P/LA-95 through 181-SAT-P/LA-95.

[16] Astrolink, FCC File Numbers 187-SAT-AMEND-95, and 188/189-SAT-P/LA-95.

[17] ITU Recommendation ITU-R RPN.618-4, 1996

[18] Allnutt, J. E.; Satellite-to-ground Radiowave Propagation, London: Peter Peregrinus Ltd., 1989

[19] Van de Hulst, H. C.; Light Scattering by Small Particles,London: Dover, 1958.

[20] Proceedings of NAPEX VI, Fairbanks, AL, 1996

[21] A. W. Dissanayake and N. J. McEwan, "Radar and attenuating properties of rain and bright band," IEE Conf. Publ. 169-2, pp. 125-129, 1978

[22] G. Ortgies, F. Rucker, and F. Dintelman, "Statistics of clear-air attenuation on satellite links at 20 and 30 GHz," Electron. Lett., vol. 26, pp. 358 - 360, 1990

[23] Cox, D. C., Arnold, H. W.; Results from the 19- and 28-GHz COMSTAR Satellite Propagation Experiments at Crawford Hill, Proc. IEEE, Vol. 70, pp. 458-488, 1982

[24] Paraboni, A., Riva, C.; A New Method for Prediction of Fade Duration Statistics in Satellite Links Above 10 GHz Int. Jrnl. Satellite Communications, Vol. 12, pp. 387 - 394, 1994.

[25] th ACTS Propagation Workshop; Reston, VA, November 1996

[26] Belvis, B. C.; Losses due to rain on radomes and antenna reflecting surfaces IEEE Trans. Antennas and Prop., January 1965, pp.175 - 176

[27] F. Gargione et al., "Advanced Communications Technology Satellite (ACTS): Design and On-Orbit Performance Measurements". International Journal of Satellite Communications, Vol. 14, Issue 3, May/June 1996.

[28] COMSAT Laboratories, "ACTS Up-Link Power Control Experiment," Final Report Submitted to NASA Lewis Research Center under Contract NAS 326402, March 1995.

[29] J. S. Snyder et al., "Pseudo-Bit -Error- Rate Measurement for 120 Mbit/s TDMA," *COMSAT Technical Review*, Volume 14, Number 2, Fall 1984, pp. 285-311.

[30] INTELSAT Document IESS-308 (Rev. 6B), "Performance Characteristics for Intermediate Data Rate (IDR) Digital Carriers," 4 December 1992.

[31] M. E. Jones, E. K. Koh, and D. E. Weinreich, "INTELSAT TDMA Link Design and Transmission Simulation," COMSAT Technical Review, Vol. 16, No. 1, Spring 1986, pp. 53-125.

[32] O. Shimbo, *Transmission Analysis in Communication Systems*, Vol. 2. Maryland: Computer Science Press, 1988, Chapters 2 and 3.

[33] R. J. Schertler, "Summary Report on Key ACTS Experiments," 16th International Communications Satellite Systems Conference Record, Washington, DC, February 25-29, 1996, pp. 738-748.

[34] B. K. Levitt, "Rain Compensation Algorithm for ACTS Mobile Terminal," IEEE Journal on Selected Areas in Communications, Vol. 10, No. 2, February 1992, pp. 358-363.

[35] N. Lay and K. Dessouky, "A Communication Protocol for Mobile Satellite Systems Affected by Rain Attenuation ," IEEE Journal on Selected Areas in Communications, Vol. 10, No. 6, August 1992, pp. 1037-1047.

[36] E. H. Satorius and L. H. Tong, "Analysis of a Rain Compensation Algorithm for K/Ka-Band Communications," International Journal of Satellite Communications, Vol. 14, No. 3, May-June 1996, pp. 297-311.

[37] L.T. Vuong, H. Paul, and D. Cole, "Matrix Amplifier and Routing System (MARS)," prepared for the U.S. Air Force Space and Missile Systems Center (SMC/MCX), Los Angeles AFB, CA, August 11, 1993 [no performing organization report number is shown].

[38] "TRP Active Transmit Phased Array Project Review," 11 March 1997. An ARPA, NASA, SS/L, SRC joint development effort for a 20-GHz active transmit phased array.

[39] M. Hecht, "ACTS Dual Power TWTA Study," NASA/ACTS-MCP-457, 88-CS-2604, RCA Astro-Space Division, East Windsor, NJ (June 3, 1988).

[40] D. Ginsburg, ATM Solutions for Enterprise Internetworking. England: Addison-Wesley, 1996, Chapter 3.

[41] The ATM Forum, Traffic Management Specification v4.0, April 1996.

[42] COMSAT Laboratories marketing brochure for ATM Link Accelerator™ (ALA-2000™).

[43] J. W. Marshall and A. Q. Le, "Approaches and Requirements for Tactical SATCOM ATM Integration," MILCOM Conference Record, San Diego, 5-8 November 1995, pp. 212-216.

[44] European Telecommunications Standards ETS 300 421, "Digital broadcasting systems for television, sound and data services; Framing structure, channel coding and modulation for 11/12 GHz satellite services". December, 1994.

APPENDIX A — FADE MEASUREMENT TECHNIQUE ERROR ANALYSIS RESULTS

Bent Pipe with Back-off		
Low Cost Beacon Receiver		
Source of Error	**Residual Error, [±dB]**	**Comments**
Beacon power fluctuations at receive terminal	0.31	Fade estimate errors caused by satellite beacon power and pointing errors are much less than propagation effects. Propagation effects are dominated by frequency scaling of gaseous absorption.
Receive antenna pointing errors and efficiency variations	0.90	Dominated by inaccurate frequency scaling of feed window wetting.
Receive gain fluctuations	1.00	Residual error will be related to the worst case day-to-day temperature change at a constant time of day.
Beacon power level measurement accuracy	0.75	Expensive beacon receivers can provide ±0.25 dB accuracy. Accuracy of low cost receiver is estimated to be ±0.75 dB.
RSS Error	1.57	Worst case values above are interpreted as two sigma values. Error is less than value 95% of time.
Mean square error	0.79	Half of two sigma value.
Degradation estimate accuracy	±1.25 dB	Beacon receiver measures fading on path while comparison is performed on accuracy of degradation estimate. Terminal must assume system and sky noise temperature and calculate degradation from fade measurement.

Bent Pipe with Back-off		
Automatic Gain Control Signal Measurement		
Source of Error	**Residual Error, [±dB]**	**Comments**
Transmit power variations across frequency band	1.50	Uplink transmit power variations with frequency are approximately ±1.5 dB.
Transmit power variations over temperature	0.50	Typically ±2 dB from -40°C to 50°C. Time of day correction removes all but the worst case day to day temperature variation at constant time-of-day which is approximately ±0.5 dB/10°C.
Accuracy of uplink compensation	1.00	If signal is not regenerated on the satellite then uplink fading must be compensated for at the transmit station. Downlink C/N and BER will be affected by residual fade.
Satellite motion	0.33	Received signal power fluctuations caused by satellite motion are more significant for narrow beam antennas. ±0.05° satellite orientation error produces ±0.33 dB signal level variation at receive terminal in 0.3° beam.
Satellite gain variations across frequency band	0.50	Gain variations across the transponder do not affect (C/N)up but (C/N)down is affected. Apply half of the typical error for a link with (C/N)up = (C/N)down.
Satellite gain variations at a fixed frequency	0.50	Thermal gain variations of the transponder do not affect (C/N)up but (C/N)down is affected. Apply half of the typical error for a link with (C/N)up = (C/N)down.
Downlink propagation effects	0.31	Propagation effects are dominated by frequency scaling of gaseous absorption.
LNA gain fluctuations	1.00	LNA gain variations affect signal and noise equally.
RSS of worst case errors	2.28	Error is less than this value 95% of the time.
RSS error	1.14	RMS error or one sigma error.
Mean square error in fade estimate	1.75	[Eb/No] clear-sky =9 dB
Mean square error in degradation estimate	3.94	Fade =2±1.75 dB, Tm=280 ±10, Ts=230±10

Bent Pipe with Back-off		
Pseudo-Bit Error Rate		
Source of Error		**Comments**
Transmit power variations across frequency band	1.50	Uplink transmit power variations with frequency are approximately ±1.5 dB.
Transmit power variations over temperature	0.50	Typically ±2 dB from -40°C to 50°C. Time of day correction removes all but the worst case day to day temperature variation at constant time-of-day which is approximately ±0.5 dB/10°C.
Accuracy of uplink compensation	1.00	If signal is not regenerated on the satellite then uplink fading must be compensated for at the transmit station. Downlink C/N and BER will be affected by residual fade.
Satellite motion	0.33	Received signal power fluctuations caused by satellite motion are more significant for narrow beam antennas. ±0.05° satellite orientation error produces ±0.33 dB signal level variation at receive terminal in 0.3° beam.
Satellite gain variations across frequency band	0.50	Gain variations across the transponder do not affect (C/N)up but (C/N)down is affected. Apply half of the typical error for a link with (C/N)up = (C/N)down.
Satellite gain variations at a fixed frequency	0.50	Gain variations across the transponder do not affect (C/N)up but (C/N)down is affected. Apply half of the typical error for a link with (C/N)up = (C/N)down.
Downlink propagation effects	0.31	Propagation effects are dominated by frequency scaling of gaseous absorption.
LNA gain fluctuations	0.00	LNA gain variations affect signal and noise equally.
Fade measurement accuracy	0.50	Channel BER=0.01, 95% confidence interval is 0.5 dB.
RSS error	2.11	Square root of the sum of the worst case errors.
Mean square error	1.06	Mean square or one sigma error.

Bent Pipe with Back-off		
Bit Error Rate Measurement on Channel Coded Data		
Source of Error		**Comments**
Transmit power variations across frequency band	1.50	Uplink transmit power variations with frequency are approximately ±1.5 dB.
Transmit power variations over temperature	0.50	Typically ±2 dB from -40°C to 50°C. Time of day correction removes all but the worst case day to day temperature variation at constant time-of-day which is approximately ±0.5 dB/10°C.
Accuracy of uplink compensation	1.00	If signal is not regenerated on the satellite then uplink fading must be compensated for at the transmit station. Downlink C/N and BER will be affected by residual fade.
Satellite motion	0.33	Received signal power fluctuations caused by satellite motion are more significant for narrow beam antennas. ±0.05° satellite orientation error produces ±0.33 dB signal level variation at receive terminal in 0.3° beam.
Satellite gain variations across frequency band	0.50	Gain variations across the transponder do not affect (C/N)up but (C/N)down is affected. Apply half of the typical error for a link with (C/N)up = (C/N)down.
Satellite gain variations at a fixed frequency	0.50	Thermal gain variations of the transponder do not affect (C/N)up but (C/N)down is affected. Apply half of the typical error for a link with (C/N)up = (C/N)down.
Downlink propagation effects	0.31	Propagation effects are dominated by frequency scaling of gaseous absorption.
LNA gain fluctuations	0.00	LNA gain variations affect signal and noise equally.
Fade measurement accuracy	0.30	Channel BER=5E-4, 95% confidence interval is 0.3 dB.
RSS error	2.07	Square root of the sum of the worst case errors.
Mean square error	1.04	Mean square or one sigma error.

Bent Pipe with Back-off		
Bit Error Rate Measurement from Known Data Pattern		
Source of Error		**Comments**
Transmit power variations across frequency band	1.50	Uplink transmit power variations with frequency are approximately ±1.5 dB.
Transmit power variations over temperature	0.50	Typically ±2 dB from -40°C to 50°C. Time of day correction removes all but the worst case day to day temperature variation at constant time-of-day which is approximately ±0.5 dB/10°C.
Accuracy of uplink compensation	1.00	If signal is not regenerated on the satellite then uplink fading must be compensated for at the transmit station. Downlink C/N and BER will be affected by residual fade.
Satellite motion	0.33	Received signal power fluctuations caused by satellite motion are more significant for narrow beam antennas. ±0.05° satellite orientation error produces ±0.33 dB signal level variation at receive terminal in 0.3° beam.
Satellite gain variations across frequency band	0.50	Gain variations across the transponder do not affect (C/N)up but (C/N)down is affected. Apply half of the typical error for a link with (C/N)up = (C/N)down.
Satellite gain variations at a fixed frequency	0.50	Gain variations across the transponder do not affect (C/N)up but (C/N)down is affected. Apply half of the typical error for a link with (C/N)up = (C/N)down.
Downlink propagation effects	0.31	Propagation effects are dominated by frequency scaling of gaseous absorption.
LNA gain fluctuations	0.00	LNA gain variations affect signal and noise equally.
Fade measurement accuracy	0.50	Channel BER=0.01, 95% confidence interval is ±0.5 dB.
Total Error	2.11	Square root of the sum of the worst case errors.
Mean square error	1.06	Mean square or one sigma error.

Bent Pipe with Back-off		
Signal to Noise Ratio Measurement		
Source of Error		**Comments**
Transmit power variations across frequency band	1.50	Uplink transmit power variations with frequency are approximately ±1.5 dB.
Transmit power variations over temperature	0.50	Typically ±2 dB from -40°C to 50°C. Time of day correction removes all but the worst case day to day temperature variation at constant time-of-day which is approximately ±0.5 dB/10°C.
Accuracy of uplink compensation	1.00	If signal is not regenerated on the satellite then uplink fading must be compensated for at the transmit station. Downlink C/N and BER will be affected by residual fade.
Satellite motion	0.33	Received signal power fluctuations caused by satellite motion are more significant for narrow beam antennas. ±0.05° satellite orientation error produces ±0.33 dB signal level variation at receive terminal in 0.3° beam.
Satellite gain variations across frequency band	0.50	Gain variations across the transponder do not affect (C/N)up but (C/N)down is affected. Apply half of the typical error for a link with (C/N)up = (C/N)down.
Satellite gain variations at a fixed frequency	0.50	Thermal gain variations of the transponder do not affect (C/N)up but (C/N)down is affected. Apply half of the typical error for a link with (C/N)up = (C/N)down.
Downlink propagation effects	0.31	Propagation effects are dominated by frequency scaling of gaseous absorption.
LNA gain fluctuations	0.00	LNA gain variations affect signal and noise equally.
Fade measurement accuracy	0.10	For Eb/No > 5 dB, 95% confidence interval is 0.1 dB.
RSS error	2.05	Square root of the sum of the worst case errors.
Mean square error	1.03	Mean square or one sigma error.

Bent Pipe with Saturated Transponder		
Low Cost Beacon Receiver		
Source of Error	**Residual Error, [±dB]**	**Comments**
Beacon power fluctuations at receive terminal	0.31	Fade estimate errors caused by satellite beacon power and pointing errors are much less than propagation effects. Propagation effects are dominated by frequency scaling of gaseous absorption.
Receive antenna pointing errors and efficiency variations	0.90	Dominated by inaccurate frequency scaling of feed window wetting.
Receive gain fluctuations	1.00	Residual error will be related to the worst case day-to-day temperature change at a constant time of day.
Beacon power level measurement accuracy	0.75	Expensive beacon receivers can provide ±0.25 dB accuracy. Accuracy of low cost receiver is estimated to be ±0.75 dB.
RSS Error	1.57	Worst case values above are interpreted as two sigma values. Error is less than value 95% of time.
Mean square error	0.79	
Degradation estimate accuracy	±1.25 dB	Beacon receiver measures fading on path while comparison is performed on accuracy of degradation estimate. Terminal must assume system and sky noise temperature and calculate degradation from fade measurement.

Bent Pipe with Saturated Transponder		
Automatic Gain Control Signal Measurement		
Source of Error	**Residual Error, [±dB]**	**Comments**
Transmit power variations across frequency band	0.15	Uplink transmit power variations with frequency of ±1.5 dB will be reduced to approximately ±0.15 dB in saturated transponder.
Transmit power variations over temperature	0.05	Uplink transmit power variations with temperature of ±0.5 dB will be reduced to approximately ±0.05 dB in saturated transponder.
Accuracy of uplink compensation	0.10	Uplink compensation errors of ±1.0 dB will be reduced to approximately ±0.1 dB in saturated transponder.
Satellite motion	0.33	Received signal power fluctuations caused by satellite motion are more significant for narrow beam antennas. ±0.05° satellite orientation error produces ±0.33 dB signal level variation at receive terminal in 0.3° beam.
Satellite gain variations across frequency band	0.50	Gain variations across the transponder do not affect (C/N)up but (C/N)down is affected. Apply half of the typical error for a link with (C/N)up = (C/N)down.
Satellite gain variations at a fixed frequency	0.50	Thermal gain variations of the transponder do not affect (C/N)up but (C/N)down is affected. Apply half of the typical error for a link with (C/N)up = (C/N)down.
Downlink propagation effects	0.31	Propagation effects are dominated by frequency scaling of gaseous absorption.
LNA gain fluctuations	1.00	LNA gain variations affect signal and noise equally.
RSS of worst case errors	1.32	Error is less than this value 95% of the time.
RSS error	0.66	RMS error or one sigma error.
Mean square error in fade estimate	0.95	[Eb/No] clear-sky =9 dB
Mean square error in degradation estimate	2.17	Fade =5±1.5 dB, Tm=280 ±10, Ts=230±10

Bent Pipe with Saturated Transponder		
Pseudo-Bit Error Rate		
Source of Error		**Comments**
Transmit power variations across frequency band	0.15	Uplink transmit power variations with frequency of ±1.5 dB will be reduced to approximately ±0.15 dB in saturated transponder.
Transmit power variations over temperature	0.05	Uplink transmit power variations with temperature of ±0.5 dB will be reduced to approximately ±0.05 dB in saturated transponder.
Accuracy of uplink compensation	0.10	Uplink compensation errors of ±1.0 dB will be reduced to approximately ±0.1 dB in saturated transponder.
Satellite motion	0.33	Received signal power fluctuations caused by satellite motion are more significant for narrow beam antennas. ±0.05° satellite orientation error produces ±0.33 dB signal level variation at receive terminal in 0.3° beam.
Satellite gain variations across frequency band	0.50	Gain variations across the transponder do not affect (C/N)up but (C/N)down is affected. Apply half of the typical error for a link with (C/N)up = (C/N)down.
Satellite gain variations at a fixed frequency	0.50	Gain variations across the transponder do not affect (C/N)up but (C/N)down is affected. Apply half of the typical error for a link with (C/N)up = (C/N)down.
Downlink propagation effects	0.31	Propagation effects are dominated by frequency scaling of gaseous absorption.
LNA gain fluctuations	0.00	LNA gain variations affect signal and noise equally.
Fade measurement accuracy	0.50	Channel BER=0.01, 95% confidence interval is 0.3 dB.
RSS error	0.99	Square root of the sum of the worst case errors.
Mean square error	0.50	Mean square or one sigma error.

Bent Pipe with Saturated Transponder		
Bit Error Rate Measurement on Channel Coded Data		
Source of Error		**Comments**
Transmit power variations across frequency band	0.15	Uplink transmit power variations with frequency of ±1.5 dB will be reduced to approximately ±0.15 dB in saturated transponder.
Transmit power variations over temperature	0.05	Uplink transmit power variations with temperature of ±0.5 dB will be reduced to approximately ±0.05 dB in saturated transponder.
Accuracy of uplink compensation	0.10	Uplink compensation errors of ±1.0 dB will be reduced to approximately ±0.1 dB in saturated transponder.
Satellite motion	0.33	Received signal power fluctuations caused by satellite motion are more significant for narrow beam antennas. ±0.05° satellite orientation error produces ±0.33 dB signal level variation at receive terminal in 0.3° beam.
Satellite gain variations across frequency band	0.50	Gain variations across the transponder do not affect (C/N)up but (C/N)down is affected. Apply half of the typical error for a link with (C/N)up = (C/N)down.
Satellite gain variations at a fixed frequency	0.50	Gain variations across the transponder do not affect (C/N)up but (C/N)down is affected. Apply half of the typical error for a link with (C/N)up = (C/N)down.
Downlink propagation effects	0.31	Propagation effects are dominated by frequency scaling of gaseous absorption.
LNA gain fluctuations	0.00	LNA gain variations affect signal and noise equally.
Fade measurement accuracy	0.30	Channel BER=5E-4, 95% confidence interval is 0.3 dB.
RSS error	0.91	Square root of the sum of the worst case errors.
Mean square error	0.46	Mean square or one sigma error.

Bent Pipe with Saturated Transponder		
Bit Error Rate Measurement from Known Data Pattern		
Source of Error		**Comments**
Transmit power variations across frequency band	0.15	Uplink transmit power variations with frequency of ±1.5 dB will be reduced to approximately ±0.15 dB in saturated transponder.
Transmit power variations over temperature	0.05	Uplink transmit power variations with temperature of ±0.5 dB will be reduced to approximately ±0.05 dB in saturated transponder.
Accuracy of uplink compensation	0.10	Uplink compensation errors of ±1.0 dB will be reduced to approximately ±0.1 dB in saturated transponder.
Satellite motion	0.33	Received signal power fluctuations caused by satellite motion are more significant for narrow beam antennas. ±0.05° satellite orientation error produces ±0.33 dB signal level variation at receive terminal in 0.3° beam.
Satellite gain variations across frequency band	0.50	Gain variations across the transponder do not affect (C/N)up but (C/N)down is affected. Apply half of the typical error for a link with (C/N)up = (C/N)down.
Satellite gain variations at a fixed frequency	0.50	Gain variations across the transponder do not affect (C/N)up but (C/N)down is affected. Apply half of the typical error for a link with (C/N)up = (C/N)down.
Downlink propagation effects	0.31	Propagation effects are dominated by frequency scaling of gaseous absorption.
LNA gain fluctuations	0.00	LNA gain variations affect signal and noise equally.
Fade measurement accuracy	0.50	Channel BER=0.01, 95% confidence interval is ±0.5 dB.
Total Error	0.99	Square root of the sum of the worst case errors.
Mean square error	0.50	Mean square or one sigma error.

Bent Pipe with Saturated Transponder		
Signal to Noise Ratio Measurement		
Source of Error		**Comments**
Transmit power variations across frequency band	0.15	Uplink transmit power variations with frequency of ±1.5 dB will be reduced to approximately ±0.15 dB in saturated transponder.
Transmit power variations over temperature	0.05	Uplink transmit power variations with temperature of ±0.5 dB will be reduced to approximately ±0.07 dB in saturated transponder.
Accuracy of uplink compensation	0.10	Uplink compensation errors of ±1.0 dB will be reduced to approximately ±0.1 dB in saturated transponder.
Satellite motion	0.33	Received signal power fluctuations caused by satellite motion are more significant for narrow beam antennas. ±0.05° satellite orientation error produces ±0.33 dB signal level variation at receive terminal in 0.3° beam.
Satellite gain variations across frequency band	0.50	Gain variations across the transponder do not affect (C/N)up but (C/N)down is affected. Apply half of the typical error for a link with (C/N)up = (C/N)down.
Satellite gain variations at a fixed frequency	0.50	Gain variations across the transponder do not affect (C/N)up but (C/N)down is affected. Apply half of the typical error for a link with (C/N)up = (C/N)down.
Downlink propagation effects	0.31	Propagation effects are dominated by frequency scaling of gaseous absorption.
LNA gain fluctuations	0.00	LNA gain variations affect signal and noise equally.
Fade measurement accuracy	0.10	For Eb/No > 5 dB, 95% confidence interval is 0.1 dB.
RSS error	0.87	Square root of the sum of the worst case errors.
Mean square error	0.43	Mean square or one sigma error.

On-board Processing		
Low Cost Beacon Receiver		
Source of Error	**Residual Error, [±dB]**	**Comments**
Beacon power fluctuations at receive terminal	0.31	Fade estimate errors caused by satellite beacon power and pointing errors are much less than propagation effects. Propagation effects are dominated by frequency scaling of gaseous absorption.
Receive antenna pointing errors and efficiency variations	0.90	Dominated by inaccurate frequency scaling of feed window wetting.
Receive gain fluctuations	1.00	Residual error will be related to the worst case day-to-day temperature change at a constant time of day.
Beacon power level measurement accuracy	0.75	Expensive beacon receivers can provide ±0.25 dB accuracy. Accuracy of low cost receiver is estimated to be ±0.75 dB.
RSS Error	1.57	Worst case values above are interpreted as two sigma values. Error is less than value 95% of time.
Mean square error	0.79	
Degradation estimate accuracy	±1.25 dB	Beacon receiver measures fading on path while comparison is performed on accuracy of degradation estimate. Terminal must assume system and sky noise temperature and calculate degradation from fade measurement.

On-board Processing		
Automatic Gain Control Signal Measurement		
Source of Error	**Residual Error, [±dB]**	**Comments**
Transmit power variations across frequency band	0.00	Uplink transmit power variations will not affect downlink power.
Transmit power variations over temperature	0.00	Uplink transmit power variations will not affect downlink power.
Accuracy of uplink compensation	0.00	Uplink compensation errors will not affect downlink power.
Satellite motion	0.33	Received signal power fluctuations caused by satellite motion are more significant for narrow beam antennas. ±0.05° satellite orientation error produces ±0.33 dB signal level variation at receive terminal in 0.3° beam.
Satellite gain variations across frequency band	0.50	Gain variations across the transponder do not affect (C/N)up but (C/N)down is affected. Apply half of the typical error for a link with (C/N)up = (C/N)down.
Satellite gain variations at a fixed frequency	0.50	Thermal gain variations of the transponder do not affect (C/N)up but (C/N)down is affected. Apply half of the typical error for a link with (C/N)up = (C/N)down.
Downlink propagation effects	0.31	Propagation effects are dominated by frequency scaling of gaseous absorption.
LNA gain fluctuations	1.00	LNA gain variations affect signal and noise equally.
RSS of worst case errors	1.31	Error is less than this value 95% of the time.
RSS error	0.65	RMS error or one sigma error.
Mean square error in fade estimate	0.95	[Eb/No] clear-sky =9 dB
Mean square error in degradation estimate	2.17	Fade =2±1.5 dB, Tm=280 ±10, Ts=230±10

On-board Processing		
Pseudo-Bit Error Rate		
Source of Error		**Comments**
Transmit power variations across frequency band	0.15	Uplink transmit power variations with frequency of ±1.5 dB will be reduced to approximately ±0.15 dB in saturated transponder.
Transmit power variations over temperature	0.05	Uplink transmit power variations with temperature of ±0.5 dB will be reduced to approximately ±0.05 dB in saturated transponder.
Accuracy of uplink compensation	0.10	Uplink compensation errors of ±1.0 dB will be reduced to approximately ±0.1 dB in saturated transponder.
Satellite motion	0.33	Received signal power fluctuations caused by satellite motion are more significant for narrow beam antennas. ±0.05° satellite orientation error produces ±0.33 dB signal level variation at receive terminal in 0.3° beam.
Satellite gain variations across frequency band	0.50	Gain variations across the transponder do not affect (C/N)up but (C/N)down is affected. Apply half of the typical error for a link with (C/N)up = (C/N)down.
Satellite gain variations at a fixed frequency	0.50	Gain variations across the transponder do not affect (C/N)up but (C/N)down is affected. Apply half of the typical error for a link with (C/N)up = (C/N)down.
Downlink propagation effects	0.31	Propagation effects are dominated by frequency scaling of gaseous absorption.
LNA gain fluctuations	0.00	LNA gain variations affect signal and noise equally.
Fade measurement accuracy	0.50	Channel BER=0.01, 95% confidence interval is 0.3 dB.
RSS error	0.99	Square root of the sum of the worst case errors.
Mean square error	0.50	Mean square or one sigma error.

On-board Processing		
Bit Error Rate Measurement on Channel Coded Data		
Source of Error		**Comments**
Transmit power variations across frequency band	0.00	Uplink transmit power variations will not affect downlink power.
Transmit power variations over temperature	0.00	Uplink transmit power variations will not affect downlink power.
Accuracy of uplink compensation	0.00	Uplink compensation errors will not affect downlink power.
Satellite motion	0.33	Received signal power fluctuations caused by satellite motion are more significant for narrow beam antennas. ±0.05° satellite orientation error produces ±0.33 dB signal level variation at receive terminal in 0.3° beam.
Satellite gain variations across frequency band	0.50	Gain variations across the transponder do not affect (C/N)up but (C/N)down is affected. Apply half of the typical error for a link with (C/N)up = (C/N)down.
Satellite gain variations at a fixed frequency	0.50	Gain variations across the transponder do not affect (C/N)up but (C/N)down is affected. Apply half of the typical error for a link with (C/N)up = (C/N)down.
Downlink propagation effects	0.31	Propagation effects are dominated by frequency scaling of gaseous absorption.
LNA gain fluctuations	0.00	LNA gain variations affect signal and noise equally.
Fade measurement accuracy	0.30	Channel BER=5E-4, 95% confidence interval is 0.3 dB.
RSS error	0.89	Square root of the sum of the worst case errors.
Mean square error	0.45	Mean square or one sigma error.

On-board Processing		
Bit Error Rate Measurement from Known Data Pattern		
Source of Error		**Comments**
Transmit power variations across frequency band	0.00	Uplink transmit power variations will not affect downlink power.
Transmit power variations over temperature	0.00	Uplink transmit power variations will not affect downlink power.
Accuracy of uplink compensation	0.00	Uplink compensation errors will not affect downlink power.
Satellite motion	0.33	Received signal power fluctuations caused by satellite motion are more significant for narrow beam antennas. ±0.05° satellite orientation error produces ±0.33 dB signal level variation at receive terminal in 0.3° beam.
Satellite gain variations across frequency band	0.50	Gain variations across the transponder do not affect (C/N)up but (C/N)down is affected. Apply half of the typical error for a link with (C/N)up = (C/N)down.
Satellite gain variations at a fixed frequency	0.50	Gain variations across the transponder do not affect (C/N)up but (C/N)down is affected. Apply half of the typical error for a link with (C/N)up = (C/N)down.
Downlink propagation effects	0.31	Propagation effects are dominated by frequency scaling of gaseous absorption.
LNA gain fluctuations	0.00	LNA gain variations affect signal and noise equally.
Fade measurement accuracy	0.50	Channel BER=0.01, 95% confidence interval is ±0.5 dB.
Total Error	0.98	Square root of the sum of the worst case errors.
Mean square error	0.49	Mean square or one sigma error.

On-board Processing		
Signal to Noise Ratio Measurement		
Source of Error		**Comments**
Transmit power variations across frequency band	0.00	Uplink transmit power variations will not affect downlink power.
Transmit power variations over temperature	0.00	Uplink transmit power variations will not affect downlink power.
Accuracy of uplink compensation	0.00	Uplink compensation errors will not affect downlink power.
Satellite motion	0.33	Received signal power fluctuations caused by satellite motion are more significant for narrow beam antennas. ±0.05° satellite orientation error produces ±0.33 dB signal level variation at receive terminal in 0.3° beam.
Satellite gain variations across frequency band	0.50	Gain variations across the transponder do not affect (C/N)up but (C/N)down is affected.
Satellite gain variations at a fixed frequency	0.50	Gain variations across the transponder do not affect (C/N)up but (C/N)down is affected. Apply half of the typical error for a link with (C/N)up = (C/N)down.
Downlink propagation effects	0.31	Propagation effects are dominated by frequency scaling of gaseous absorption. Apply half of the typical error for a link with (C/N)up = (C/N)down.
LNA gain fluctuations	0.00	LNA gain variations affect signal and noise equally.
Fade measurement accuracy	0.10	For Eb/No > 5 dB, 95% confidence interval is 0.1 dB.
RSS error	0.85	Square root of the sum of the worst case errors.
Mean square error	0.42	Mean square or one sigma error.

APPENDIX B — HEXAGONAL ARRAY NUMEROLOGY AND ACTIVE AREA FOR CIRCULAR ELEMENTS

Hexagonal array numerology is presented followed by calculation of the active area of a hexagonal array of circular feed horns. It is determined that the ratio of active area to total area is about 0.91 for large arrays.

In a hexagonal array the total numbers of elements, $\underline{n}$, for regular hexagonal fill areas are 7, 19, 37, 61, 91, 127, etc. The number of elements on a principal diagonal of the hexagonal area can be defined as:

number of elements on principal diagonal = 2k+1

where k=1 for n=7, k=2 for n=19, k=3 for n=37, etc. With this nomenclature, $\underline{n}$ may be expressed as a function of $\underline{k}$ as:

$$n = 6(1+(k-1)/2)k + 1$$

Let the hexagonal fill area be inscribed within the smallest circle such that no part of the hexagonal area is outside of the circle. The diameter of this circle is equal to $(2k+1)\ D_h$, where D_h is the diameter of an individual feed horn.

The active area of the feed array is equal to the area of all of the $\underline{n}$ [$= 6(1+(k-1)/2)k + 1$] feed horn apertures, or nA_h, where $A_h = \pi(D_h/2)^2$ is the area of a single feed horn aperture. The total area of the feed array is the active area plus the area taken by all of the interstitial areas between the feed horns. Each such interstitial area, A_i, is obtained as follows:

A_i = (area of an equilateral triangle with vertices at the centers of three adjacent feed horns) - 3 (one-sixth the area of a single feed horn aperture)

$$= (1/2)\ D_h\ D_h \cos(30°) - (3/6)\pi(D_h/2)^2$$

$$= 0.16125\ (D_h/2)^2 = 0.0513275\pi\ (D_h/2)^2$$

It is easy to count the number of interstitial areas, $\underline{i}$, for each hexagonal array and establish a functional relationship with $\underline{k}$. The result of this effort is:

$$\underline{i} = 6k^2$$

The ratio $R_{a/t}$ of active area to total area of a hexagonal array is then given by:

$$R_{a/t} = \text{(active area)}/[\text{(active area)} + \text{(interstitial area)}]$$

$$= nA_h/[nA_h + 6k^2A_i]$$

$$= n\pi(D_h/2)^2/[n\pi(D_h/2)^2 + 6k^2\, 0.0513275\, \pi(D_h/2)^2]$$

$$= [6(1+(k-1)/2)k + 1]/[6(1+(k-1)/2)k + 1 + 6k^2\,(0.0513275)]$$

$$= [3k^2 + 3k + 1]/[3.308k^2 + 3k + 1]$$

Values for $R_{a/t}$ are given in Table B-1.

To obtain an array with 1323 active elements, the value of k should be about 21. Therefore, the diameter of the array is 43 feed horns. For any given feed-horn spacing, in wavelengths, the diameter may be calculated.

For example, if horn spacing is 2.6 wavelengths at 19.2 GHz, the array diameter is given by:

$$\text{array diameter} = 43 \times 2.6\ (11.785/19.2) \text{ inches}$$

$$= 68.6 \text{ inches}$$

Table B-1. Table of Values of $R_{a/t}$ for k=1,2, ..., 6

k	n (number of feeds in regular hexagonal grid array) $6[1+(k-1)/2]k+1$	i (number of interstices within regular hexagonal grid array) $6k^2$	$R_{a/t}$ (ratio of active area to total area of array)*
0	1	0	1
1	7	6	0.9579
2	19	24	0.9391
3	37	54	0.9303
4	61	96	0.9253
5	91	150	0.9220
6	127	216	0.9197
7	169	282	0.9180
8	217	384	0.9167
9	271	486	0.9157
10	331	600	0.9149
11	397	726	0.9142
12	469	864	0.9136
13	547	1014	0.9131
14	631	1176	0.9127
15	721	1350	0.9123
16	817	1536	0.9120
17	919	1734	0.9117
18	1027	1944	0.9114
19	1141	2166	0.9112
20	1261	2400	0.9110
21	1387	2646	0.9108
22	1519	2904	0.9106
23	1657	3174	0.9105
24	1801	3456	0.9103
25	1951	3750	0.9102

* $R_{a/t} = [3k^2 + 3k + 1]/[3.308k^2 + 3k + 1]$

REPORT DOCUMENTATION PAGE

Form Approved
OMB No. 0704-0188

1. AGENCY USE ONLY (*Leave blank*)	2. REPORT DATE	3. REPORT TYPE AND DATES COVERED
	December 1997	Final Contractor Report

4. TITLE AND SUBTITLE

Rain Fade Compensation for Ka-Band Communications Satellites

5. FUNDING NUMBERS

WU-315-90-2C
NAS3-27559

6. AUTHOR(S)

W. Carl Mitchell, Lan Nguyen, Asoka Dissanayake, and Brian Markey

7. PERFORMING ORGANIZATION NAME(S) AND ADDRESS(ES)

Space Systems/LORAL
3825 Fabian Way
Palo Alto, California 94303–4604

8. PERFORMING ORGANIZATION REPORT NUMBER

E–11024

9. SPONSORING/MONITORING AGENCY NAME(S) AND ADDRESS(ES)

National Aeronautics and Space Administration
Lewis Research Center
Cleveland, Ohio 44135–3191

10. SPONSORING/MONITORING AGENCY REPORT NUMBER

NASA CR—97-206591
SS/L TR01363

11. SUPPLEMENTARY NOTES

W. Carl Mitchell, Space Systems/Loral, 3825 Fabian Way, Palo Alto, California 94303–4606; Lan Nguyen, Asoka Dissanayake, and Brian Markey, COMSAT Laboratories, Clarksburg, Maryland. Project Manager, Clifford H. Arth, Space Communications Office, NASA Lewis Research Center, organization code, (216) 433–3460.

12a. DISTRIBUTION/AVAILABILITY STATEMENT

Unclassified - Unlimited
Subject Category: 17 Distribution: Nonstandard

This publication is available from the NASA Center for AeroSpace Information, (301) 621–0390.

12b. DISTRIBUTION CODE

13. ABSTRACT ***(Maximum 200 words)***

This report provides a review and evaluation of rain fade measurement and compensation techniques for Ka-band satellite systems. This report includes a description of and cost estimates for performing three rain fade measurement and compensation experiments. The first experiment deals with rain fade measurement techniques while the second one covers the rain fade compensation techniques. The third experiment addresses a feedback flow control technique for the ABR service (for ATM-based traffic). The following conclusions were observed in this report; a sufficient system signal margin should be allocated for all carriers in a network, that is a fixed clear-sky margin should be typically in the range of 4-5 dB and should be more like 15 dB in the up link for moderate and heavy rain zones; to obtain a higher system margin it is desirable to combine the uplink power control technique with the technique that implements the source information rate and FEC code rate changes resulting in a 4-5 dB increase in the dynamic part of the system margin. The experiments would assess the feasibility of the fade measurements and compensation techniques, and ABR feedback control technique.

14. SUBJECT TERMS

ACTS; Rain fade; Ka-band; Satellites

15. NUMBER OF PAGES

164

16. PRICE CODE

A08

17. SECURITY CLASSIFICATION OF REPORT	18. SECURITY CLASSIFICATION OF THIS PAGE	19. SECURITY CLASSIFICATION OF ABSTRACT	20. LIMITATION OF ABSTRACT
Unclassified	Unclassified	Unclassified	